Identification of the trail-following pheromone receptor in termites

Souleymane Diallo[1,2], Kateřina Kašparová[1,3], Josef Šulc[1], Jibin Johny[2], Jan Křivánek[1], Jana Nebesářová[3,4], David Sillam-Dussès[5], Pavlína Kyjaková[1], Jiří Vondrášek[1], Aleš Machara[1], Ondřej Lukšan[1]*, Ewald Grosse-Wilde[2] & Robert Hanus[1]*

[1]Institute of Organic Chemistry and Biochemistry of the Czech Academy of Sciences, Prague, Czech Republic

[2]Czech University of Life Sciences, Prague, Czech Republic

[3]Faculty of Science, Charles University, Prague, Czech Republic

[4]Biology Centre of the Czech Academy of Sciences, Prague, České Budějovice, Czech Republic

[5]University Sorbonne Paris Nord, 93430 Villetaneuse, France

*Corresponding authors

ABSTRACT

Chemical communication is the cornerstone of eusocial insect societies since it mediates the social hierarchy, division of labor, and concerted activities of colony members. The chemistry of social insect pheromones received considerable attention in both major groups of social insects, the eusocial Hymenoptera and termites. By contrast, current knowledge on molecular mechanisms of social insect pheromone detection by odorant receptors (ORs) is limited to hymenopteran social insects and no OR was yet functionally characterized in termites, the oldest eusocial insect clade. Here, we present the first OR deorphanization in termites. We selected four OR sequences from the previously annotated antennal transcriptome of the termite *Prorhinotermes simplex* (Rhinotermitidae), expressed them in Empty Neuron *Drosophila*, and functionally characterized using single sensillum recording (SSR) and a panel of termite semiochemicals. In one of the selected ORs, PsimOR14, we succeeded in obtaining strong and reliable responses to the main component of *P. simplex* trail-following pheromone, the monocyclic diterpene neocembrene. PsimOR14 showed a narrow tuning to neocembrene; only one additional compound out of 67 tested (geranylgeraniol) generated non-negligible responses. Subsequently, we used SSR in *P. simplex* workers and identified the olfactory sensillum specifically responding to neocembrene, thus likely expressing *PsimOR14*. We report on homology-based modelling of neocembrene binding by PsimOR14 and show how different ligands impact the receptor dynamicity using molecular dynamics simulations. Finally, we demonstrate that *PsimOR14* is significantly more expressed in worker antennae compared to soldiers, which correlates with higher sensitivity of workers to neocembrene.

INTRODUCTION

Chemical communication is the cornerstone of eusocial insect societies. It mediates the social hierarchy and division of labor, social cohesion and concerted activities of colony members. Different clades of eusocial insects have independently evolved chemical signals acting in similar social contexts, such as trail, alarm and queen pheromones, colony and caste recognition cues, and other signals. The convergent evolution of chemical signaling is the best manifested by many similarities between ants and termites, in spite of the great evolutionary distance between these two dominant groups of social insects with great ecological significance (Leonhardt et al., 2016; Tuma et al. 2020).

Since the identification of the multigene family of insect odorant receptors (ORs) expressed in antennae and maxillary palps of *Drosophila melanogaster* (Clyne et al., 1999), neurophysiology of insect olfaction has seen great progress in terms of phylogenetic reconstructions of OR evolution across taxa, functional characterizations (deorphanisations) of multiple ORs and ultimately their recent structural characterizations (Butterwick et al., 2018; del Mármol et al., 2021; Wang et al., 2024; Zhao et al. 2024). Even though the insect ORs have seven transmembrane domains like the ORs known from vertebrates, they do not share many tangible sequence similarities. Insect ORs have an inverted membrane topology in the dendrites of olfactory sensory neurons compared to vertebrate ORs (Benton et al., 2006; Clyne et al., 1999) and unlike the vertebrate ORs known to act as GPCR receptors, insect ORs function as odorant-gated ion channels (Sato et al., 2008; Wicher et al., 2008). While the ORs from the basal wingless insect lineage Archaeognatha are homotetramers (del Mármol et al., 2021; Brand et al., 2018), ORs of all other Insecta form heteromeric complexes with a highly conserved coreceptor protein (ORCo) (Brand et al., 2018; Butterwick et al., 2018; Larsson et al., 2004; Sato et al., 2008). As recently shown in mosquitoes and aphids, these complexes consist of one OR and three ORCo subunits (Wang et al., 2024; Zhao et al. 2024).

The OR repertoire is greatly variable across Insecta and ranges from units in the wingless Archaeognatha and basal winged order Odonata to tens or hundreds ORs identified in most other flying insects (Robertson, 2019; Yan et al., 2020). Insect ORs often lack a clear orthology pattern across phylogeny, because the OR family evolved via rapid birth-and-death process, accompanied by multiple gene duplications, pseudogenizations, and losses. Lineage-specific expansions,

together with a considerable variability in OR ligand specificities (from broad to narrow tuning) allow for a rapid response of olfactory system to ecological and life history changes (Andersson et al., 2015; Benton, 2015; Nei & Rooney, 2005; Robertson, 2019). Ecology-driven plasticity in OR evolution has been convincingly demonstrated by comparisons of specialist vs. generalist insects, the former often having much lower repertoires of ORs and other chemosensory proteins (Robertson, 2019).

The knowledge on OR function and ligand specificities has historically been obtained mainly from deorphanisation studies on *Drosophila* and other holometabolan insects using various heterologous expression systems. Recently, this bias was in part compensated by OR deorphanisations in more basal taxa, e.g., the wingless Archaeognatha (del Mármol et al., 2021), or the hemimetabolous aphids (Zhang et al., 2017, 2019a) and locusts (Guo et al., 2020; Chang et al., 2023).

Within social insects, eusocial Hymenoptera received considerable attention both in terms of OR repertoire reconstructions and functional characterizations with multiple ORs being deorphanized in ants (Pask et al., 2017; Slone et al., 2017) and the honey bee (e.g., Gomez Ramirez et al., 2023; Wanner et al., 2007). The amassed knowledge suggests that the complex communication and orientation capabilities in the colonies of eusocial Hymenoptera are facilitated by the greatly expanded repertoire of ORs, especially that of the 9-exon subfamily in ants and paper wasps participating in the detection of cuticular hydrocarbons (CHCs) as important cues in contact chemoreception of colony and caste identity and fertility status in eusocial insects (Engsontia et al., 2015; Legan et al., 2021; McKenzie et al., 2016; Pask et al., 2017; Zhou et al., 2015). The 9-exon subfamily and the overall OR richness have been inherited by the extant eusocial Hymenoptera from the ancestor of Aculeata (McKenzie et al., 2016), and also solitary aculeate taxa display large OR repertoires (Obiero et al., 2021); this preadaptation might had been important for the repeated emergence of eusociality and the related complex communication. This is supported by the reduction of OR array (including 9-exon genes) in parasitic ant taxa, along with the simplification of their behavioral repertoire (Jongepier et al., 2022).

The multiple convergences in biology and life histories between termites and ants call for comparison of olfactory detection of chemical signals and environmental cues in the two groups. Yet, despite relatively good knowledge on chemistry of termite pheromones and recognition cues (reviewed in Bagnères & Hanus, 2015; Bordereau & Pasteels, 2011; Mitaka & Akino, 2021), molecular aspects of olfaction remain largely understudied in termites. Termite ORs were so far

only addressed with respect to their diversity, inferred from genome assemblies (Harrison et al., 2018; Terrapon et al., 2014) or whole-body transcriptomes (Mitaka et al., 2016), recently complemented by comprehensive search for chemosensory protein repertoire using the antennal transcriptomes of three termite species (Johny et al., 2023). Termite ORs are organized in relatively conserved, highly orthologous pattern and their total numbers range from 28 to 69 (Johny et al., 2023; Terrapon et al., 2014). These numbers are lower than in their solitary cockroach relative *Blattella germanica* (Harrison et al., 2018), and dramatically lower than in ants, having up to over 400 ORs (Engsontia et al., 2015; Legan et al., 2021; McKenzie et al., 2016; Pask et al., 2017; Zhou et al., 2015). Thus, termites clearly contradict the paradigm on eusociality as a driver of OR richness, even though their chemical communication is by far more complex than in solitary insects and includes pheromone components from a variety of chemical classes, such as fatty-acyl derived alcohols, aldehydes and ketones, terpenoids, and, last, but not least, the CHCs. Independently of eusocial Hymenoptera, termites evolved an intricate communication system using CHCs as kin- and nestmate discrimination cues and as indicators of caste identity and fertility status (reviewed in Bagnères & Hanus, 2015; Mitaka & Akino, 2021). Therefore, compared to ants, the termite social evolution seemingly adopted a different trajectory to accommodate the needs of chemical communication, including CHC detection.

One of alternative hypotheses springs from observations that termites possess an extraordinarily rich set of ionotropic receptors (IRs), reaching up to more than one hundred in some species (Harrison et al., 2018; Johny et al., 2023; Terrapon et al., 2014). Even though the richness of IRs is shared by termites and their cockroach relatives, with *B. germanica* having the largest IR repertoire ever identified in insects (Robertson et al., 2018), IRs also underwent termite-specific expansions (Harrison et al., 2018; Johny et al., 2023). Since insect IRs have been shown to respond to volatile ligands (Benton et al., 2009), we cannot rule out that they also participate in the complex chemical communication in termites as has been previously speculated (Harrison et al., 2018). Nevertheless, since no chemosensory proteins have yet been functionally characterized in termites, ORs remain the prime candidates for pheromone detection.

Here, we report on the first OR deorphanization in termites. We build on the knowledge about the chemical ecology of the Cuban subterranean termite *Prorhinotermes simplex* (Rhinotermitidae) (Hanus et al., 2006, 2009; Jirošová et al., 2017; Piskorski et al., 2007), on the annotated repertoire of 50 ORs from *P. simplex* antennal transcriptome (Johny et al., 2023), on additional *P. simplex*

sequencing data (caste-specific head transcriptomes, draft genome assembly), and on laboratory culture of the species. We select four *P. simplex* OR sequences, study their function by means of the Empty Neuron *Drosophila* expression system and single-sensillum recording (SSR) using panels of biologically relevant ligands including the *P. simplex* pheromones and chemically related compounds. We identify PsimOR14 as the pheromone receptor narrowly tuned to the monocyclic diterpene neocembrene, known as the major component of the trail-following pheromone (TFP) (Sillam-Dussès et al., 2009). We demonstrate strong and selective response of PsimOR14 to neocembrene, with only one additional ligand, geranylgeraniol, generating non-negligible receptor response. We further report on homology-based modelling of neocembrene binding by PsimOR14 and perform molecular dynamics simulations to estimate the impact of ligand binding on PsimOR14 dynamicity. Finally, we identify the *P. simplex* olfactory sensillum specifically responding to neocembrene and document worker caste-biased expression of PsimOR14 accompanied by significantly higher sensitivity to neocembrene compared to *P. simplex* soldiers.

RESULTS

Phylogenetic reconstruction and candidate OR selection

In the first step, we reconstructed the phylogeny of termite ORs and ORCos using published protein sequences from two species in combination with our antennal transcriptome data on three species and the bristletail *Lepisma saccharina* as basal insect outgroup. In the resulting tree, all ORCo sequences and ORs from *L. saccharina* were basally situated, while majority of termite OR sequences were organized into two large sister clusters, both of which were further split into several sub-branches mostly containing one sequences from all five termite species (Fig. 1A and Supplementary Fig. S1). Only a few exceptions to this highly orthologous pattern were spotted, such as isolated sequences or species-specific expansions with a maximum of four paralogs.

Out of the 50 ORs identified in *P. simplex*, 26 sequences represented full open reading frames with at least 6 undisputed transmembrane domains predicted using TMHMM-2.0. From these, we selected four sequences (PsimOR9, 14, 30 and 31) situated in different parts (subbranches) of the tree (Fig. 1) and used them for transgenic *D. melanogaster* generation and SSR screening.

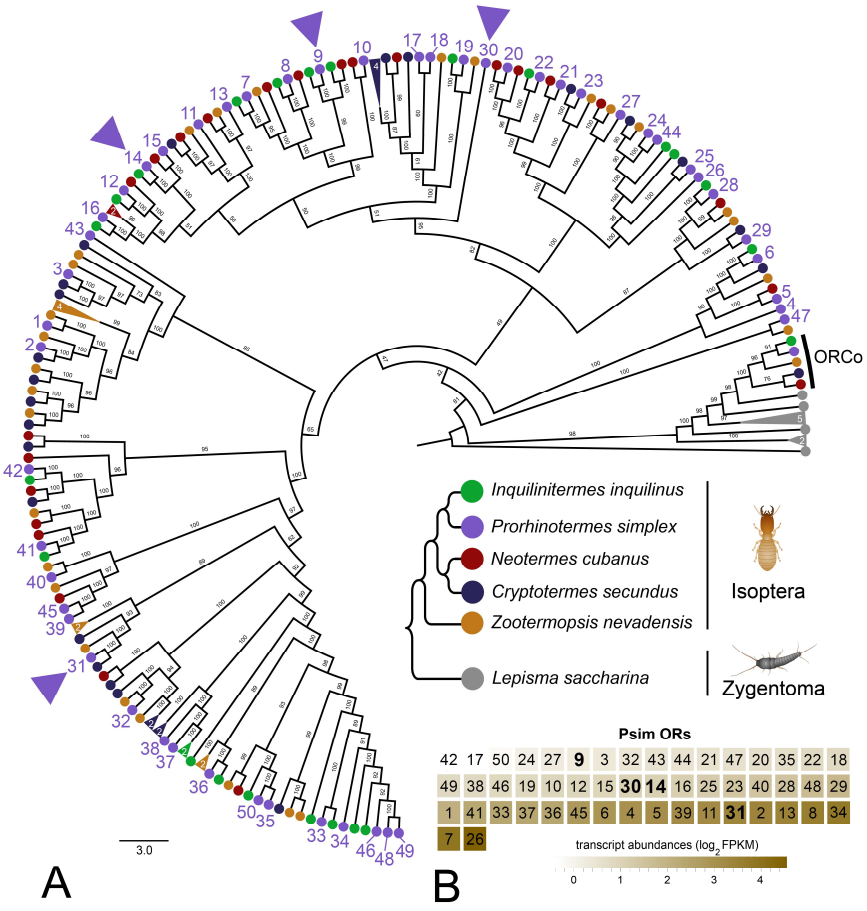

Fig. 1. Phylogenetic reconstruction of termite ORs and their transcript abundances in *P. simplex* workers. A. Phylogenetic tree is based on 182 protein sequences from five species of termites and the bristletail *Lepisma saccharina* as a basal insect outgroup, and also includes the sequences of ORCo. The topology and branching supports were inferred using the IQ-TREE maximum likelihood algorithm with the JTT+F+R8 model and supported by 10,000 iterations of ultrafast bootstrap approximation. Protein sequences of termite ORs can be found under the same labeling in Johny et al. (2023). *Lepisma saccharina* sequences are listed in Thoma et al. (2019). Arrowheads highlight the four ORs from *Prorhinotermes simplex* selected for functional characterization. Fully annotated version of the tree is provided as Supplementary Fig. S1. **B.** Heatmap shows the transcript abundances of 50 ORs identified in the RNAseq data from *P. simplex* worker antennae available in NCBI SRA archive under accession SRX17749141.

Functional characterization of *P. simplex* ORs in *D. melanogaster* ab3 sensillum

We expressed the four selected *P. simplex* ORs in the recently improved version of the *Drosophila melanogaster* Empty Neuron system (Chahda et al., 2019); the crossing scheme for fly generation adapted from Gonzales et al. (Gonzalez et al., 2016) is shown in Supplementary Fig. S2. Spontaneous SSR firing rates of the four transgenic lines showed an expected pattern with no abnormal bursts, indicating that the ORs were functional. The flies were first subjected to SSR screening with Panel 1, consisting of 11 semiochemicals relevant to termite chemical communication and structurally related compounds. As shown in Fig. 2A, PsimOR9 and PsimOR30 did not provide any strong response to any of the tested compounds, and PsimOR31 broadly and weakly responded to several compounds. By contrast, PsimOR14 systematically and strongly responded to stimulations by the monocyclic diterpene hydrocarbon neocembrene, which is the main component of the trail-following pheromone in the genus *Prorhinotermes* (Sillam-Dussès et al., 2009). Additionally, a moderate PsimOR14 response was also recorded for the linear diterpene alcohol geranylgeraniol, while all other compounds in the panel, including two other terpenoids, only elicited weak or no responses (Fig. 2A, Supplementary Tables S1–S4).

We then compared the responses of *Drosophila* ab3 sensillum in PsimOR14 expressing flies with those of W^{1118} flies. As evidenced in Fig. 2B, W^{1118} ab3 sensillum did not show any significant neuronal response to Panel 1 compounds, while the transgenic PsimOR14 line generated an average Δ spike number of >50 spikes/s for neocembrene and a minor secondary response of ~25 Δ spikes/s for geranylgeraniol. Characteristic responses for both lines to the two compounds are depicted in Fig. 2C. In the next step, we tested the dose-response behavior of PsimOR14 flies to neocembrene, and recorded an exponentially increasing neuronal response over the range of 0.01–10 ng to ED50 = ~24 ng and a lack of saturation at the dose of 500 ng (Fig. 2D, Supplementary Tables S5, S6).

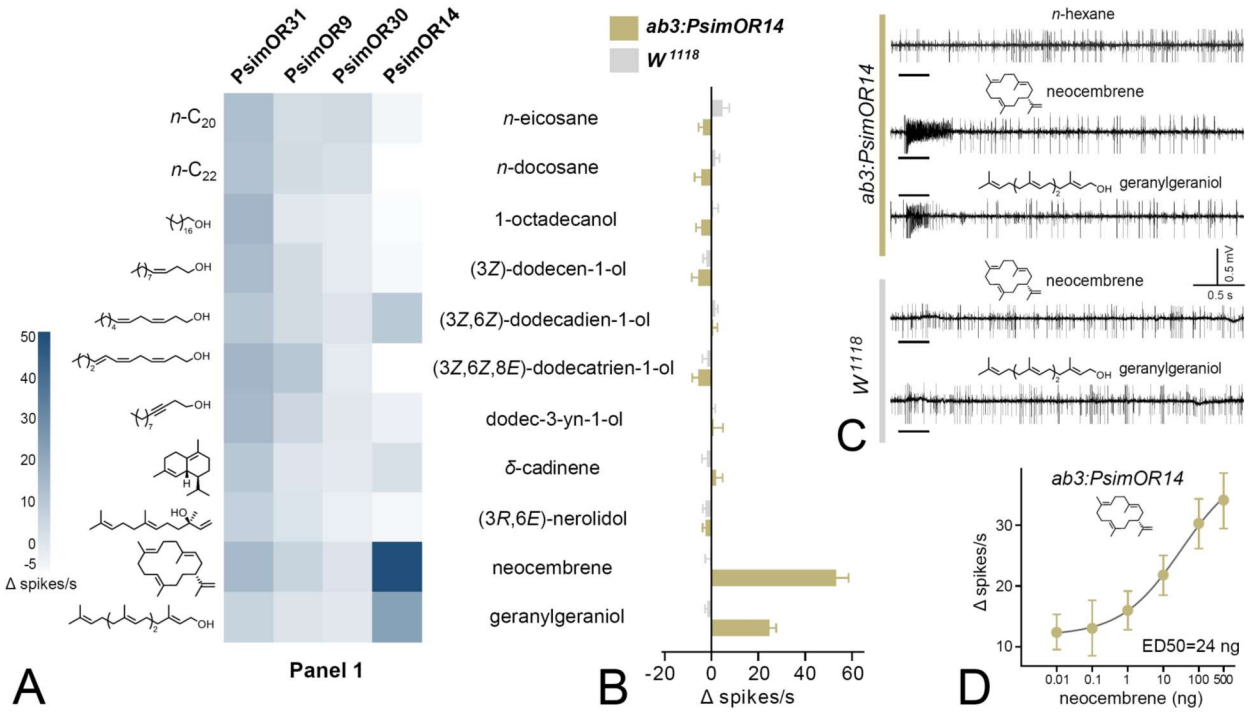

Fig. 2. SSR responses of transgenic *D. melanogaster* ab3 sensillum expressing PsimOR9, 14, 30 and 31 to the initial screening of 11 volatiles with biological relevance for termites. A. Heatmap showing the average responses of the four ORs as Δ spikes/s from 3–6 independent replicates. **B.** Comparison of SSR responses of transgenic *Drosophila melanogaster* ab3A neurons expressing PsimOR14 (*ab3A:PsimOR14)* and W^{1118} *D. melanogaster*. The bars show the average Δ spikes/s values from five independent replicates ± SEM. **C.** Characteristic SSR traces of *ab3A:PsimOR14* and W^{1118} flies for 1 µg dose of neocembrene and geranylgeraniol. **D.** Dose response curve of *ab3A:PsimOR14* SSR responses to neocembrene. The graph shows average Δ spikes/s values ± SEM based on nine replicates (8 in case of 100 ng and 4 in case of 500 ng stimulations). The curve fit and ED50 value were calculated using log(agonist) vs. response non-linear algorithm with least square fit method and the constraint of minimal response > 0. The raw data for all graphs is provided in Supplementary Tables S1–S6.

PsimOR14 is narrowly tuned to neocembrene, the main trail-following pheromone component

To further address the specificity of PsimOR14 tuning, we tested three additional panels containing 56 frequently occurring insect semiochemicals from various chemical classes. As shown in Fig. 3A, none of these compounds, including multiple terpenoids (mono-, sesqui-, di-), generated a strong response, suggesting a narrow tuning of PsimOR14 to neocembrene. The narrow tuning of PsimOR14 is evident also from the tuning curve depicted in Fig. 3B, with the receptor lifetime sparseness value 0.88 (Supplementary Tables S7–S9). These results confirm that PsimOR14 is a

pheromone receptor adaptively tuned to detect the main trail-following pheromone component neocembrene.

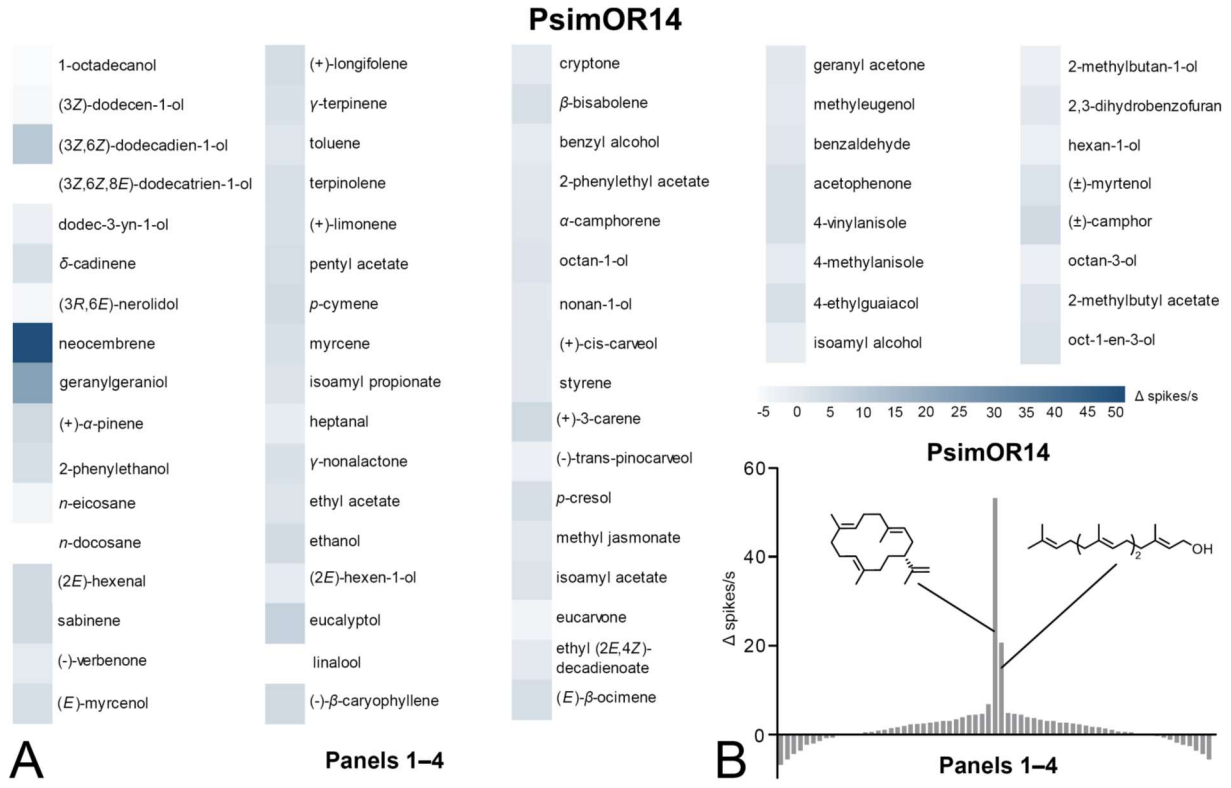

Fig. 3. SSR responses of transgenic *D. melanogaster* ab3 sensillum expressing PsimOR14 to the complete set of 67 compounds (Panels 1–4). A. Heatmap showing the average responses as Δ spikes/s from 3–6 independent replicates. **B.** Tuning curve of PsimOR14 for the 67 compounds contained in panels 1–4. The raw data is provided in Supplementary Tables S7–S9.

Identification of *P. simplex* olfactory sensillum responding to neocembrene

Our next goal was to identify the antennal olfactory sensillum responsible for neocembrene detection by *P. simplex* workers using a combination of SSR measurements with scanning electron microscopy (SEM) and high-resolution SEM (HR-SEM) imaging. Since no previous study reported SSR responses of termite olfactory sensilla to pheromones or environmental cues, we decided to search for the neocembrene-detecting sensillum on the last flagellomere, known to harbor by far the most sensilla in termite workers (Castillo et al., 2021).

In SSR experiments with the termite-relevant compounds from Panel 1, we obtained strong response to both neocembrene and geranylgeraniol from a short multiporous grooved sensillum situated in the apical part of the last antennal segment (Fig. 4A,B). The response of this sensillum to neocembrene was confirmed on workers originating from two different colonies. Detailed view on spontaneous firing pattern of the neocembrene-responding sensillum revealed three different spike amplitudes (Fig. 4C), suggesting the potential presence of as many as three olfactory sensory neurons (a–c). Comparison with spike amplitudes upon neocembrene and geranylgeraniol stimulations then indicated that the responses are generated by the neuron labeled as b.

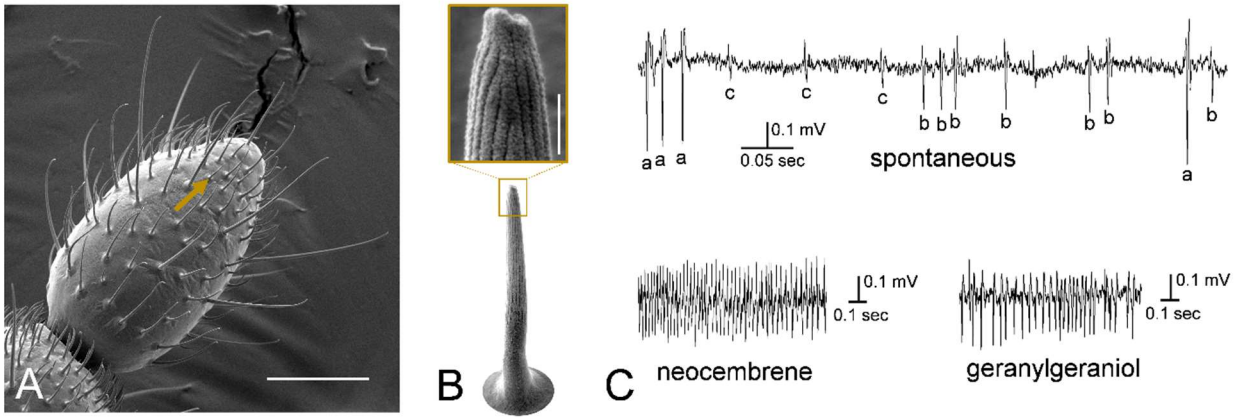

Fig. 4. Neocembrene-responding sensillum in *P. simplex* workers. A. SEM photograph of the last flagellomere of *P. simplex* worker. Arrow shows a small multiporous grooved sensillum responding to neocembrene and geranylgeraniol. Scale bar represents 50 µm. **B.** HR-SEM view on the neocembrene-responding sensillum. Scale bar in the inset represents 500 nm. **C.** Detailed view on SSR traces recorded from the neocembrene-responding sensillum during spontaneous firing, and upon stimulation with neocembrene and geranylgeraniol.

The SSR response spectrum of neocembrene sensillum to Panel 1 was markedly similar to that of ab3A neuron of PsimOR14-expressing *Drosophila* (Fig. 5A). None of the compounds elicited higher average responses than 10 Δ spikes/s, except for neocembrene and geranylgeraniol; their average Δ spikes/s were even slightly higher than those of heterologously expressed PsimOR14, reaching ~65 and ~29, respectively (Fig. 5A, B). Likewise, the dose-response experiment with neocembrene indicated a higher sensitivity threshold and lower ED50 = 0.016 ng (Fig. 5C, Supplementary Tables S10, S11).

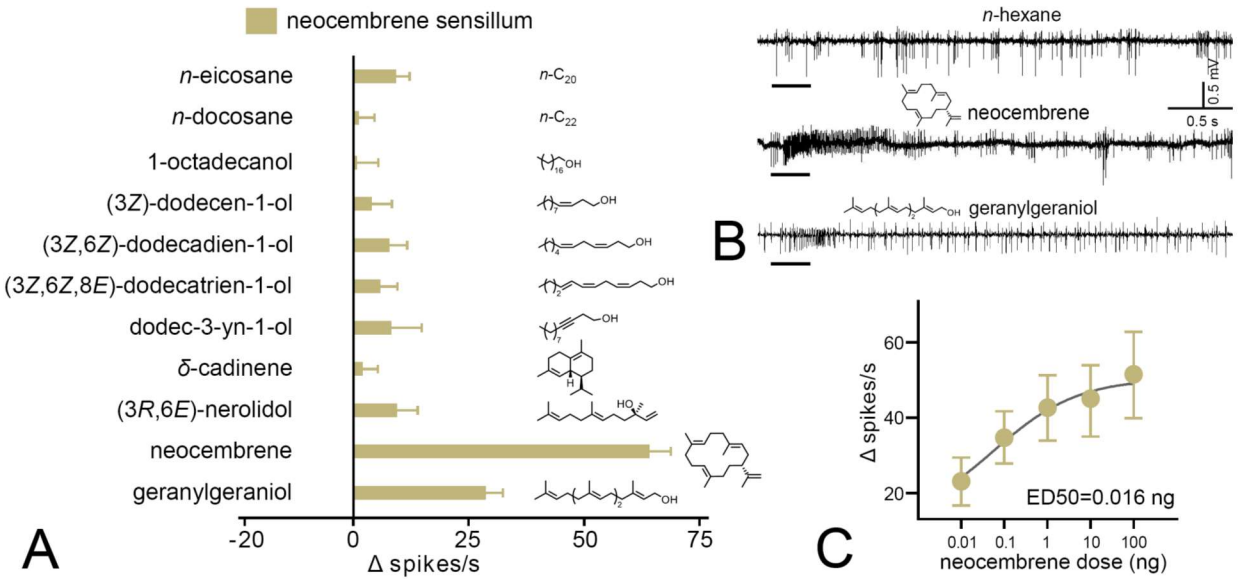

Fig. 5. SSR responses of the neocembrene-responding sensillum on the last flagellomere of *P. simplex* worker. **A.** SSR responses to panel 1. The bars show the average Δ spikes/s values from 8–17 replicates ± SEM. The raw data is provided in Supplementary Table S10. **B.** Characteristic SSR traces of the neocembrene-detecting sensillum for neocembrene and geranylgeraniol. **C.** Dose response curve of the SSR responses to neocembrene by the neocembrene-responding sensillum. The graph shows average Δ spikes/s values ± SEM based on 9–11 replicates. The curve fit and ED50 value were calculated using log(agonist) vs. response non-linear algorithm with least square fit method and the constraint of minimal response > 0. The raw data is provided in Supplementary Table S11.

PsimOR14 gene and protein structure, protein modeling, ligand docking, MM/PBSA, molecular dynamics (MD) simulations

Mapping the *PsimOR14* transcript sequence on *P. simplex* draft genome revealed that the gene consists of six exons and is situated on the same locus and in close vicinity of *PsimOR15*, with which it shares the exon-intron boundaries, suggesting a recent diversification of the two genes via duplication, as also supported by their high sequence similarity (Fig. 6A, Fig. 1A). Transcript (Fig. 6B) and protein (Fig. 6C) structures of PsimOR14 showed the presence of seven transmembrane domains (S1-S7) with the largest extracellular loop between S3 and S4 and the longest intracellular loop between S4 and S5.

Fig. 6D shows the initial PsimOR14 model obtained using AlphaFold 2. Three terpenoid ligands, i.e., the best agonists neocembrene and geranylgeraniol, and a weak agonist (+)-limonene, were selected for docking into the identified binding site. Dockings are visualized in Fig. 6E, the final

scores of the best-ranked poses are shown in Table 1. The predicted docking scores indicated neocembrene as the best ligand, followed by geranylgeraniol and (+)-limonene, in line with the ranking of their biological effect in SSR assays (Table 1). (+)-Limonene ranked as the worst agonist also according to the binding free energy calculated in MM/PBSA analysis, while the best energy score was obtained for geranylgeraniol followed by neocembrene (Table 1). Both docking and MM/PBSA analysis suggested that primarily Van der Waals interactions facilitate the binding, only in case of geranylgeraniol non-negligible contribution of electrostatic interactions has been recorded. Per-residue decomposition results (Fig. 6C, Supplementary Tables S13) showed that all three ligands bind two hydrophobic patches made out of residues from S3 and S4 (Cys154, Ala157, Val158; Thr221, Leu224, Ala225, Tyr228). Neocembrene and (+)-limonene only bind these patches, while geranylgeraniol also interacts with additional residues (Table S13).

MD simulations of per atom explored volumes in PsimOR14 apoform and upon ligand binding delimited three regions with high dynamicity, i.e. the N-terminal region, the extracellular S3-S4 loop and especially the intracellular S4-S5 loop (Fig. 6F). Binding of each of the three ligands reduced the overall protein dynamicity; this protein stabilization did not differ dramatically among the three ligands. By contrast, binding of geranylgeraniol and neocembrene led to a conspicuous dynamicity increase in a portion of the S4-S5 loop, compared to both the apoform and (+)-limonene binding (Fig. 6G).

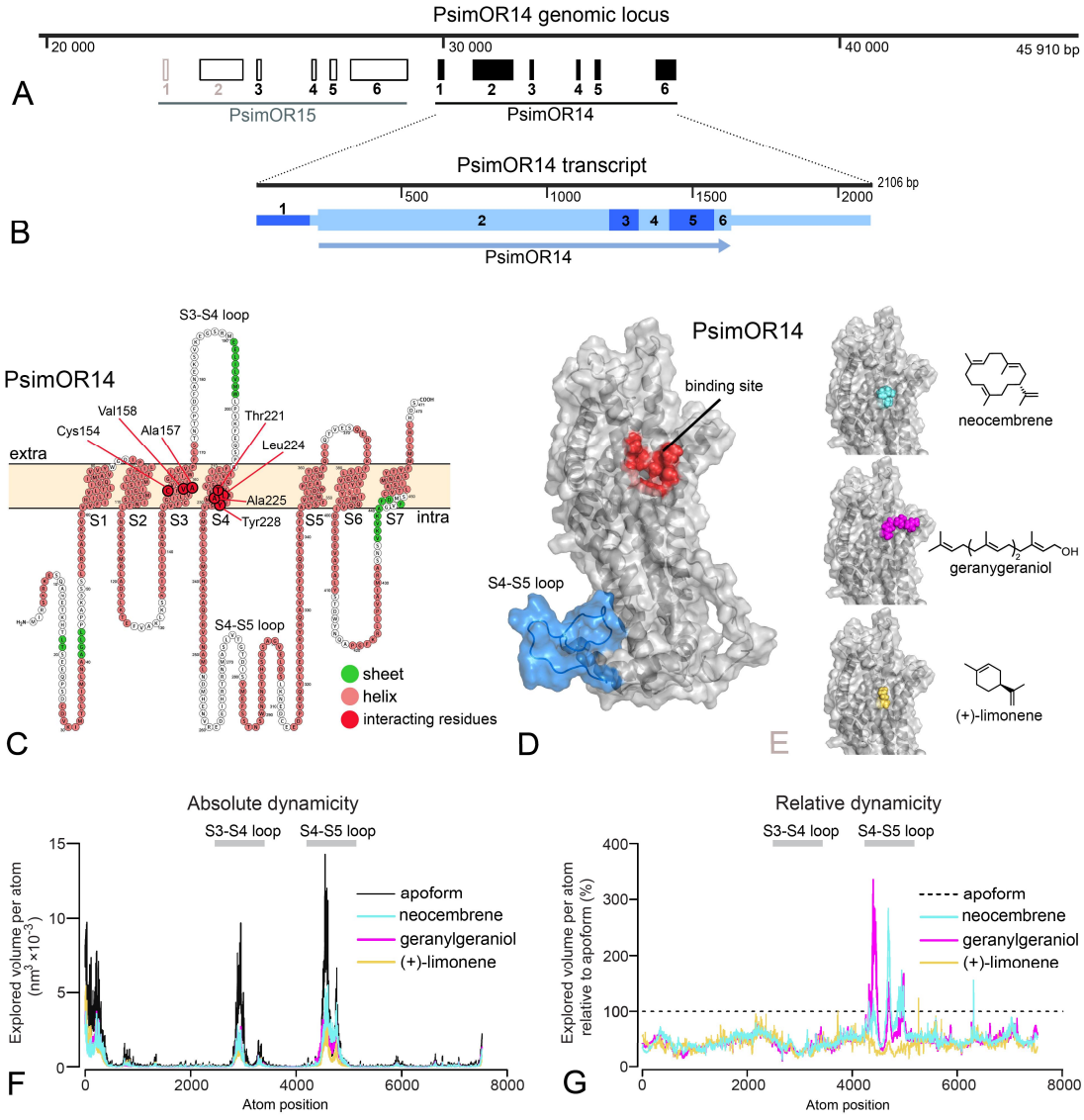

Fig. 6. PsimOR14 gene, transcript and protein structures, docking and MD simulations. A. Genomic locus containing *PsimOR14* and *PsimOR15*. *PsimOR14* gene consists of 1 non-coding and 5 protein coding exons. **B.** *PsimOR14* transcript with 6 exons, showing the protein-coding (higher boxes) and untranslated regions (lower boxes), and ORF (arrow). **C.** Transmembrane architecture of PsimOR14. In red are shown seven residues interacting with neocembrene. Light blue ellipse shows the intracellular loop the most impacted by ligand binding. **D.** Modelled apoform of PsimOR14. Red region denotes the binding site identified via docking, light blue region represents the intracellular S4-S5 loop. **E.** Holoforms of PsimOR14 with three docked ligands. **F.** Absolute PsimOR4 dynamicity expressed as average volumes explored by atoms per simulation step in PsimOR14 apoform and upon binding the three studied ligands. **G.** Relative PsimOR14 dynamicity expressed as average explored atom volumes upon ligand binding relative to the volumes in PsimOR14 apoform. Nucleotide and protein sequences of PsimOR14 are provided in Supplementary Table S12 and as NCBI entry under accession OR921181.

Caste-biased PsimOR14 expression and antennal sensitivity to neocembrene

We next decided to compare the expression pattern of PsimOR14 between *P. simplex* workers and soldiers, along with the sensitivity of the two castes to its preferred ligand, neocembrene. Both DESeq2 and EdgeR differential expression analyses of RNAseq read counts from heads (including antennae) of workers and soldiers revealed that PsimOR14 is significantly more expressed in workers, being among three the most upregulated ORs in workers (Fig. 7A, Supplementary Table S14). Subsequent EAG measurements were in line with this observation and indicated significantly stronger responses to neocembrene in workers (p=0.012) (Fig. 7B, Supplementary Table S15).

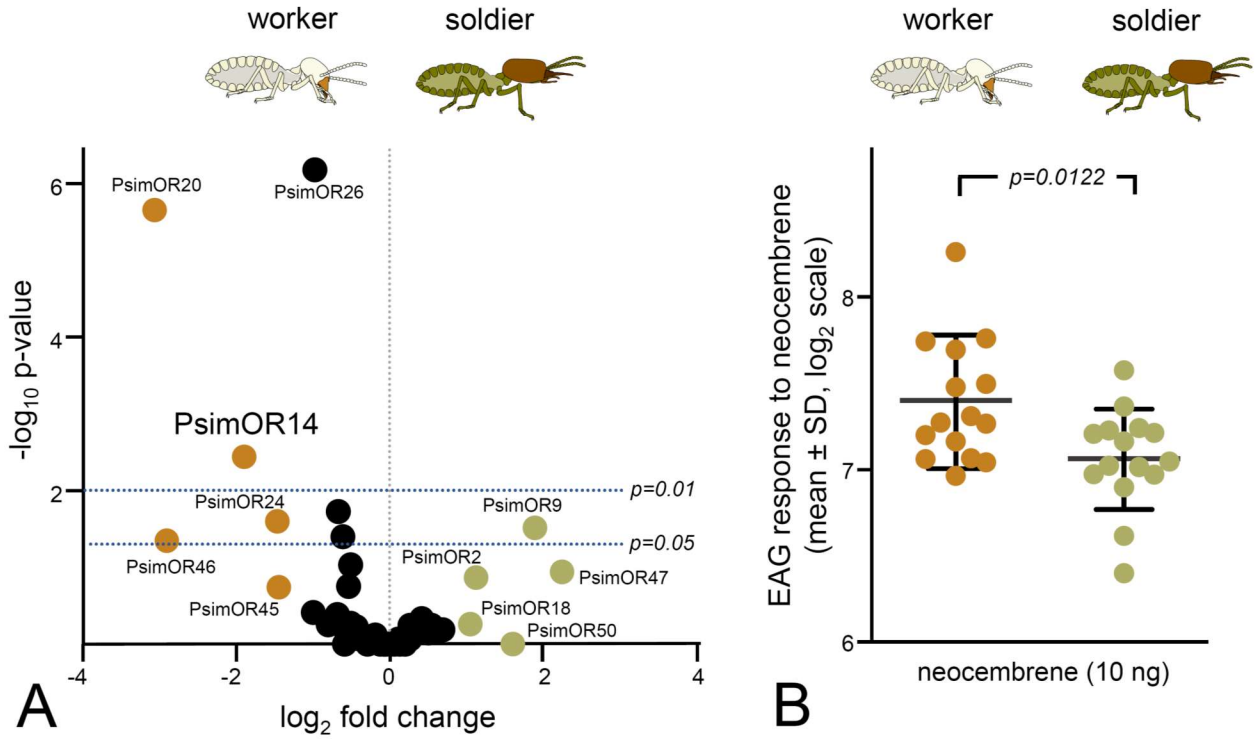

Fig. 7. Caste comparison of *PsimOR14* expression and EAG responses between *P. simplex* workers and soldiers. **A.** Volcano plot representing edgeR differential gene expression analysis of all 50 *P. simplex* ORs in RNAseq data from soldier and workers heads (including antennae) sequenced in three independent biological replicates per caste. Colored dots mark ORs reaching absolute value of $\log_2$ fold change ≥ 1, horizontal lines represent p-value thresholds of 0.05 and 0.01. Numeric values of the edgeR and DESeq2 differential expression analysis are provided in Supplementary Table S14. Based on SRA archives accessible under SRX18952230–32 and SRX18952237–39. **B.** EAG responses of whole antenna preparations of workers and soldiers to neocembrene at a dose of 10 ng (mean ± SD shown on $\log_2$ scale). Inter-caste differences were compared using t-test on $\log_2$-transformed data. Raw data is shown in Supplementary Table S15.

DISCUSSION

Identification of PsimOR14 as the pheromone receptor narrowly tuned to neocembrene in *P. simplex* represents the first OR deorphanisation in termites and confirms that the trail-following communication is mediated by odorant receptors. This assumption, validated here for the monocyclic diterpene neocembrene, is indirectly supported by previous experiments in two termite species having a C_{12} fatty alcohol as TFP; ORCo silencing in these species impaired the ability to follow the foraging trail (Gao et al., 2020). Because trail-following in termites has the shared evolutionary origin with courtship communication and both neocembrene and C_{12} alcohols also occur as sex-pairing pheromone components (Bagnères & Hanus, 2015; Bordereau & Pasteels, 2011; Sillam-Dussès, 2010), it is likely that the two communication modalities share identical or closely related ORs. Future OR deorphanizations should test this hypothesis and provide an insight on how the functional diversification of trail-following and sex attraction is imprinted into the OR evolution.

Neurophysiological characteristics of *D. melanogaster* ab3A neuron expressing PsimOR14 showed expected patterns of spontaneous firing rates of units of Hz (6.87 ± 4.73, mean ± SD) and maximum firing rates of 90 spikes/s at the highest used neocembrene doses (1 µg), though not reaching the reported maxima for ab3A responses with genuine and exogenous receptors, which may be well over 100 spikes/s (e.g., Chahda et al., 2019). This confirms that co-expression of termite ORs with the *Drosophila* ORCo using the Empty Neuron system is a suitable technique for termite OR characterizations. PsimOR14 has a narrow tuning to neocembrene with receptor lifetime sparseness equal to 0.88. ORs detecting pheromone components (pheromone receptors) and other volatiles with high biological importance, such as key food or host attractants, are often expressed in specialized sensilla and are highly selective, in contrast to the broad tuning of ORs sensing the general environmental stimuli (e.g., Carey et al., 2010; Fleischer & Krieger, 2018). Such a high selectivity is the best known for sex pheromone receptors, e.g. in moths (reviewed in Zhang & Löfstedt, 2015) or *Drosophila* (reviewed in Haverkamp, et al. 2018), mostly tuned to a single compound, even though in some cases the respective ORs can be adaptively shaped to selectively detect more pheromone compounds (Díaz-Morales et al., 2024; Mariette et al., 2024). Thus, the narrow tuning of PsimOR14 is in line with expectations from a pheromone receptor, especially when considering the ancient origin of trail-following from sex-pairing behavior and the great importance of TFP for concerted foraging in these blind insects. Nevertheless, due to the low

coverage of insect diversity by OR deorphanization studies and their strong bias towards derived Holometabola, it remains difficult to make any general considerations about the OR selectivity relative to the receptor function across Insecta. This has been recently demonstrated by a comprehensive functional characterization of ORs in migratory locust unveiling an unexpected design of the olfactory information decoding, consisting of a large set of narrowly tuned ORs for environmental cues (Chang et al., 2023).

With average Δ spike/s over 20, the linear diterpene alcohol geranylgeraniol was the only other agonist with non-negligible response. None of the remaining compounds elicited a Δ spike of more than 7, despite the presence of multiple other compounds derived from terpenoid scaffolds in the tested panels. It is difficult to attribute any adaptive significance to this observation since there is no record of geranylgeraniol in communication context in termites. Therefore, the observed significant biological activity, high docking score and high ranking in free energy comparison, may be due to non-adaptive binding affinity of PsimOR14 to the non-native ligand (see also below). Interestingly, another related terpene alcohol, the monoterpene linalool, had the biggest negative Δ spike score (-6.8) and the absolute spikes/s ranged from 0 to 5 (1.5 ± 1.9, mean ± SD), suggesting a possible inverse agonist function of linalool.

The neocembrene-sensing sensilla identified using SSR in *P. simplex* workers provided a response pattern to Panel 1 very similar to that of *PsimOR14*-expressing ab3 *Drosophila* sensillum, e.g., strong response to neocembrene followed by geranylgeraniol, supporting independently the results obtained from transgenic *Drosophila*. No other important responses to termite pheromone components from the Panel 1, which also included the minor *P. simplex* TFP component (3*Z*,6*Z*,8*E*)-dodecatrien-1-ol, were recorded, in spite of the likely presence of two additional olfactory neurons housed in the neocembrene-detecting sensillum. The function of these additional neurons remains elusive and examples from other insects offer multiple scenarios. A neuron expressing a highly selective pheromone receptor may co-exist with functionally independent neurons detecting environmental cues (e.g., Tateishi et al. 2020), or the co-habitation of several neurons may generate more complex interactions such as lateral inhibition of the neighboring neurons (Su et al., 2012; Zhang et al., 2019b). However, it must be noted, that our SSR analyses focused a specific sensillum defined by its topology on the last flagellomere and we did not perform a comprehensive mapping of olfactory sensilla on the entire worker antenna. Therefore, also our

image on the distribution of neocembrene-detecting sensilla and the pattern of neurons housed in these sensilla is incomplete.

The basic PsimOR14 protein architecture with seven transmembrane domains is typical for insect ORs. Likewise, the docking experiments identified a binding site defined by a binding pocket deep in the transmembrane region, homologous to that in previously studied insect ORs, and confirmed the nature of the ligand binding to mainly rely on hydrophobic interactions (e.g., del Mármol et al., 2021; Pettersson & Cattaneo, 2023; Yuvaraj et al., 2021). In case of PsimOR14, mainly the residues from S3 and S4 interacted with the studied ligands; these transmembrane domains were shown to participate in ligand binding also in other studied insect ORs (e.g., del Mármol et al., 2021; Yuvaraj et al., 2021; Wang et al., 2024; Zhao et al. 2024).

The calculated binding scores for the three tested ligands correlated with observed biological effects of the ligands. The MM/PBSA data also in part corroborated the SSR measurements by estimating (+)-limonene as the worst agonist; by contrast, geranylgeraniol and not neocembrene ranked as the best ligand. This may potentially be explained by the additional residues interacting with geranylgeraniol compared to neocembrene and (+)-limonene, and the relatively higher contribution of electrostatic interactions in geranylgeraniol binding. Moreover, in systems where ligand binding induces allosteric effects, as is the case of insect ORs, the simple binding affinity does not provide a complete picture of receptor signal transduction function.

In contrast to the general protein stabilization upon binding of the three tested ligands, some parts of the intracellular S4-S5 loop showed a significant increase in the dynamics upon binding of the biologically active ligands geranylgeraniol and neocembrene, compared to apoform and the weak agonist (+)-limonene binding. What is the mechanistic role of this allosteric transmission of the binding effect to the intracellular loop remains elusive. However, the impact of the S4-S5 loop on OR function has previously been reported for the MhOR5 from *Machilis hrabei* (del Mármol et al., 2021); replacement of the loop with a short linker increased the receptor response to native ligand. Interestingly, in some insect ORs this loop has been reduced to a short sequence of a few residues (e.g., Wang et al., 2024).

PsimOR14 does not belong to the most expressed *P. simplex* ORs (Fig. 1B). However, interestingly, it is among those having the most caste-biased expression with significantly higher transcript abundance in antennae of workers compared to soldiers. Accordingly, also the electrophysiological responses of workers to neocembrene were significantly stronger in workers.

Termite soldiers are known to lay pheromone trails, to detect TFPs and to participate in foraging and field exploration in a number of termite species, though the behavioral patterns of soldiers and workers during these activities differ (Kaib, 1990; Traniello, 1981; Traniello & Busher, 1985). This has also been demonstrated in a close relative to our model, the congeneric species *Prorhinotermes inopinatus* (Rupf & Roisin, 2008). Yet, differences in sensitivity of termite workers and soldiers have not previously been addressed at the electrophysiological level. Caste-biased *PsimOR14* expression and neocembrene sensitivity may represent olfactory information filtering adaptive to the different tasks of the two castes, as documented, e.g., in ants (Caminer et al., 2023).

Genus *Prorhinotermes* is the most basally situated termite taxon known to have a terpenoid component as a part of its pheromone repertoire (Sillam-Dussès et al., 2009). The acquisition of terpenoid pheromone components is undoubtedly due to the evolution of terpene biosynthesis in basal Neoisoptera, which has led to the fascinating diversity of defensive terpenoids produced by soldiers of Neoisoptera in their frontal gland (Gössinger, 2019). In line with general observations on pheromone evolution (Steiger et al., 2010), some of these defensive terpenoids from the frontal gland gained via exaptation a novel function of alarm pheromones (Dolejšová et al., 2014; Roisin et al., 1990; Šobotník et al., 2008, 2010). Likewise, the cyclic diterpenes probably became part of trail-following pheromones and sex-pairing pheromones by co-opting the terpenoid biosynthesis in exocrine glands other than the defensive frontal gland of soldiers. Beside the occurrence of neocembrene in the sub-basal *Prorhinotermes*, it only occurs as a pheromone component in much later diverging representatives of the subfamily Nasutitermitinae (Bordereau & Pasteels, 2011). Once reliable genome or antennal transcriptome of Nasutitermitinae become available, it would be of interest to search in these species for OR orthologs of PsimOR14 and test whether they have retained the function of neocembrene detection.

Insect ORs are frequently organized in tandem arrays (e.g., Bohbot et al., 2007; McKenzie and Kronauer, 2018; Robertson and Wanner, 2006). Likewise, the genomic locus of *PsimOR14* contains a likely tandem copy paralog of *PsimOR15* gene. The two genes share the gene architecture, and their transcripts are equally represented in worker antennal transcriptome, though *PsimOR15* does not display the caste-biased expression. Thanks to the close similarity of both genes, *PsimOR15* is a candidate for potential pheromone receptor function.

Future research in termites should also aim at finding the ORs or other chemosensory proteins involved in the detection of CHCs. In spite of the similarities in CHC roles in termites and ants,

ranging from nestmate recognition to fertility signaling, termite OR sequences do not show any conspicuous expansions analogous to 9-exon subfamily in ants. Therefore, finding the chemosensory principle of CHC detection in termites would bring another piece of knowledge about the fascinating convergent evolution in these two unrelated major groups of eusocial insects. Yet another appealing target for OR deorphanization is the search for pheromone receptors of queen pheromones, the central signals ensuring the reproductive dominance of queens in the colonies of social insects. In the honeybee and ants, narrowly tuned ORs responding to main queen pheromone components were already described (Wanner et al., 2007; Pask et al., 2017). In termites, queen pheromones were so far only identified in two species (Dolejšová et al., 2022; Matsuura et al. 2010). They are volatile and were shown to act as airborne signals via olfaction (Dolejšová et al., 2022), it is thus reasonable to expect a selective OR responsible for their detection.

MATERIALS AND METHODS

Termites

Multiple laboratory colonies of *P. simplex*, originating from previous field collections in Cuba and Florida, are held in the Institute of Organic Chemistry and Biochemistry, Czech Academy of Sciences. Colonies are reared in glass vivaria at 27°C and 80% relative humidity in clusters of spruce wood slices.

The data reported here were collected from three mature Cuban colonies. The first one was used for antennal transcriptome sequencing and assembly followed by phylogenetic analysis, as described in Johny et al. (2023). The second one was used for RNA extraction for OR cloning, SSR, SEM and HR-SEM. The third one was used for caste-specific head transcriptomes (head + antennae) of workers and soldiers, for caste-specific EAG recordings, and for SSR confirmation of the neocembrene-detecting sensillum. For all experiments with workers, 4th or 5th stage workers were selected as the most abundant developmental stages, recognized according to body size and head width.

RNA extraction, OR cloning and construct generation

Total RNA was extracted from 20 pairs of dissected *P. simplex* antennae using PureLink RNA Mini Kit (Invitrogen, Carlsbad, CA, USA) following the manufacturer's protocol and quantified using NanoDrop spectrophotometer (Thermo, Delaware, USA). From the total RNA, 2 µg was

used to synthesize the cDNA using SuperScript IV Reverse Transcriptase (Invitrogen, Carlsbad, CA, USA) according to manufacturer's instructions. The efficiency of cDNA synthesis was evaluated by amplification of ORCo. The list of primers is provided in Supplementary Table S16. The full-length open reading frame (ORF) of each selected PsimORs was PCR-amplified from the cDNA using the DreamTaq Green PCR Master Mix (Invitrogen, USA) and gene-specific primers (Supplementary Table S16). Amplification products were purified by QIAquick Gel Extraction Kit (Qiagen, Germany), cloned into pCR8/GW/TOPO vector using the TOPO TA Cloning Kit (Invitrogen, USA) and transformed into OneShot TOP10 competent cells (Invitrogen, USA). Positive colonies were selected based on colony-PCRs using primers GW1 and GW2, recombinant plasmids were isolated using the QIAprep 2.0 Spin Miniprep Columns (Qiagen, Germany) and sequences were verified by Sanger sequencing (Eurofins Genomics, Germany).

The expression vector constructs were prepared using the Gateway LR recombination cloning technology (Invitrogen, USA) based on recombination of the phage-like attachment sites attL/R in pCR8/GW/TOPO with the bacteria-like attachment site attB in pUASg.attb vector (obtained from *Drosophila* Genomics Resource Center, Bloomington, USA). The resulting constructs pUASg.attB-PsimOR were purified using the QIAprep 2.0 Spin Miniprep Columns (Qiagen, Germany) and insert sequences were verified by Sanger sequencing at Eurofins Genomics (Germany). All primers used for Sanger sequencing and colony-PCR are listed in Supplementary Table S16).

Fly lines

D. melanogaster lines used in the Empty Neuron system were kindly provided by Dr. Thomas O. Auer (from Richard Benton Lab, University of Lausanne, Switzerland). The wild type W^{1118} line, used as a control, was kindly provided by Prof. Michal Žurovec (Biology Centre, Czechia). All *Drosophila melanogaster* lines were reared in an incubator which was set at 24±2˚C with relative humidity of 50±5%. Flies were fed with in-house prepared diet based on standard cornmeal food. The fly lines used are listed in Supplementary Table S17.

Transgenic expression of termite ORs in *D. melanogaster* ab3A neuron

Selected PsimORs were expressed in the *Drosophila melanogaster* Empty Neuron system for functional screening. Transgenic *D. melanogaster* UAS-PsimOR lines were generated by

BestGene Inc. (Chino Hills, CA, USA) by injecting pUASg.attB-PsimOR vectors into fly embryos expressing the integrase PhiC31 and carrying an attP landing site resulting in flies with genotype w−; +; UAS-PsimOR (w+)/+.

The recent CRISPR-Cas9-engineered empty neuron line Or22ab^{-Gal4} (Chahda et al., 2019) was used as Δhalo genetic background for the expression of UAS-PsimOR in Dmel ab3 sensilla. The fly crossing scheme was adapted from (Gonzalez et al., 2016) with a modification at the F3 crossing. Final homozygote lines with UAS-PsimOR and Or22ab^{-Gal4} were generated and used for the electrophysiological recordings. The full description of the crossing scheme is provided in Supplementary Fig. S2.

Chemicals

For SSR measurements, we used a total of 67 chemicals organized into four panels. The initial screening Panel 1 contained 11 compounds biologically relevant to termites, i.e. components of termite pheromones and cuticular hydrocarbons known from Neoisoptera and structurally related compounds. This panel was used for initial SSR screening of PsimOR9, 14, 30 and 31 in transgenic *D. melanogaster* and for SSR experiments with *P. simplex* workers. For detailed analysis of Psim OR14, three additional panels were used, consisting of 56 frequently occurring insect semiochemicals (e.g., terpenoids, fatty acid esters, fatty alcohols and aldehydes, etc.). Panel 1 compounds were diluted in *n*-hexane to 100 ng/µL, panel 2–4 compounds were diluted in paraffin oil to 10^{-3} v/v. List of all compounds tested and their origin are listed in Supplementary Table S18.

Organic synthesis

For the purpose of SSR experiments, we synthesized (*Z*)-dodec-3-en-1-ol, (3*Z*,6*Z*)-dodeca-3,6-dien-1-ol, (3*Z*,6*Z*,8*E*)-dodecatrien-1-ol, and dodec-3-yn-1-ol, and included these compounds into Panel 1. The *de novo* organic synthesis of these fatty alcohols is described in the Supplementary Information file.

Electrophysiology

SSR recordings on *Drosophila* ab3 sensillum were performed as described previously (Benton & Dahanukar, 2023; Olsson & Hansson, 2013). We used 2–4 days old flies for one recording per each

548 to avoid neuronal adaptations from multiple stimulations. To expose more ab3 sensilla, the fly
549 preparation was done with arista down (Keesey et al., 2022).
550 In termites, the olfactory sensilla situated on the last antennal flagellomere of workers were targeted
551 for SSR, since their number increases towards the distal end of termite antennae, the last segment
552 being significantly more populated by olfactory sensilla than any other segment (Castillo et al.,
553 2021). The grounding electrode was carefully inserted into the clypeus and the antenna was fixed
554 on a microscope slide using a glass electrode. To avoid the antennal movement, the microscope
555 slide was covered with double-sided tape and the three distal antennal segments were attached to
556 the slide.
557 The sensilla were observed under the Nikon FN1 eclipse microscope at 60× magnification. For all
558 electrophysiological measurements, the recording electrode was brought into contact with the base
559 of the sensillum using a Kleindiek Nanotechnik MM3A micromanipulator connected to a cubic
560 micromanipulator device. Using Syntech stimulus delivery system (CS55 model, Syntech,
561 Germany), the odorant stimulus was administered as a 0.3 s pulse by inserting the tip of the glass
562 Pasteur pipette through an opening into the delivery tube (situated 4 cm from the tube outlet)
563 carrying a purified air stream (0.4 L/min). The tube outlet was placed approximately 1 cm from the
564 antenna. The experiments were conducted at 25–26 °C.
565 From each diluted odorant (100 ng/µL), 10 µL were pipetted on 1 cm diameter filter paper disk
566 placed in a glass Pasteur pipette in the screening experiment, while the doses ranging from 0.01 to
567 500 ng of neocembrene per filter paper were used in the dose-response experiments.
568 The signal was amplified and digitally converted using Syntech IDAC-4. The neuronal cells were
569 sorted based on their amplitude and the spikes were counted using the AutoSpike v3.9software
570 (Syntech Ockenfels, Germany). Δ spike was calculated by subtracting the number of spikes during
571 1 second post-stimulation from the number of spikes generated 1 second before the stimulation. In
572 dose response experiments and measurements on termite antennae, the counting periods were 0.5
573 s. Δ spike values were corrected by subtracting the response generated by the solvent and converted
574 into Δ spike/s (Benton & Dahanukar, 2023; Olsson & Hansson, 2013). The receptor lifetime
575 sparseness value was calculated according to Chang et al. (2023).
576 EAG experiment addressing the caste-specificity of antennal responses to neocembrene was
577 performed with 15 workers and 15 soldiers; each individual was only used for one stimulation
578 series consisting of air–hexane–neocembrene (10 ng)–hexane–air. Brain and antennal tip were

placed between two Ag/AgCl electrodes containing Ringer's solution and connected to a high impedance (10^{14} Ω) amplifier (Syntech, Buchenbach, Germany). The antennal preparation was placed into a stream of cleaned air (500 mL/min), into which the stimuli were injected from Pasteur pipettes containing a 1.5 cm^2 filter paper impregnated with 10 µL of the tested solution. Odor injections were controlled by a foot switch-operated Syntech stimulus controller and maximal negative deflection was measured using Syntech EagPro software. Pasteur pipettes containing odorant stimuli were changed after three stimulations. Air responses were used for data normalization, the responses log_2-transformed to reduce heteroscedasticity and comply with assumptions for parametric testing (Bartlett test for equal variances, and Shapiro-Wilk normality test), and then compared between workers and soldiers using Student's t-test.

Scanning electron microscopy

For SEM, 10 workers with intact antennae were cold-anesthetized and decapitated with micro-scissors. Heads were desiccated in increasing ethanol concentrations (60, 80, 90, and 96%, each for 2 h) followed by 12 h in acetone. Heads were then attached to aluminium holders for microscopy using adhesive tape, and differentially oriented to allow axial, dorsal, ventral, and lateral views. The samples were gold-coated for regular SEM (4 nm gold layer) and high-resolution SEM (HR-SEM, 2 nm) using sputter coater Bal-Tec SCD 050. Last antennal segments were inspected and photographed under scanning electron microscope JEOL 6380 LV (SEM). Surface of particular sensilla were studied using high resolution field emission scanning electron microscope JSM-IT800 (HR-SEM) and Olympus Soft Imaging Solution software. Working distance for all samples was 4.0–4.1 mm and accelerating voltage 2.0 kV.

Bioinformatics

For phylogenetic reconstruction of termite ORs, we used 182 OR protein sequences originating from five termite species, i.e. *Neotermes cubanus*, *Prorhinotermes simplex*, *Inquilinitermes inquilinus* (Johny et al., 2023), *Zootermopsis nevadensis* (Terrapon et al., 2014) and *Cryptotermes secundus* (Harrison et al., 2018), and the bristletail *Lepisma saccharina* (Thoma et al., 2019) as a basal insect outgroup. For all species also the ORCo sequence was included. Sequences were aligned by means of the MUSCLE algorithm and used for reconstructing the phylogenetic tree with

609 the IQ-TREE maximum likelihood algorithm (Nguyen et al., 2015) using the JTT+F+R8
610 substitution model and 10,000 ultrafast bootstrap replicates.
611 The gene structures of *PsimORs* were characterized by local alignment of full-length transcript
612 sequences from Johny et al. (2023) to our in-house genome assembly using BLAST (for details on
613 genome assembly see Koubová et al., 2021) and confirmed with genomic mapping of the RNAseq
614 data from *P. simplex* antennae available under accession SRX17749141 in NCBI SRA archives
615 using STAR aligner v2.7.10b (Dobin et al., 2013). The mapping results were further used for
616 abundance estimations of all ORs and ORCo in antennal transcriptome reported in Johny et al.
617 (2023). Read counts were obtained with featureCounts tool from the Subread package
618 (https://subread.sourceforge.net/) and normalized according to the FPKM (Fragments Per Kilobase
619 Million) method.
620 Differential OR expression analysis in *P. simplex* soldier and worker heads (including antennae)
621 was performed using the RNAseq data from our previous sequencing project and available as SRA
622 archives under accessions SRX18952230–32 and SRX18952237–39. The data was obtained from
623 sequencing of three biological replicates of each caste. Read counts obtained using STAR mapping
624 and featureCounts estimations were statistically evaluated using the DESeq2 Bioconductor
625 package in R and edgeR.
626 PsimOR14 secondary structure was predicted using online tools Jpred 4.0.0
627 (www.compbio.dundee.ac.uk/jpred) and TMHMM2.0
628 (https://services.healthtech.dtu.dk/services/TMHMM-2.0), schematic model was generated using
629 Protter (https://wlab.ethz.ch/protter).
630
631 **Protein modeling**
632 PsimOR14 structure was modelled in its monomeric membrane-free form using AlphaFold2
633 (Jumper et al., 2021; Mirdita et al., 2022). The best model was refined by MD relaxation,
634 employing GROMACS 2021.3 and CHARMM36m (Abraham et al., 2015; Huang et al., 2017).
635 After solvation and neutralization by Na^+ ions in TIP3P CHARMM water in a 1.5 nm padded box,
636 temperature and pressure equilibration followed. Six different simulations with differing starting
637 velocities were produced, followed by 150 ns periodic simulated annealing independently for each
638 replica (0.5 ns at 300 K, then 0.5 ns at 320 K, repeating). The lowest potential energy structure was
639 chosen. Neocembrene, geranylgeraniol and (+)-limonene structures were sourced from PubChem

(13th Feb 2023) and parametrized using CgenFF 4.6, employing CHARMM-GUI for the conversion (Jo et al., 2008; Kim et al., 2023; Vanommeslaeghe et al., 2010). The binding site was predicted based on DEET binding region of *Mh*OR5 from *Machilis hrabei* (7LIG) (del Mármol et al., 2021). Using DockThor webserver, ligands were docked with all bonds treated as rotatable, centered around the expected binding site with maximized box size (40 units). The best binder was then selected for each complex (Santos et al., 2020).

MM/PBSA simulations

Complex topologies were built in GROMACS. Simulations included 9 replicas for liganded (14 μs each) and 6 for unliganded PsimOR14 (6.9 μs), with different starting velocities. Convergence was assessed by ligand backbone RMSD distributions. Replicas were concatenated, split into 1.5 ns frames, and analyzed with MM/PBSA (ff19SB+GAFF2, linearized PB with diel=2, SASA for apolar contributions, optimized CHARMM radii) using gmx_MMPBSA v1.6.3 and AmberTools 20 (Case et al., 2023; Guedes et al., 2021; Tian et al., 2020; Wang et al., 2004). For each liganded PsimOR14 (neocembrene, geranylgeraniol and limonene) 9 replica trajectories were separately analyzed, along with apoform PsimOR14 trajectories (6 replicas). All trajectories were PBC-corrected, cleaned, and fitted to the first frame of the PsimOR14 trajectory.

Atom positions were marked in 3D space per frame, and the convex hull algorithm approximated the volume explored by each atom. This compared dynamic behavior between trajectories, with unliganded PsimOR14 as the baseline. The average total volume explored by atoms was compared.

CONFLICT OF INTERESTS

The authors declare no competing interests.

AUTHOR CONTRIBUTIONS

SD – SSR, fly transgenesis, SEM; KK – EAG; JŠ, JV – docking, molecular dynamics; JJ – RNA extraction, cloning and vector constructions, fly transgenesis; JK – insect culture, SEM; JN – SEM, HR-SEM; DSD – advising; PK – chemical analysis; AM – organic synthesis; OL – bioinformatics; RH, EGW, OL, SD – conception, supervision, statistics, writing. All authors contributed to the manuscript writing and approved its final version.

DATA AVAILABILITY

Nucleotide and protein sequences of termite ORs used for phylogenetic reconstruction and functional characterizations were published in Johny et al. (2023) and the raw sequencing data was previously deposited in NCBI SRA archive as PRJNA885453 bioproject. Transcript abundances of *P. simplex* ORs were also inferred from the antennal transcriptome data, available at NCBI under SRX17749141. Sequences of PsimOR14 studied in detail in the present paper are listed in the Supplementary Table S12 and deposited at NCBI as OR921181 entry. Origin of the *P. simplex* draft genome assembly is reported in Koubová et al. (2021). Differential expression of *P. simplex* ORs in workers and soldiers was studied using caste-specific head transcriptomes available at NCBI as SRA archives under accessions SRX18952230-32 and SRX18952237-39.

ACKNOWLEDGMENTS

This study was supported by Czech Science Foundation (No. 20-17194S) and Institute of Organic Chemistry and Biochemistry, CAS (RVO: 61388963). We thank M. Hyliš and the Viničná Microscopy Core Facility (VMCF of the Faculty of Science, Charles University) supported by the MEYS CR (LM2023050 Czech-BioImaging) for their support and assistance with microscopy techniques. We also thank Martina Hajdušková (www.biographix.cz) for insect drawings used in Fig. 1A.

REFERENCES

Abraham, M. J., Murtola, T., Schulz, R., Páll, S., Smith, J. C., Hess, B. & Lindahl, E. (2015). GROMACS: High performance molecular simulations through multi-level parallelism from laptops to supercomputers. *SoftwareX* **1–2**, 19–25.

Andersson, M. N., Löfstedt, C. & Newcomb, R. D. (2015) Insect olfaction and the evolution of receptor tuning. *Front Ecol Evol* **3**, 53.

Bagnères, A. G. & Hanus, R. (2015) Communication and social regulation in termites. *In* Social recognition in invertebrates (L. Aquiloni and E. Tricarico, eds.), pp. 193-248. Springer International Publishing.

Benton, R. (2015) Multigene family evolution: Perspectives from insect chemoreceptors. *Trends Ecol Evol* **30**, 590-600.

Benton, R. & Dahanukar, A. (2023) Chemosensory coding in *Drosophila* single sensilla. *Cold Spring Harb Protoc* **2023**, pdb.top107803.

Benton, R., Sachse, S., Michnick, S. W. & Vosshall, L. B. (2006) Atypical membrane topology and heteromeric function of *Drosophila* odorant receptors in vivo. *PLoS Biol* **4**, e20.

Benton, R., Vannice, K. S., Gomez-Diaz, C. & Vosshall, L. B. (2009) Variant ionotropic glutamate receptors as chemosensory receptors in *Drosophila*. *Cell* **136**, 149-162.

Bohbot, J., Pitts, R. J., Kwon, H. W., Rützler, M., Robertson, H. M. & Zwiebel, L. J. (2007). Molecular characterization of the Aedes aegypti odorant receptor gene family. *Insect Mol Biol* 16, 525-537.

Bordereau, C. & Pasteels, J. M. (2011) Pheromones and chemical ecology of dispersal and foraging in termites. *In* Biology of termites: A modern synthesis (D. E. Bignell, Y. Roisin and N. Lo, eds.), pp. 279-320. Springer.

Brand, P., Robertson, H. M., Lin, W., Pothula, R., Klingeman, W. E., Jurat-Fuentes, J. L. & Johnson, B. R. (2018) The origin of the odorant receptor gene family in insects. *Elife* **7**, e38340.

Butterwick, J. A., Del Marmol, J., Kim, K. H., Kahlson, M. A., Rogow, J. A., Walz, T. & Ruta, V. (2018) Cryo-EM structure of the insect olfactory receptor Orco. *Nature* **560**, 447-452.

Caminer, M. A., Libbrecht, R., Majoe, M., Ho, D. V., Baumann, P. & Foitzik, S. (2023) Task-specific odorant receptor expression in worker antennae indicates that sensory filters regulate division of labor in ants. *Commun Biol* **6**, 1004.

Carey, A. F., Wang, G., Su, C.-Y., Zwiebel, L. J. & Carlson, J. R. (2010) Odorant reception in the malaria mosquito *Anopheles gambiae*. *Nature* **464**, 66-71.

Case, D. A., Aktulga, H. M., Belfon, K., Cerutti, D. S., Cisneros, G. A., Cruzeiro, V. W. D., Forouzesh, N., Giese, T. J., Götz, A. W., et al. (2023). AmberTools. *J Chem Inf Model* **63**, 6183–6191.

Castillo, P., Le, N. & Sun, Q. (2021) Comparative antennal morphometry and sensilla organization in the reproductive and non-reproductive castes of the Formosan subterranean termite. *Insects* **12**, 576.

Chahda, J. S., Soni, N., Sun, J. S., Ebrahim, S. A. M., Weiss, B. L. & Carlson, J. R. (2019) The molecular and cellular basis of olfactory response to tsetse fly attractants. *PLoS Genet* **15**, e1008005.

Chang, H., Unni, A. P., Tom, M. T., Cao, Q., Liu, Y., Wang, G., Llorca, L. C., Brase, S., Bucks, S., et al. (2023) Odorant detection in a locust exhibits unusually low redundancy. *Curr Biology* **33**, 5427-5438.e5.

Clyne, P. J., Warr, C. G., Freeman, M. R., Lessing, D., Kim, J. & Carlson, J. R. (1999) A novel family of divergent seven-transmembrane proteins: candidate odorant receptors in *Drosophila*. *Neuron* **22**, 327-338.

del Mármol, J., Yedlin, M. A. & Ruta, V. (2021) The structural basis of odorant recognition in insect olfactory receptors. *Nature* **597**, 126-131.

Díaz-Morales, M., Khallaf, M. A., Stieber, R., Alali, I., Hansson, B. S. & Knaden, M. (2024) The ortholog receptor Or67d in *Drosophila bipectinata* is able to detect two different pheromones. *J Chem Ecol* **50**, 610–619.

Dobin, A., Davis, C. A., Schlesinger, F., Drenkow, J., Zaleski, C., Jha, S., Batut, P., Chaisson, M. & Gingeras, T. R. (2013) STAR: ultrafast universal RNA-seq aligner. *Bioinformatics* **29**, 15-21.

Dolejšová, K., Krasulová, J., Kutalová, K. & Hanus, R. (2014) Chemical alarm in the termite *Termitogeton planus* (Rhinotermitidae). *J Chem Ecol* **40**, 1269-1276.

Dolejšová, K., Křivánek, J., Štáfková, J., Horáček, N., Havlíčková, J., Roy, V., Kalinová, B., Roy, A., Kyjaková, P. & Hanus, R. (2022) Identification of a queen primer pheromone in higher termites. *Commun Biol* **5**, 1165.

Engsontia, P., Sangket, U., Robertson, H. M. & Satasook, C. (2015) Diversification of the ant odorant receptor gene family and positive selection on candidate cuticular hydrocarbon receptors. *BMC Res Notes* **8**, 380.

Fleischer, J. & Krieger, J. (2018) Insect pheromone receptors – Key elements in sensing intraspecific chemical signals. *Frontiers Cell Neurosci* **12**, 425.

Gao, Y., Huang, Q. & Xu, H. (2020) Silencing Orco impaired the ability to perceive trail pheromones and affected locomotion behavior in two termite species. *J Econ Entomol* **113**, 2941-2949.

Gomez Ramirez, W. C., Thomas, N. K. T., Muktar, I. J. & Riabinina, O. (2023) The neuroecology of olfaction in bees. *Curr Opin Insect Sci* **56**, 101018.

Gonzalez, F., Witzgall, P. & Walker, W. B. (2016) Protocol for heterologous expression of insect odourant receptors in *Drosophila*. *Front Ecol Evol* **4**, 24.

Gössinger, E. (2019) Chemistry of the secondary metabolites of termites. *In* Progress in the Chemistry of organic natural products 109 (A. D. Kinghorn, H. Falk, S. Gibbons, J. i. Kobayashi, Y. Asakawa and J.-K. Liu, eds.), pp. 1-384. Springer International Publishing.

Guedes, I. A., Barreto, A. M. S., Marinho, D., Krempser, E., Kuenemann, M. A., Sperandio, O., Dardenne, L. E., & Miteva, M. A. (2021). New machine learning and physics-based scoring functions for drug discovery. *Sci Rep* **11**, 3198.

Guo, X., Yu, Q., Chen, D., Wei, J., Yang, P., Yu, J., Wang, X. & Kang, L. (2020) 4-Vinylanisole is an aggregation pheromone in locusts. *Nature* **584**, 584-588.

Hanus, R., Šobotník, J., Valterová, I. & Lukáš, J. (2006) The ontogeny of soldiers in *Prorhinotermes simplex* (Isoptera, Rhinotermitidae). *Insectes Soc* **53**, 249-257.

Hanus, R., Luxová, A., Šobotník, J., Kalinová, B., Jiroš, P., Křeček, J., Bourguignon, T. & Bordereau, C. (2009) Sexual communication in the termite *Prorhinotermes simplex* (Isoptera, Rhinotermitidae) mediated by a pheromone from female tergal glands. *Insectes Soc* **56**, 111-118.

Harrison, M. C., Jongepier, E., Robertson, H. M., Arning, N., Bitard-Feildel, T., Chao, H., Childers, C. P., Dinh, H., Doddapaneni, H., et al. (2018) Hemimetabolous genomes reveal molecular basis of termite eusociality. *Nat Ecol Evol* **2**, 557-566.

Haverkamp, A., Hansson, B. S. & Knaden, M. (2018) Combinatorial codes and labeled lines: How insects use olfactory cues to find and judge food, mates, and oviposition sites in complex environments. *Front Physiol* **9**, 49.

Huang, J., Rauscher, S., Nawrocki, G., Ran, T., Feig, M., de Groot, B. L., Grubmüller, H., & MacKerell, A. D., Jr. (2017). CHARMM36m: an improved force field for folded and intrinsically disordered proteins. *Nat Methods* **14**, 71–73.

Jirošová, A., Jančařík, A., Menezes, R. C., Bazalová, O., Dolejšová, K., Vogel, H., Jedlička, P., Buček, A., Brabcová, J., et al. (2017) Co-option of the sphingolipid metabolism for the production of nitroalkene defensive chemicals in termite soldiers. *Insect Biochem Mol Biol* **82**, 52-61.

Jo, S., Kim, T., Iyer, V. G., & Im, W. (2008). CHARMM-GUI: a web-based graphical user interface for CHARMM. *J Comput Chem* **29**, 1859–1865.

Johny, J., Diallo, S., Lukšan, O., Shewale, M., Kalinová, B., Hanus, R. & Große-Wilde, E. (2023) Conserved orthology in termite chemosensory gene families. *Front Ecol Evol* **10**, 1065947.

Jongepier, E., Séguret, A., Labutin, A., Feldmeyer, B., Gstöttl, C., Foitzik, S., Heinze, J. & Bornberg-Bauer, E. (2022) Convergent loss of chemoreceptors across independent origins of slave-making in ants. *Mol Biol Evol* **39**, msab305.

Jumper, J., Evans, R., Pritzel, A., Green, T., Figurnov, M., Ronneberger, O., Tunyasuvunakool, K., Bates, R., Žídek, A., et al. (2021). Highly accurate protein structure prediction with AlphaFold. *Nature* **596**, 583 – 589.

Kaib, M. (1990) Multiple functions of exocrine secretions in termite communication: exemplified by *Schedorhinotermes lamanianus*. *In* Social insects and the environment (G. K. Veeresh, B. Mallik and C. A. Viraktamath, eds.), pp. 37-38. E. J. Brill.

Keesey, I. W., Zhang, J., Depetris-Chauvin, A., Obiero, G. F., Gupta, A., Gupta, N., Vogel, H., Knaden, M. & Hansson, B. S. (2022) Functional olfactory evolution in *Drosophila suzukii* and the subgenus *Sophophora*. *iScience* **25**, 104212.

Kim, S., Chen, J., Cheng, T., Gindulyte, A., He, J., He, S., Li, Q., Shoemaker, B. A., Thiessen, P. A., et al. (2023). PubChem 2023 update. *Nucleic Acids Res* 51, D1373–D1380.

Koubová, J., Pangrácová, M., Jankásek, M., Lukšan, O., Jehlík, T., Brabcová, J., Jedlička, P., Křivánek, J., Čapková Frydrychová, R. & Hanus, R. (2021) Long-lived termite kings and queens activate telomerase in somatic organs. *Proc Roy Soc B: Biol Sci* **288**, 20210511.

Larsson, M. C., Domingos, A. I., Jones, W. D., Chiappe, M. E., Amrein, H. & Vosshall, L. B. (2004) Or83b encodes a broadly expressed odorant receptor essential for *Drosophila* olfaction. *Neuron* **43**, 703-714.

Legan, A. W., Jernigan, C. M., Miller, S. E., Fuchs, M. F. & Sheehan, M. J. (2021) Expansion and accelerated evolution of 9-exon odorant receptors in polistes paper wasps. *Mol Biol Evol* **38**, 3832-3846.

Leonhardt, Sara D., Menzel, F., Nehring, V. & Schmitt, T. (2016) Ecology and evolution of communication in social insects. *Cell* **164**, 1277-1287.

Mariette, J., Carcaud, J., Louis, T., Lacassagne, E., Servais, I., Montagné, N., Chertemps, T., Jacquin-Joly, E., Meslin, C., et al. (2024). Evolution of queen pheromone receptor tuning in four honeybee species (Hymenoptera, Apidae, Apis). *iScience* **27**, 111243.

McKenzie, S. K., Fetter-Pruneda, I., Ruta, V. & Kronauer, D. J. C. (2016) Transcriptomics and neuroanatomy of the clonal raider ant implicate an expanded clade of odorant receptors in chemical communication. *Proc Natl Acad Sci USA* **113**, 14091-14096.

McKenzie, S. K. & Kronauer, D. J. C. (2018). The genomic architecture and molecular evolution of ant odorant receptors. *Genome Res* 28, 1757-1765.

Matsuura, K., Himuro, C., Yokoi, T., Yamamoto Y., Vargo E. L. & Keller L. (2010) Identification of a pheromone regulating caste differentiation in termites. *Proc Natl Acad Sci USA* **107**, 12963-12968.

Mirdita, M., Schütze, K., Moriwaki, Y., Heo, L., Ovchinnikov, S., & Steinegger, M. (2022). ColabFold: making protein folding accessible to all. *Nat Methods* **19**, 679–682.

Mitaka, Y. & Akino, T. (2021) A review of termite pheromones: Multifaceted, context-dependent, and rational chemical communications. *Front Ecol Evol* **8**, 595614.

Mitaka, Y., Kobayashi, K., Mikheyev, A., Tin, M. M. Y., Watanabe, Y. & Matsuura, K. (2016) Caste-specific and sex-specific expression of chemoreceptor genes in a termite. *PLoS One* **11**, e0146125.

826 Nei, M. & Rooney, A. P. (2005) Concerted and birth-and-death evolution of multigene families. *Annu Rev*
827 *Genet* **39**, 121-152.
828 Nguyen, L. T., Schmidt, H. A., von Haeseler, A. & Minh, B. Q. (2015) IQ-TREE: a fast and effective
829 stochastic algorithm for estimating maximum-likelihood phylogenies. *Mol Biol Evol* **32**, 268-274.
830 Obiero, G. F., Pauli, T., Geuverink, E., Veenendaal, R., Niehuis, O. & Große-Wilde, E. (2021)
831 Chemoreceptor diversity in apoid wasps and its reduction during the evolution of the pollen-
832 collecting lifestyle of bees (Hymenoptera: Apoidea). *Genome Biol Evol* **13**, evaa269.
833 Olsson, S. B. & Hansson, B. S. (2013) Electroantennogram and single sensillum recording in insect
834 antennae. *In* Pheromone Signaling: Methods and Protocols (K. Touhara, ed.), pp. 157-177. Humana
835 Press.
836 Pask, G. M., Slone, J. D., Millar, J. G., Das, P., Moreira, J. A., Zhou, X. F., Bello, J., Berger, S. L., Bonasio,
837 R., et al. (2017) Specialized odorant receptors in social insects that detect cuticular hydrocarbon
838 cues and candidate pheromones. *Nat Commun* **8**, 297.
839 Pettersson, J. H. & Cattaneo, A. M. (2023) Heterologous investigation of metabotropic and ionotropic
840 odorant receptors in ab3A neurons of *Drosophila melanogaster*. *Front Mol Biosci* **10**, 1275901.
841 Piskorski, R., Hanus, R., Vašíčková, S., Cvačka, J., Šobotník, J., Svatoš, A. & Valterová, I. (2007)
842 Nitroalkenes and sesquiterpene hydrocarbons from the frontal gland of three *Prorhinotermes*
843 termite species. *J Chem Ecol* **33**, 1787-1794.
844 Robertson, H. M. (2019) Molecular evolution of the major arthropod chemoreceptor gene families. *Annu*
845 *Rev Entomol* **64**, 227-242.
846 Robertson, H. M. & Wanner, K. W. (2006). The chemoreceptor superfamily in the honey bee, Apis
847 mellifera: Expansion of the odorant, but not gustatory, receptor family. *Genome Res* 16, 1395-1403.
848 Robertson, H. M., Baits, R. L., Walden, K. K. O., Wada-Katsumata, A. & Schal, C. (2018) Enormous
849 expansion of the chemosensory gene repertoire in the omnivorous German cockroach *Blattella*
850 *germanica*. *J Exp Zool B Mol Dev Evol* **330**, 265-278.
851 Roisin, Y., Everaerts, C., Pasteels, J. M. & Bonnard, O. (1990) Caste-dependent reactions to soldier
852 defensive secretion and chiral alarm/recruitment pheromone in *Nasutitermes princeps*. *J Chem Ecol*
853 **16**, 2865-2875.
854 Rupf, T. & Roisin, Y. (2008) Coming out of the woods: do termites need a specialized worker caste to
855 search for new food sources? *Naturwissenschaften* **95**, 811-819.
856 Santos, K. B., Guedes, I. A., Karl, A. L. M., & Dardenne, L. E. (2020). Highly flexible ligand docking:
857 Benchmarking of the DockThor program on the LEADS-PEP protein–peptide data set. *J Chem Inf*
858 *Model* **60**, 667–683.
859 Sato, K., Pellegrino, M., Nakagawa, T., Nakagawa, T., Vosshall, L. B. & Touhara, K. (2008) Insect olfactory
860 receptors are heteromeric ligand-gated ion channels. *Nature* **452**, 1002-1006.
861 Sillam-Dussès, D. (2010) Trail pheromones and sex pheromones in termites. Nova Novinka, Nova Science
862 Publishers, 79 pp.
863 Sillam-Dussès, D., Kalinová, B., Jiroš, P., Březinová, A., Cvačka, J., Hanus, R., Šobotník, J., Bordereau, C.
864 & Valterová, I. (2009) Identification by GC-EAD of the two-component trail-following pheromone
865 of *Prorhinotermes simplex* (Isoptera, Rhinotermitidae, Prorhinotermitinae). *J Insect Physiol* **55**,
866 751-757.
867 Slone, J. D., Pask, G. M., Ferguson, S. T., Millar, J. G., Berger, S. L., Reinberg, D., Liebig, J., Ray, A. &
868 Zwiebel, L. J. (2017) Functional characterization of odorant receptors in the ponerine ant,
869 *Harpegnathos saltator*. *Proc Natl Acad Sci USA* **114**, 8586-8591.
870 Šobotník, J., Hanus, R., Kalinová, B., Piskorski, R., Cvačka, J., Bourguignon, T. & Roisin, Y. (2008) (*E*,*E*)-
871 alpha-farnesene, an alarm pheromone of the termite *Prorhinotermes canalifrons*. *J Chem Ecol* **34**,
872 478-86.
873 Šobotník, J., Jirošová, A. & Hanus, R. (2010) Chemical warfare in termites. *J Insect Physiol* **56**, 1012-21.
874 Steiger, S., Schmitt, T. & Schaefer, H. M. (2010) The origin and dynamic evolution of chemical information
875 transfer. *Proc Roy Soc B: Biol Sci* **278**, 970-979.

Su, C.-Y., Menuz, K., Reisert, J. & Carlson, J. R. (2012) Non-synaptic inhibition between grouped neurons in an olfactory circuit. *Nature* **492**, 66–71.

Tateishi, K., Nishimura, Y., Sakuma, M., Yokohari, F. & Watanabe, H. (2020) Sensory neurons that respond to sex and aggregation pheromones in the nymphal cockroach. *Sci Rep* **10**, 1995.

Terrapon, N., Li, C., Robertson, H. M., Ji, L., Meng, X., Booth, W., Chen, Z., Childers, C. P., Glastad, K. M., et al. (2014) Molecular traces of alternative social organization in a termite genome. *Nat Commun* **5**, 3636.

Thoma, M., Missbach, C., Jordan, M. D., Grosse-Wilde, E., Newcomb, R. D. & Hansson, B. S. (2019) Transcriptome surveys in silverfish suggest a multistep origin of the insect odorant receptor gene family. *Front Ecol Evol* **7**, 281.

Tian, C., Kasavajhala, K., Belfon, K. A. A., Raguette, L., Huang, H., Migues, A. N., Bickel, J., Wang, Y., Pincay, J., et al. (2020). ff19SB: Amino-acid-specific protein backbone parameters trained against quantum mechanics energy surfaces in solution. *J Chem Theory Comput* **16**, 528–552.

Traniello, J. F. A. (1981) Enemy deterrence in the recruitment strategy of a termite: soldier-organized foraging in *Nasutitermes costalis*. *Proc Natl Acad Sci USA* **78**, 1976-1979.

Traniello, J. F. A. & Busher, C. (1985) Chemical regulation of polyethism during foraging in the Neotropical termite *Nasutitermes costalis*. *J Chem Ecol* **11**, 319-332.

Tuma, J., Eggleton, P. & Fayle T. M. (2020) Ant-termite interactions: an important but under-explored ecological linkage. *Biol Rev* **95**, 555-572.

Vanommeslaeghe, K., Hatcher, E., Acharya, C., Kundu, S., Zhong, S., Shim, J., Darian, E., Guvench, O., Lopes, P., et al. (2010). CHARMM general force field: A force field for drug-like molecules compatible with the CHARMM all-atom additive biological force fields. *J Comput Chem* **31**, 671–690.

Wang, J., Wolf, R. M., Caldwell, J. W., Kollman, P. A. & Case, D. A. (2004). Development and testing of a general amber force field. *J Comput Chem* **25**, 1157–1174.

Wang, Y., Qiu, L., Wang, B., Guan, Z., Dong, Z., Zhang, J., Cao, S., Yang, L., Wang, B., et al. (2024) Structural basis for odorant recognition of the insect odorant receptor OR-Orco heterocomplex. *Science* **384**, 1453-1460.

Wanner, K. W., Nichols, A. S., Walden, K. K., Brockmann, A., Luetje, C. W. & Robertson, H. M. (2007) A honey bee odorant receptor for the queen substance 9-oxo-2-decenoic acid. *Proc Natl Acad Sci USA* **104**, 14383-14388.

Wicher, D., Schafer, R., Bauernfeind, R., Stensmyr, M. C., Heller, R., Heinemann, S. H. & Hansson, B. S. (2008) *Drosophila* odorant receptors are both ligand-gated and cyclic-nucleotide-activated cation channels. *Nature* **452**, 1007-1011.

Yan, H., Jafari, S., Pask, G., Zhou, X., Reinberg, D. & Desplan, C. (2020) Evolution, developmental expression and function of odorant receptors in insects. *J Exp Biol* **223**, jeb208215.

Yuvaraj, J. K., Roberts, R. E., Sonntag, Y., Hou, X.-Q., Grosse-Wilde, E., Machara, A., Zhang, D.-D., Hansson, B. S., Johanson, U., et al. (2021) Putative ligand binding sites of two functionally characterized bark beetle odorant receptors. *BMC Biology* **19**, 16.

Zhang, D.-D. & Löfstedt, C. (2015) Moth pheromone receptors: gene sequences, function, and evolution. *Front Ecol Evol* **3**, 105.

Zhang, R., Wang, B., Grossi, G., Falabella, P., Liu, Y., Yan, S., Lu, J., Xi, J. & Wang, G. (2017) Molecular basis of alarm pheromone detection in aphids. *Curr Biol* **27**, 55-61.

Zhang, R.-B., Liu, Y., Yan, S.-C. & Wang, G.-R. (2019a) Identification and functional characterization of an odorant receptor in pea aphid, *Acyrthosiphon pisum*. *Insect Sci* **26**, 58-67.

Zhang, Y., Tsang, T. K., Bushong, E. A., Chu, L.-A., Chiang, A.-S., Ellisman, M. H., Reingruber, J. & Su, C.-Y. (2019b). Asymmetric ephaptic inhibition between compartmentalized olfactory receptor neurons. *Nat Commun* **10**, 1560.

Zhao, J., Chen, A. Q., Ryu, J. & del Mármol, J. (2024) Structural basis of odor sensing by insect heteromeric odorant receptors. *Science* **384**, 1460-1467.

926 Zhou, X., Rokas, A., Berger, S. L., Liebig, J., Ray, A. & Zwiebel, L. J. (2015) Chemoreceptor evolution in
927 Hymenoptera and its implications for the evolution of eusociality. *Genome Biol Evol* **7**, 2407-2416.

928 **Tables**

929 Table 1. Docking scores and energy values inferred from the docking experiment and from
930 MM/PBSA simulations for binding interactions of neocembrene, geranylgeraniol and (+)-limonene
931 with PsimOR14.
932

ligand	docking experiment			MM/PBSA E (kcal/mol) ± SD			
	docking score	VDWAALS	electrostatic (kcal/mol)	ΔTOTAL	ΔVDWAALS	ΔEEL	ΔGSOLV
neocembrene	-8.658	-19.777	-0.223	-28.72 ± 1.46	-26.92 ± 1.24	-0.29 ± 0.56	-1.51 ± 0.10
geranylgeraniol	-8.331	-18.786	-11.137	-36.98 ± 1.22	-35.47 ± 0.96	-0.77 ± 0.56	-0.73 ± 0.27
(+)-limonene	-7.638	-16.134	-0.561	-20.02 ± 2.63	-20.57 ± 2.30	-0.35 ± 0.47	0.89 ± 2.21

933

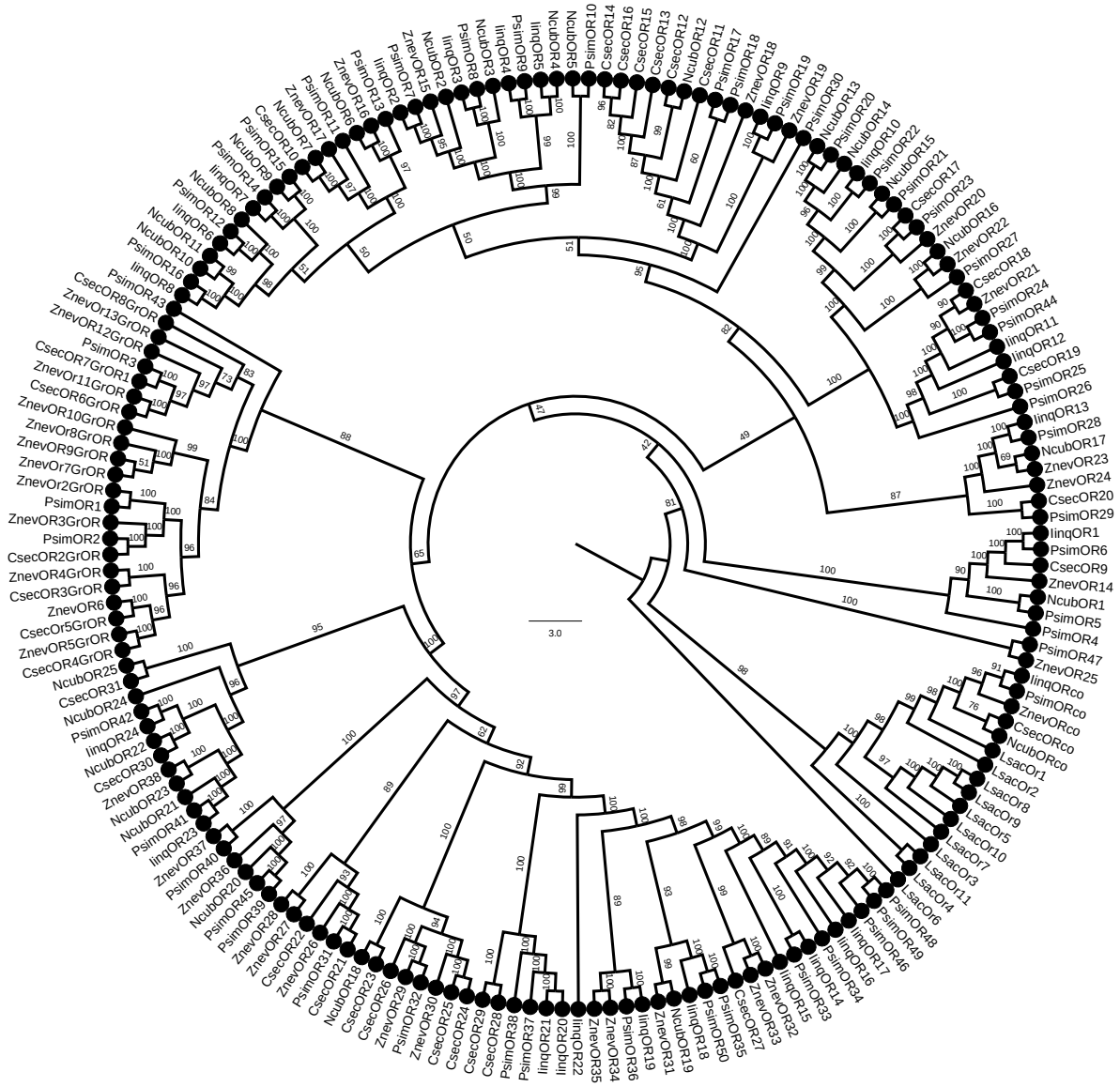

Fig. S1. Full version of the phylogenetic tree of termite ORs shown in Fig. 1 of the main text. Protein sequences of termite ORs can be found under the same labeling in Johny et al. (2023). *Lepisma saccharina* sequences used as basal insect outgroup are listed in Thoma et al. (2019). The topology and branching supports were inferred using the IQ-TREE maximum likelihood algorithm with the JTT+F+R8 model and supported by 10,000 iterations of ultrafast bootstrap approximation.

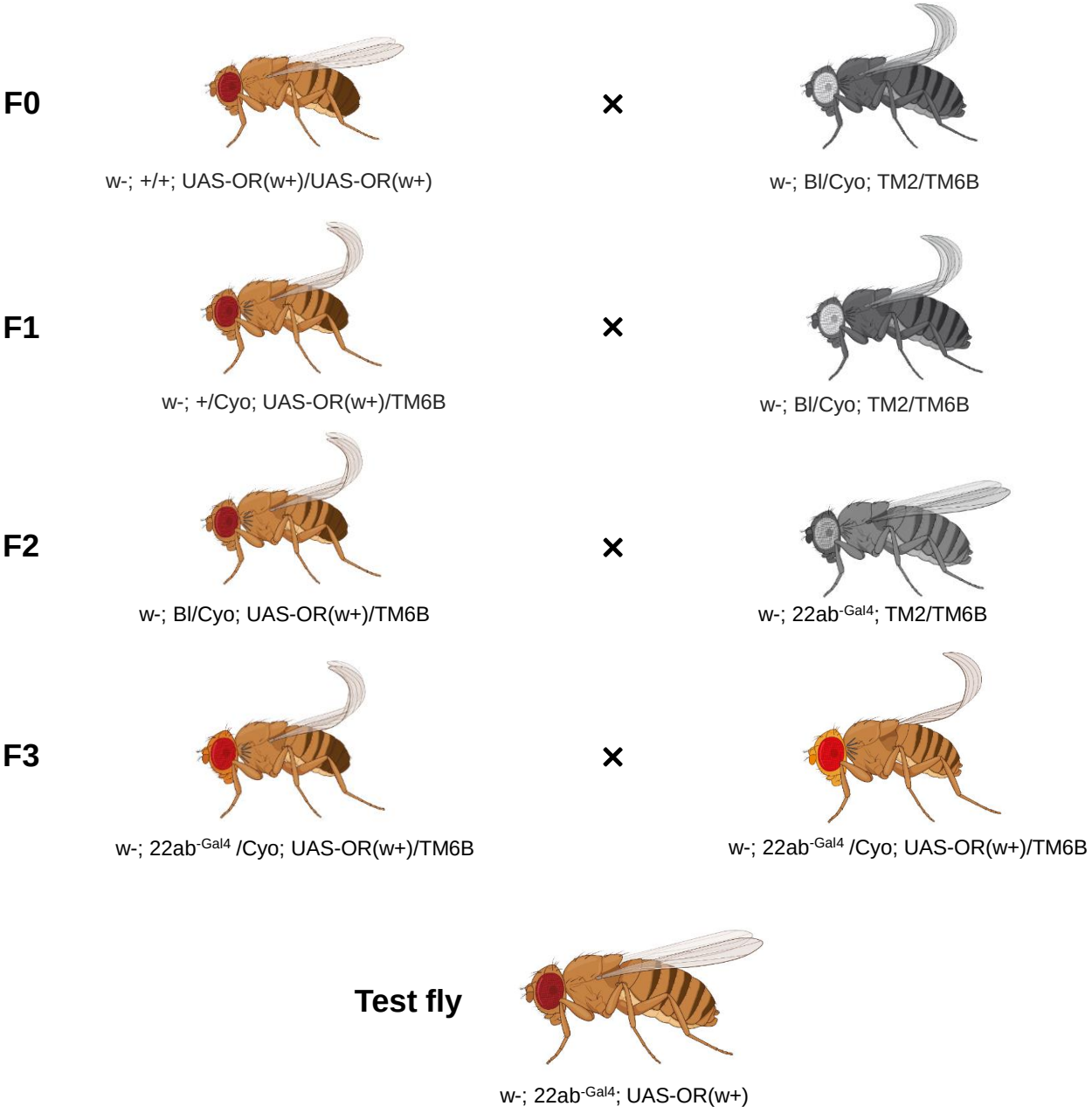

Fig. S2. Crossing scheme of termite ORs heterologous expression using *Drosophila melanogaster* empty neurons in ab3 sensilla.

Table S1. SSR responses to Panel 1 for PsimOR9. Related to Fig. 2.

Replicate	Compound	Pre-stimulation spikes	Post-stimulation spikes	Generated spikes	Δ Spikes/s
1	hexane	8	5	-3	
1	(3*Z*,6*Z*)-dodecadien-1-ol	6	9	3	6
1	(3*Z*)-dodecen-1-ol	11	10	-1	2
1	(3*Z*,6*Z*,8*E*)-dodecatrien-1-ol	5	12	7	10
1	*n*-eicosane	4	9	5	8
1	1-octadecanol	10	5	-5	-2
1	*n*-docosane	10	11	1	4
1	dodec-3-yn-1-ol	1	8	7	10
1	neocembrene	9	11	2	5
1	*δ*-cadinene	3	0	-3	0
1	(3*R*,6*E*)-nerolidol	0	0	0	3
2	hexane	6	3	-3	
2	(3*Z*,6*Z*)-dodecadien-1-ol	9	7	-2	1
2	(3*Z*)-dodecen-1-ol	10	8	-2	1
2	(3*Z*,6*Z*,8*E*)-dodecatrien-1-ol	4	13	9	12
2	*n*-eicosane	12	2	-10	-7
2	1-octadecanol	8	6	-2	1
2	*n*-docosane	11	12	1	4
2	dodec-3-yn-1-ol	9	10	1	4
2	neocembrene	8	13	5	8
2	*δ*-cadinene	12	15	3	6
2	(3*R*,6*E*)-nerolidol	8	14	6	9
2	geranylgeraniol	12	10	-2	1
3	hexane	6	5	-1	
3	(3*Z*,6*Z*)-dodecadien-1-ol	10	17	7	8
3	(3*Z*)-dodecen-1-ol	9	14	5	6
3	(3*Z*,6*Z*,8*E*)-dodecatrien-1-ol	6	19	13	14
3	*n*-eicosane	4	15	11	12
3	1-octadecanol	13	11	-2	-1
3	*n*-docosane	7	12	5	6
3	dodec-3-yn-1-ol	8	11	3	4
3	neocembrene	11	18	7	8
3	*δ*-cadinene	10	18	8	9
3	(3*R*,6*E*)-nerolidol	14	11	-3	-2
3	geranylgeraniol	7	12	5	6
4	hexane	11	10	-1	
4	(3*Z*,6*Z*)-dodecadien-1-ol	12	17	5	6
4	(3*Z*)-dodecen-1-ol	4	15	11	12
4	(3*Z*,6*Z*,8*E*)-dodecatrien-1-ol	3	8	5	6
4	*n*-eicosane	3	3	0	1
4	1-octadecanol	2	2	0	1
4	*n*-docosane	5	10	5	6
4	dodec-3-yn-1-ol	4	12	8	9
4	neocembrene	2	9	7	8
4	*δ*-cadinene	6	5	-1	0
4	(3*R*,6*E*)-nerolidol	1	4	3	4
4	geranylgeraniol	3	5	2	3
5	hexane	10	8	-2	
5	(3*Z*,6*Z*)-dodecadien-1-ol	7	8	1	3
5	(3*Z*)-dodecen-1-ol	9	9	0	2
5	(3*Z*,6*Z*,8*E*)-dodecatrien-1-ol	5	15	10	12
5	*n*-eicosane	6	12	6	8
5	1-octadecanol	9	16	7	9
5	*n*-docosane	8	10	2	4
5	dodec-3-yn-1-ol	6	9	3	5
5	neocembrene	1	5	4	6
5	*δ*-cadinene	5	0	-5	-3
5	(3*R*,6*E*)-nerolidol	4	2	-2	0
5	geranylgeraniol	3	1	-2	0

Table S2. SSR responses to Panel 1 for PsimOR14. Related to Fig. 2.

Replicate	Compound	Pre-stimulation spikes	Post-stimulation spikes	Generated spikes	Δ Spikes/s
1	hexane	7	3	-4	
1	1-octadecanol	10	6	-4	0
1	(3*Z*,6*Z*)-dodecadien-1-ol	6	7	1	5
1	(3*Z*)-dodecen-1-ol	16	8	-8	-4
1	dodec-3-yn-1-ol	8	18	10	14
1	(3*Z*,6*Z*,8*E*)-dodecatrien-1-ol	13	12	-1	3
1	(3*R*,6*E*)-nerolidol	15	8	-7	-3
1	geranylgeraniol	4	22	18	22
1	*n*-docosane	13	10	-3	1
1	*n*-eicosane	10	8	-2	2
1	neocembrene	14	62	48	52
1	*δ*-cadinene	13	22	9	13
2	hexane	8	9	1	
2	1-octadecanol	5	3	-2	-3
2	(3*Z*,6*Z*)-dodecadien-1-ol	7	3	-4	-5
2	(3*Z*)-dodecen-1-ol	13	3	-10	-11
2	dodec-3-yn-1-ol	9	3	-6	-7
2	(3*Z*,6*Z*,8*E*)-dodecatrien-1-ol	13	3	-10	-11
2	(3*R*,6*E*)-nerolidol	6	5	-1	-2
2	geranylgeraniol	4	38	34	33
2	*n*-docosane	8	2	-6	-7
2	*n*-eicosane	7	2	-5	-6
2	neocembrene	4	55	51	50
2	*δ*-cadinene	4	5	1	0
3	hexane	17	15	-2	
3	1-octadecanol	11	6	-5	-3
3	(3*Z*,6*Z*)-dodecadien-1-ol	10	13	3	5
3	(3*Z*)-dodecen-1-ol	17	7	-10	-8
3	dodec-3-yn-1-ol	10	7	-3	-1
3	(3*Z*,6*Z*,8*E*)-dodecatrien-1-ol	18	5	-13	-11
3	(3*R*,6*E*)-nerolidol	17	14	-3	-1
3	geranylgeraniol	15	41	26	28
3	*n*-docosane	20	12	-8	-6
3	*n*-eicosane	13	4	-9	-7
3	neocembrene	18	90	72	74
3	*δ*-cadinene	12	6	-6	-4
4	hexane	6	7	1	
4	1-octadecanol	15	3	-12	-13
4	(3*Z*,6*Z*)-dodecadien-1-ol	7	7	0	-1
4	(3*Z*)-dodecen-1-ol	14	5	-9	-10
4	dodec-3-yn-1-ol	16	9	-7	-8
4	(3*Z*,6*Z*,8*E*)-dodecatrien-1-ol	12	6	-6	-7
4	(3*R*,6*E*)-nerolidol	12	6	-6	-7
4	geranylgeraniol	2	28	26	25
4	*n*-docosane	16	4	-12	-13
4	*n*-eicosane	7	1	-6	-7
4	neocembrene	12	57	45	44
4	*δ*-cadinene	5	7	2	1
5	hexane	8	6	-2	
5	1-octadecanol	8	3	-5	-3
5	(3*Z*,6*Z*)-dodecadien-1-ol	6	3	-3	-1
5	(3*Z*)-dodecen-1-ol	2	5	3	5
5	dodec-3-yn-1-ol	2	6	4	6
5	(3*Z*,6*Z*,8*E*)-dodecatrien-1-ol	8	4	-4	-2
5	(3*R*,6*E*)-nerolidol	10	8	-2	0
5	geranylgeraniol	6	20	14	16
5	*n*-docosane	6	7	1	3
5	*n*-eicosane	6	4	-2	0
5	neocembrene	5	49	44	46
5	*δ*-cadinene	10	7	-3	-1

Table S3. SSR responses to Panel 1 for PsimOR30. Related to Fig. 2.

Replicate	Compound	Pre-stimulation spikes	Post-stimulation spikes	Generated spikes	Δ Spikes/s
1	hexane	1	0	-1	
1	(3*Z*,6*Z*)-dodecadien-1-ol	1	5	4	5
1	(3*Z*)-dodecen-1-ol	7	3	-4	-3
1	(3*Z*,6*Z*,8*E*)-dodecatrien-1-ol	4	6	2	3
1	*n*-eicosane	4	8	4	5
1	1-octadecanol	5	6	1	2
1	*n*-docosane	5	6	1	2
1	dodec-3-yn-1-ol	4	2	-2	-1
1	neocembrene	5	3	-2	-1
1	δ-cadinene	5	3	-2	-1
1	(3*R*,6*E*)-nerolidol	2	3	1	2
1	geranylgeraniol	4	2	-2	-1
2	hexane	4	4	0	
2	(3*Z*,6*Z*)-dodecadien-1-ol	5	6	1	1
2	(3*Z*)-dodecen-1-ol	5	8	3	3
2	(3*Z*,6*Z*,8*E*)-dodecatrien-1-ol	7	7	0	0
2	*n*-eicosane	7	7	0	0
2	1-octadecanol	9	6	-3	-3
2	*n*-docosane	5	11	6	6
2	dodec-3-yn-1-ol	9	7	-2	-2
2	neocembrene	9	11	2	2
2	δ-cadinene	5	7	2	2
2	(3*R*,6*E*)-nerolidol	11	8	-3	-3
2	geranylgeraniol	10	7	-3	-3
3	hexane	8	5	-3	
3	(3*Z*,6*Z*)-dodecadien-1-ol	7	5	-2	1
3	(3*Z*)-dodecen-1-ol	6	5	-1	2
3	(3*Z*,6*Z*,8*E*)-dodecatrien-1-ol	9	5	-4	-1
3	*n*-eicosane	2	10	8	11
3	1-octadecanol	7	7	0	3
3	*n*-docosane	8	8	0	3
3	dodec-3-yn-1-ol	3	7	4	7
3	neocembrene	7	11	4	7
3	δ-cadinene	8	7	-1	2
3	(3*R*,6*E*)-nerolidol	7	3	-4	-1
3	geranylgeraniol	5	10	5	8

Table S4. SSR responses to Panel 1 for PsimOR31. Related to Fig. 2.

Replicate	Compound	Pre-stimulation spikes	Post-stimulation spikes	Generated spikes	Δ Spikes/s
1	hexane	5	6	1	
1	(3*Z*,6*Z*)-dodecadien-1-ol	5	24	19	18
1	(3*Z*)-dodecen-1-ol	5	25	20	19
1	(3*Z*,6*Z*,8*E*)-dodecatrien-1-ol	3	27	24	23
1	*n*-eicosane	3	25	22	21
1	1-octadecanol	5	25	20	19
1	*n*-docosane	6	27	21	20
1	dodec-3-yn-1-ol	4	28	24	23
1	neocembrene	6	19	13	12
1	δ-cadinene	3	19	16	15
1	(3*R*,6*E*)-nerolidol	5	16	11	10
1	geranylgeraniol	3	10	7	6
2	hexane	3	2	-1	
2	(3*Z*,6*Z*)-dodecadien-1-ol	5	5	0	1
2	(3*Z*)-dodecen-1-ol	4	9	5	6
2	(3*Z*,6*Z*,8*E*)-dodecatrien-1-ol	2	7	5	6
2	*n*-eicosane	5	10	5	6
2	1-octadecanol	6	6	0	1
2	*n*-docosane	5	4	-1	0
2	dodec-3-yn-1-ol	7	6	-1	0
2	neocembrene	2	5	3	4
2	δ-cadinene	2	10	8	9
2	(3*R*,6*E*)-nerolidol	2	2	0	1
3	hexane	4	3	-1	
3	(3*Z*,6*Z*)-dodecadien-1-ol	9	7	-2	-1
3	(3*Z*)-dodecen-1-ol	3	14	11	12
3	(3*Z*,6*Z*,8*E*)-dodecatrien-1-ol	8	14	6	7
3	*n*-eicosane	9	21	12	13
3	1-octadecanol	6	21	15	16
3	*n*-docosane	6	27	21	22
3	dodec-3-yn-1-ol	10	18	8	9
3	neocembrene	9	17	8	9
3	δ-cadinene	7	20	13	14
3	(3*R*,6*E*)-nerolidol	6	14	8	9
3	geranylgeraniol	10	21	11	12
4	hexane	13	15	2	
4	(3*Z*,6*Z*)-dodecadien-1-ol	20	17	-3	-5
4	(3*Z*)-dodecen-1-ol	15	19	4	2
4	(3*Z*,6*Z*,8*E*)-dodecatrien-1-ol	14	21	7	5
4	*n*-eicosane	18	22	4	2
4	1-octadecanol	19	22	3	1
4	*n*-docosane	16	20	4	2
4	dodec-3-yn-1-ol	11	23	12	10
4	neocembrene	8	22	14	12
4	δ-cadinene	10	24	14	12
4	(3*R*,6*E*)-nerolidol	16	21	5	3
4	geranylgeraniol	12	21	9	7
5	hexane	11	10	-1	
5	(3*Z*,6*Z*)-dodecadien-1-ol	17	18	1	2
5	(3*Z*)-dodecen-1-ol	5	16	11	12
5	(3*Z*,6*Z*,8*E*)-dodecatrien-1-ol	8	12	4	5
5	*n*-eicosane	17	14	-3	-2
5	1-octadecanol	7	13	6	7
5	*n*-docosane	11	16	5	6
5	dodec-3-yn-1-ol	10	15	5	6
5	neocembrene	0	15	15	16
6	hexane	24	25	1	
6	(3*Z*,6*Z*)-dodecadien-1-ol	21	46	25	24
6	(3*Z*)-dodecen-1-ol	18	44	26	25
6	(3*Z*,6*Z*,8*E*)-dodecatrien-1-ol	14	44	30	29
6	*n*-eicosane	17	43	26	25
6	1-octadecanol	10	44	34	33
6	*n*-docosane	12	38	26	25
6	dodec-3-yn-1-ol	17	47	30	29
6	neocembrene	11	32	21	20
6	δ-cadinene	19	27	8	7
6	(3*R*,6*E*)-nerolidol	7	26	19	18
6	geranylgeraniol	9	19	10	9

Table S5. SSR responses to Panel 1 for PsimOR14 vs. W^{1118}. Related to Fig. 2.

Fly line	Replicate	Compound	Pre-stimulation spikes	Post-stimulation spikes	Generated spikes	Δ Spikes/s
PsimOR14	1	hexane	7	3	-4	
PsimOR14	1	(3*Z*,6*Z*)-dodecadien-1-ol	6	7	1	5
PsimOR14	1	(3*Z*)-dodecen-1-ol	16	8	-8	-4
PsimOR14	1	(3*Z*,6*Z*,8*E*)-dodecatrien-1-ol	13	12	-1	3
PsimOR14	1	*n*-eicosane	10	8	-2	2
PsimOR14	1	1-octadecanol	10	6	-4	0
PsimOR14	1	*n*-docosane	13	10	-3	1
PsimOR14	1	dodec-3-yn-1-ol	8	18	10	14
PsimOR14	1	neocembrene	14	62	48	52
PsimOR14	1	*δ*-cadinene	13	22	9	13
PsimOR14	1	(3*R*,6*E*)-nerolidol	15	8	-7	-3
PsimOR14	1	geranylgeraniol	4	22	18	22
PsimOR14	2	hexane	8	9	1	
PsimOR14	2	(3*Z*,6*Z*)-dodecadien-1-ol	7	3	-4	-5
PsimOR14	2	(3*Z*)-dodecen-1-ol	13	3	-10	-11
PsimOR14	2	(3*Z*,6*Z*,8*E*)-dodecatrien-1-ol	13	3	-10	-11
PsimOR14	2	*n*-eicosane	7	2	-5	-6
PsimOR14	2	1-octadecanol	5	3	-2	-3
PsimOR14	2	*n*-docosane	8	2	-6	-7
PsimOR14	2	dodec-3-yn-1-ol	9	3	-6	-7
PsimOR14	2	neocembrene	4	55	51	50
PsimOR14	2	*δ*-cadinene	4	5	1	0
PsimOR14	2	(3*R*,6*E*)-nerolidol	6	5	-1	-2
PsimOR14	2	geranylgeraniol	4	38	34	33
PsimOR14	3	hexane	17	15	-2	
PsimOR14	3	(3*Z*,6*Z*)-dodecadien-1-ol	10	13	3	5
PsimOR14	3	(3*Z*)-dodecen-1-ol	17	7	-10	-8
PsimOR14	3	(3*Z*,6*Z*,8*E*)-dodecatrien-1-ol	18	5	-13	-11
PsimOR14	3	*n*-eicosane	13	4	-9	-7
PsimOR14	3	1-octadecanol	11	6	-5	-3
PsimOR14	3	*n*-docosane	20	12	-8	-6
PsimOR14	3	dodec-3-yn-1-ol	10	7	-3	-1
PsimOR14	3	neocembrene	18	90	72	74
PsimOR14	3	*δ*-cadinene	12	6	-6	-4
PsimOR14	3	(3*R*,6*E*)-nerolidol	17	14	-3	-1
PsimOR14	3	geranylgeraniol	15	41	26	28
PsimOR14	4	hexane	6	7	1	
PsimOR14	4	neocembrene	12	57	45	44
PsimOR14	4	geranylgeraniol	2	28	26	25
PsimOR14	4	(3*Z*,6*Z*)-dodecadien-1-ol	7	7	0	-1
PsimOR14	4	(3*Z*)-dodecen-1-ol	14	5	-9	-10
PsimOR14	4	(3*Z*,6*Z*,8*E*)-dodecatrien-1-ol	12	6	-6	-7
PsimOR14	4	*n*-eicosane	7	1	-6	-7
PsimOR14	4	1-octadecanol	15	3	-12	-13
PsimOR14	4	*n*-docosane	16	4	-12	-13
PsimOR14	4	dodec-3-yn-1-ol	16	9	-7	-8
PsimOR14	4	*δ*-cadinene	5	7	2	1
PsimOR14	4	(3*R*,6*E*)-nerolidol	12	6	-6	-7
PsimOR14	5	hexane	8	6	-2	
PsimOR14	5	neocembrene	5	49	44	46
PsimOR14	5	geranylgeraniol	6	20	14	16
PsimOR14	5	(3*Z*,6*Z*)-dodecadien-1-ol	6	3	-3	-1
PsimOR14	5	(3*Z*)-dodecen-1-ol	2	5	3	5
PsimOR14	5	(3*Z*,6*Z*,8*E*)-dodecatrien-1-ol	8	4	-4	-2
PsimOR14	5	*n*-eicosane	6	4	-2	0
PsimOR14	5	1-octadecanol	8	3	-5	-3
PsimOR14	5	*n*-docosane	6	7	1	3
PsimOR14	5	dodec-3-yn-1-ol	2	6	4	6
PsimOR14	5	*δ*-cadinene	10	7	-3	-1
PsimOR14	5	(3*R*,6*E*)-nerolidol	10	8	-2	0

Fly line	Replicate	Compound	Pre-stimulation spikes	Post-stimulation spikes	Generated spikes	Δ Spikes/s
W1118	1	hexane	3	6	3	
W1118	1	(3*Z*,6*Z*)-dodecadien-1-ol	1	3	2	-1
W1118	1	(3*Z*)-dodecen-1-ol	2	4	2	-1
W1118	1	(3*Z*,6*Z*,8*E*)-dodecatrien-1-ol	4	1	-3	-6
W1118	1	*n*-eicosane	1	19	18	15
W1118	1	1-octadecanol	4	2	-2	-5
W1118	1	*n*-docosane	2	6	4	1
W1118	1	dodec-3-yn-1-ol	2	5	3	0
W1118	1	neocembrene	2	2	0	-3
W1118	1	*δ*-cadinene	1	4	3	0
W1118	1	(3*R*,6*E*)-nerolidol	3	1	-2	-5
W1118	1	geranylgeraniol	3	4	1	-2
W1118	2	hexane	1	4	3	
W1118	2	(3*Z*,6*Z*)-dodecadien-1-ol	2	4	2	-1
W1118	2	(3*Z*)-dodecen-1-ol	5	4	-1	-4
W1118	2	(3*Z*,6*Z*,8*E*)-dodecatrien-1-ol	5	3	-2	-5
W1118	2	*n*-eicosane	3	3	0	-3
W1118	2	1-octadecanol	3	2	-1	-4
W1118	2	*n*-docosane	0	5	5	2
W1118	2	dodec-3-yn-1-ol	3	3	0	-3
W1118	2	neocembrene	4	4	0	-3
W1118	2	*δ*-cadinene	6	0	-6	-9
W1118	2	(3*R*,6*E*)-nerolidol	1	3	2	-1
W1118	2	geranylgeraniol	3	4	1	-2
W1118	3	hexane	5	1	-4	
W1118	3	(3*Z*,6*Z*)-dodecadien-1-ol	5	5	0	4
W1118	3	(3*Z*)-dodecen-1-ol	5	2	-3	1
W1118	3	(3*Z*,6*Z*,8*E*)-dodecatrien-1-ol	2	4	2	6
W1118	3	n-eicosane	3	5	2	6
W1118	3	1-octadecanol	3	5	2	6
W1118	3	n-docosane	4	5	1	5
W1118	3	dodec-3-yn-1-ol	6	5	-1	3
W1118	3	neocembrene	1	5	4	8
W1118	3	δ-cadinene	4	4	0	4
W1118	3	(3*R*,6*E*)-nerolidol	6	3	-3	1
W1118	3	geranylgeraniol	4	2	-2	2
W1118	4	hexane	4	4	0	
W1118	4	(3*Z*,6*Z*)-dodecadien-1-ol	1	6	5	5
W1118	4	(3*Z*)-dodecen-1-ol	3	3	0	0
W1118	4	(3*Z*,6*Z*,8*E*)-dodecatrien-1-ol	6	4	-2	-2
W1118	4	n-eicosane	4	7	3	3
W1118	4	1-octadecanol	5	7	2	2
W1118	4	n-docosane	4	9	5	5
W1118	4	dodec-3-yn-1-ol	0	4	4	4
W1118	4	neocembrene	2	0	-2	-2
W1118	4	δ-cadinene	5	2	-3	-3
W1118	4	(3*R*,6*E*)-nerolidol	4	1	-3	-3
W1118	4	geranylgeraniol	2	0	-2	-2
W1118	5	hexane	3	8	5	
W1118	5	(3*Z*,6*Z*)-dodecadien-1-ol	6	11	5	0
W1118	5	(3*Z*)-dodecen-1-ol	9	7	-2	-7
W1118	5	(3*Z*,6*Z*,8*E*)-dodecatrien-1-ol	6	9	3	-2
W1118	5	n-eicosane	7	14	7	2
W1118	5	1-octadecanol	4	13	9	4
W1118	5	n-docosane	8	7	-1	-6
W1118	5	dodec-3-yn-1-ol	7	8	1	-4
W1118	5	neocembrene	6	8	2	-3
W1118	5	δ-cadinene	5	8	3	-2
W1118	5	(3*R*,6*E*)-nerolidol	6	6	0	-5
W1118	5	geranylgeraniol	6	6	0	-5

Table S6. SSR dose response data for neocembrene and PsimOR14 fly line. Related to Fig. 2.

	replicate	1	2	3	4	5	6	7	8	9
Dose	0.01 ng	22	10	10	6	-4	10	18	16	24
	0.1 ng	4	26	26	8	0	0	4	38	12
	1 ng	14	32	14	10	12	2	22	28	10
	10 ng	10	30	32	26	26	14	20	32	6
	100 ng	30		24	26	42	38	46	26	10
	500 ng	44		36	22	34				

Table S7. SSR responses to Panel 2 for PsimOR14. Related to Fig. 3.

Panel	Replicate	Compound	Pre-stimulation spikes	Post-stimulation spikes	Generated spikes	Δ Spikes/s
2	1	paraffin oil	6	2	-4	
2	1	myrcene	10	15	5	9
2	1	eucalyptol	2	2	0	4
2	1	(+)-3-carene	2	5	3	7
2	1	ethanol	2	6	4	8
2	1	(2*E*)-hexenal	3	5	2	6
2	1	(+)-*α*-pinene	3	2	-1	3
2	1	*p*-cymene	3	2	-1	3
2	1	(+)-limonene	4	3	-1	3
2	1	(+)-longifolene	3	2	-1	3
2	1	(-)-*β*-caryophyllene	1	2	1	5
2	1	(2*E*)-hexen-1-ol	1	0	-1	3
2	1	isoamyl propionate	0	0	0	4
2	1	sabinene	2	1	-1	3
2	1	*γ*-terpinene	0	2	2	6
2	1	terpinolene	2	0	-2	2
2	1	toluene	1	5	4	8
2	1	pentyl acetate	1	3	2	6
2	1	ethyl acetate	2	1	-1	3
2	1	heptanal	0	0	0	4
2	1	*γ*-nonalactone	2	0	-2	2
2	2	paraffin oil	0	1	1	
2	2	myrcene	6	11	5	4
2	2	eucalyptol	0	13	13	12
2	2	(+)-3-carene	6	10	4	3
2	2	ethanol	2	12	10	9
2	2	(2*E*)-hexenal	6	11	5	4
2	2	(+)-*α*-pinene	0	10	10	9
2	2	*p*-cymene	8	12	4	3
2	2	(+)-limonene	2	11	9	8
2	2	(+)-longifolene	1	10	9	8
2	2	(-)-*β*-caryophyllene	5	7	2	1
2	2	(2*E*)-hexen-1-ol	8	12	4	3
2	2	isoamyl propionate	8	8	0	-1
2	2	sabinene	6	16	10	9
2	2	*γ*-terpinene	9	7	-2	-3
2	2	terpinolene	5	10	5	4
2	2	toluene	8	8	0	-1
2	2	pentyl acetate	7	9	2	1
2	2	ethyl acetate	8	9	1	0
2	2	heptanal	10	9	-1	-2
2	2	*γ*-nonalactone	6	12	6	5
2	3	paraffin oil	5	6	1	
2	3	myrcene	2	6	4	3
2	3	eucalyptol	2	10	8	7
2	3	(+)-3-carene	0	14	14	13
2	3	ethanol	2	6	4	3
2	3	(2*E*)-hexenal	2	12	10	9
2	3	(+)-*α*-pinene	2	9	7	6
2	3	*p*-cymene	3	4	1	0
2	3	(+)-limonene	1	1	0	-1
2	3	(+)-longifolene	0	10	10	9
2	3	(-)-*β*-caryophyllene	0	10	10	9
2	3	(2*E*)-hexen-1-ol	4	1	-3	-4
2	3	(2*E*)-hexen-1-ol	3	1	-2	-3
2	3	sabinene	1	2	1	0
2	3	*γ*-terpinene	9	5	-4	-5
2	3	terpinolene	1	9	8	7
2	3	toluene	2	0	-2	-3
2	3	pentyl acetate	1	9	8	7
2	3	ethyl acetate	4	0	-4	-5
2	3	heptanal	1	4	3	2
2	3	*γ*-nonalactone	2	2	0	-1
2	4	paraffin oil	4	5	1	0
2	4	myrcene	3	1	-2	-3
2	4	eucalyptol	0	7	7	6
2	4	(+)-3-carene	2	5	3	2
2	4	ethanol	1	4	3	2
2	4	(2*E*)-hexenal	0	3	3	2
2	4	(+)-*α*-pinene	3	12	9	8
2	4	*p*-cymene	1	11	10	9
2	4	(+)-limonene	0	3	3	2
2	4	(+)-longifolene	0	8	8	7
2	4	(-)-*β*-caryophyllene	0	2	2	1
2	4	(2*E*)-hexen-1-ol	0	5	5	4
2	4	isoamyl propionate	0	5	5	4
2	4	sabinene	2	2	0	-1
2	4	*γ*-terpinene	3	9	6	5
2	4	terpinolene	7	4	-3	-4
2	4	toluene	2	2	0	-1
2	4	pentyl acetate	3	2	-1	-2
2	4	ethyl acetate	1	1	0	-1
2	4	heptanal	3	1	-2	-3
2	4	paraffin oil	6	7	1	0
2	5	myrcene	11	11	0	-1
2	5	eucalyptol	7	13	6	5
2	5	(+)-3-carene	12	11	-1	-2
2	5	ethanol	11	9	-2	-3
2	5	(2*E*)-hexenal	11	13	2	1
2	5	(+)-*α*-pinene	12	11	-1	-2
2	5	*p*-cymene	11	16	5	4
2	5	(+)-limonene	9	9	0	-1
2	5	(+)-longifolene	17	9	-8	-9
2	5	(-)-*β*-caryophyllene	6	13	7	6
2	5	(2*E*)-hexen-1-ol	9	3	-6	-7
2	5	isoamyl propionate	0	0	0	-1
2	5	sabinene	6	19	13	12
2	5	*γ*-terpinene	3	13	10	9
2	5	terpinolene	9	15	6	5
2	5	toluene	10	13	3	2
2	5	pentyl acetate	6	11	5	4
2	5	ethyl acetate	8	19	11	10
2	5	heptanal	14	7	-7	-8
2	5	*γ*-nonalactone	10	14	4	3

Table S8. SSR responses to Panel 3 for PsimOR14. Related to Fig. 3.

Panel	Replicate	Compound	Pre-stimulation spikes	Post-stimulation spikes	Generated spikes	Δ Spikes/s
3	1	paraffin oil	4	5	1	
3	1	ethyl (2*E*,4*Z*)-decadienoate	4	6	2	1
3	1	*p*-cresol	2	9	7	6
3	1	*β*-bisabolene	7	2	-5	-6
3	1	(*E*)-myrcenol	1	6	5	4
3	1	nonan-1-ol	1	8	7	6
3	1	isoamyl acetate	5	11	6	5
3	1	2-phenylethyl acetate	3	9	6	5
3	1	octan-1-ol	6	12	6	5
3	1	benzyl alcohol	12	11	-1	-2
3	1	methyl jasmonate	8	13	5	4
3	1	(*E*)-*β*-ocimene	6	14	8	7
3	1	eucarvone	10	4	-6	-7
3	1	*α*-camphorene	2	14	12	11
3	1	(-)-trans-pinocarveol	6	4	-2	-3
3	1	cryptone	8	8	0	-1
3	1	(+)-cis-carveol	12	17	5	4
3	2	paraffin oil	9	5	-4	
3	2	ethyl (2*E*,4*Z*)-decadienoate	19	11	-8	-4
3	2	*p*-cresol	15	15	0	4
3	2	*β*-bisabolene	8	14	6	10
3	2	(*E*)-myrcenol	17	16	-1	3
3	2	nonan-1-ol	17	14	-3	1
3	2	isoamyl acetate	20	16	-4	0
3	2	2-phenylethyl acetate	13	7	-6	-2
3	2	octan-1-ol	10	3	-7	-3
3	2	benzyl alcohol	3	2	-1	3
3	2	methyl jasmonate	0	1	1	5
3	2	(*E*)-*β*-ocimene	0	2	2	6
3	2	eucarvone	0	1	1	5
3	2	*α*-camphorene	0	1	1	5
3	2	(-)-trans-pinocarveol	0	1	1	5
3	2	cryptone	0	0	0	4
3	2	(+)-cis-carveol	0	0	0	4
3	3	paraffin oil	0	1	1	
3	3	ethyl (2*E*,4*Z*)-decadienoate	4	8	4	3
3	3	*p*-cresol	2	6	4	3
3	3	*β*-bisabolene	12	3	-9	-10
3	3	(*E*)-myrcenol	6	10	4	3
3	3	nonan-1-ol	5	7	2	1
3	3	isoamyl acetate	4	9	5	4
3	3	2-phenylethyl acetate	6	9	3	2
3	3	octan-1-ol	0	14	14	13
3	3	benzyl alcohol	8	7	-1	-2
3	3	methyl jasmonate	9	11	2	1
3	3	(*E*)-*β*-ocimene	2	4	2	1
3	3	eucarvone	10	1	-9	-10
3	3	*α*-camphorene	7	7	0	-1
3	3	(-)-trans-pinocarveol	5	0	-5	-6
3	3	cryptone	5	8	3	2
3	3	(+)-cis-carveol	5	6	1	0
3	4	paraffin oil	2	7	5	
3	4	ethyl (2*E*,4*Z*)-decadienoate	1	0	-1	-6
3	4	*p*-cresol	6	10	4	-1
3	4	*β*-bisabolene	3	9	6	1
3	4	(*E*)-myrcenol	2	9	7	2
3	4	nonan-1-ol	10	4	-6	-11
3	4	isoamyl acetate	1	6	5	0
3	4	2-phenylethyl acetate	0	0	0	-5
3	4	octan-1-ol	2	0	-2	-7
3	4	benzyl alcohol	1	5	4	-1
3	4	methyl jasmonate	10	3	-7	-12
3	4	(*E*)-*β*-ocimene	0	5	5	0
3	4	eucarvone	3	1	-2	-7
3	4	*α*-camphorene	1	0	-1	-6
3	4	(-)-trans-pinocarveol	9	5	-4	-9
3	4	cryptone	9	6	-3	-8
3	4	(+)-cis-carveol	1	0	-1	-6
3	5	paraffin oil	4	1	-3	
3	5	ethyl (2*E*,4*Z*)-decadienoate	1	4	3	6
3	5	*p*-cresol	0	0	0	3
3	5	*β*-bisabolene	0	15	15	18
3	5	(*E*)-myrcenol	5	5	0	3
3	5	nonan-1-ol	0	1	1	4
3	5	isoamyl acetate	4	1	-3	0
3	5	2-phenylethyl acetate	3	3	0	3
3	5	octan-1-ol	9	6	-3	0
3	5	benzyl alcohol	5	0	-5	-2
3	5	methyl jasmonate	0	1	1	4
3	5	(*E*)-*β*-ocimene	2	0	-2	1
3	5	eucarvone	9	7	-2	1
3	5	*α*-camphorene	11	4	-7	-4
3	5	(-)-trans-pinocarveol	0	0	0	3
3	5	cryptone	3	2	-1	2
3	5	(+)-cis-carveol	4	1	-3	0

Table S9. SSR responses to Panel 4 for PsimOR14. Related to Fig. 3.

Panel	Replicate	Compound	Pre-stimulation spikes	Post-stimulation spikes	Generated spikes	Δ Spikes/s
4	1	paraffin oil	6	1	-5	
4	1	(-)-verbenone	14	4	-10	-5
4	1	oct-1-en-3-ol	4	2	-2	3
4	1	acetophenone	12	20	8	13
4	1	4-vinylanisole	12	14	2	7
4	1	4-ethylguaiacol	6	2	-4	1
4	1	(±)-camphor	10	6	-4	1
4	1	octan-1-ol	16	6	-10	-5
4	1	methyleugenol	18	2	-16	-11
4	1	styrene	16	14	-2	3
4	1	benzaldehyde	20	6	-14	-9
4	1	linalool	21	0	-21	-16
4	1	4-methylanisole	20	6	-14	-9
4	1	2-methylbutan-1-ol	4	0	-4	1
4	1	isoamyl alcohol	12	0	-12	-7
4	1	2-methylbutyl acetate	18	14	-4	1
4	1	(±)-myrtenol	7	2	-5	0
4	2	paraffin oil	7	4	-3	
4	2	(-)-verbenone	2	12	10	13
4	2	oct-1-en-3-ol	7	8	1	4
4	2	acetophenone	4	10	6	9
4	2	4-vinylanisole	8	5	-3	0
4	2	4-ethylguaiacol	6	10	4	7
4	2	(±)-camphor	4	11	7	10
4	2	octan-1-ol	13	8	-5	-2
4	2	methyleugenol	5	14	9	12
4	2	styrene	10	6	-4	-1
4	2	benzaldehyde	7	11	4	7
4	2	linalool	5	5	0	3
4	2	4-methylanisole	10	4	-6	-3
4	2	2-methylbutan-1-ol	8	6	-2	1
4	2	isoamyl alcohol	11	12	1	4
4	2	2-methylbutyl acetate	10	10	0	3
4	2	(±)-myrtenol	7	9	2	5
4	2	2-phenylethanol	4	8	4	7
4	2	hexan-1-ol	9	4	-5	-2
4	2	2,3-dihydrobenzofuran	9	4	-5	-2
4	2	geranyl acetone	8	6	-2	1
4	3	paraffin oil	4	2	-2	
4	3	(-)-verbenone	12	8	-4	-2
4	3	oct-1-en-3-ol	7	5	-2	0
4	3	acetophenone	2	10	8	10
4	3	4-vinylanisole	8	12	4	6
4	3	4-ethylguaiacol	1	11	10	12
4	3	(±)-camphor	1	10	9	11
4	3	octan-1-ol	9	6	-3	-1
4	3	methyleugenol	9	6	-3	-1
4	3	styrene	3	5	2	4
4	3	benzaldehyde	11	6	-5	-3
4	3	linalool	10	1	-9	-7
4	3	4-methylanisole	3	9	6	8
4	3	2-methylbutan-1-ol	7	2	-5	-3
4	3	isoamyl alcohol	10	9	-1	1
4	3	2-methylbutyl acetate	10	6	-4	-2
4	3	(±)-myrtenol	5	3	-2	0
4	3	2-phenylethanol	2	8	6	8
4	3	hexan-1-ol	7	4	-3	-1
4	3	2,3-dihydrobenzofuran	6	9	3	5
4	3	geranyl acetone	6	9	3	5
4	4	paraffin oil	10	6	-4	
4	4	(-)-verbenone	11	5	-6	-2
4	4	oct-1-en-3-ol	7	8	1	5
4	4	acetophenone	13	3	-10	-6
4	4	4-vinylanisole	8	8	0	4
4	4	4-ethylguaiacol	7	6	-1	3
4	4	(±)-camphor	1	1	0	4
4	4	octan-1-ol	7	7	0	4
4	4	methyleugenol	14	7	-7	-3
4	4	styrene	11	6	-5	-1
4	4	benzaldehyde	5	14	9	13
4	4	linalool	8	0	-8	-4
4	4	4-methylanisole	7	5	-2	2
4	4	2-methylbutan-1-ol	5	0	-5	-1
4	4	isoamyl alcohol	9	3	-6	-2
4	4	2-methylbutyl acetate	6	9	3	7
4	4	(±)-myrtenol	3	6	3	7
4	4	2-phenylethanol	6	5	-1	3
4	4	hexan-1-ol	9	8	-1	3
4	4	2,3-dihydrobenzofuran	6	4	-2	2
4	4	geranyl acetone	10	7	-3	1
4	5	paraffin oil	8	7	-1	
4	5	(-)-verbenone	6	3	-3	-2
4	5	oct-1-en-3-ol	3	1	-2	-1
4	5	acetophenone	6	2	-4	-3
4	5	4-vinylanisole	5	3	-2	-1
4	5	4-ethylguaiacol	9	5	-4	-3
4	5	(±)-camphor	8	5	-3	-2
4	5	octan-1-ol	6	4	-2	-1
4	5	methyleugenol	7	8	1	2
4	5	styrene	7	6	-1	0
4	5	benzaldehyde	10	5	-5	-4
4	5	linalool	9	2	-7	-6
4	5	4-methylanisole	10	9	-1	0
4	5	2-methylbutan-1-ol	10	4	-6	-5
4	5	isoamyl alcohol	10	7	-3	-2
4	5	2-methylbutyl acetate	10	8	-2	-1
4	5	(±)-myrtenol	6	5	-1	0
4	5	2-phenylethanol	8	7	-1	0
4	5	hexan-1-ol	9	5	-4	-3
4	5	2,3-dihydrobenzofuran	7	6	-1	0
4	5	geranyl acetone	9	6	-3	-2
4	6	paraffin oil	9	10	1	
4	6	(-)-verbenone	7	4	-3	-4
4	6	oct-1-en-3-ol	6	8	2	1
4	6	acetophenone	12	6	-6	-7
4	6	4-vinylanisole	7	6	-1	-2
4	6	4-ethylguaiacol	8	5	-3	-4
4	6	(±)-camphor	11	14	3	2
4	6	octan-1-ol	13	5	-8	-9
4	6	methyleugenol	5	6	1	0
4	6	styrene	9	6	-3	-4
4	6	benzaldehyde	6	7	1	0
4	6	linalool	11	1	-10	-11
4	6	4-methylanisole	9	8	-1	-2
4	6	2-methylbutan-1-ol	10	4	-6	-7
4	6	isoamyl alcohol	7	7	0	-1
4	6	2-methylbutyl acetate	6	7	1	0
4	6	(±)-myrtenol	7	6	-1	-2
4	6	2-phenylethanol	10	8	-2	-3
4	6	hexan-1-ol	11	6	-5	-6
4	6	2,3-dihydrobenzofuran	12	9	-3	-4
4	6	geranyl acetone	12	9	-3	-4

Table S10. SSR responses to Panel 1 by neocembrene sensillum in *P. simplex* workers. Related to Fig. 5.

Replicate	Compound	Pre-stimulation spikes	Post-stimulation spikes	Generated spikes	Δ Spikes/s
1	hexane	8	8	0	
1	(3*Z*,6*Z*)-dodecadien-1-ol	5	8	3	6
1	(3*Z*)-dodecen-1-ol	12	21	9	18
1	(3*Z*,6*Z*,8*E*)-dodecatrien-1-ol	10	13	3	6
1	*n*-eicosane	6	8	2	4
1	1-octadecanol	5	8	3	6
1	*n*-docosane	3	5	2	4
1	(3*R*,6*E*)-nerolidol	4	16	12	24
1	neocembrene	11	34	23	46
1	*δ*-cadinene	9	12	3	6
1	dodec-3-yn-1-ol	5	6	1	2
1	geranylgeraniol	4	12	8	16
2	hexane	18	18	0	
2	(3*Z*,6*Z*)-dodecadien-1-ol	9	11	2	4
2	(3*Z*)-dodecen-1-ol	2	5	3	6
2	(3*Z*,6*Z*,8*E*)-dodecatrien-1-ol	8	6	-2	-4
2	neocembrene	3	41	38	76
2	geranylgeraniol	2	11	9	18
3	hexane	6	6	0	
3	(3*Z*,6*Z*)-dodecadien-1-ol	10	12	2	4
3	(3*Z*)-dodecen-1-ol	15	9	-6	-12
3	(3*Z*,6*Z*,8*E*)-dodecatrien-1-ol	9	11	2	4
3	neocembrene	10	46	36	72
3	geranylgeraniol	6	16	10	20
3	*δ*-cadinene	12	13	1	2
4	hexane	5	6	1	
4	(3*Z*,6*Z*)-dodecadien-1-ol	10	12	2	2
4	(3*Z*)-dodecen-1-ol	10	2	-8	-18
4	(3*Z*,6*Z*,8*E*)-dodecatrien-1-ol	9	9	0	-2
4	neocembrene	7	45	38	74
4	geranylgeraniol	3	9	6	10
5	hexane	6	10	4	
5	(3*Z*,6*Z*)-dodecadien-1-ol	7	13	6	4
5	(3*Z*)-dodecen-1-ol	6	15	9	10
5	(3*Z*,6*Z*,8*E*)-dodecatrien-1-ol	9	11	2	-4
5	neocembrene	5	51	46	84
6	hexane	12	4	-8	
6	(3*Z*,6*Z*)-dodecadien-1-ol	7	14	7	30
6	(3*Z*)-dodecen-1-ol	11	7	-4	8
6	(3*Z*,6*Z*,8*E*)-dodecatrien-1-ol	10	18	8	32
6	neocembrene	3	48	45	106
6	geranylgeraniol	9	14	5	26
7	hexane	36	33	-3	
7	(3*Z*,6*Z*)-dodecadien-1-ol	40	53	13	32
7	(3*Z*)-dodecen-1-ol	47	49	2	10
7	(3*Z*,6*Z*,8*E*)-dodecatrien-1-ol	55	64	9	24
7	*n*-eicosane	54	54	0	6
7	1-octadecanol	54	49	-5	-4
7	*n*-docosane	56	49	-7	-8
7	(3*R*,6*E*)-nerolidol	57	50	-7	-8
7	*δ*-cadinene	52	46	-6	-6
7	dodec-3-yn-1-ol	48	54	6	18
7	neocembrene	40	74	34	74
7	geranylgeraniol	17	40	23	52
8	hexane	34	32	-2	
8	neocembrene	18	46	28	60
8	geranylgeraniol	20	39	19	42
9	hexane	65	70	5	
9	(3*Z*,6*Z*)-dodecadien-1-ol	28	33	5	0
9	(3*Z*)-dodecen-1-ol	37	36	-1	-12
9	(3*Z*,6*Z*,8*E*)-dodecatrien-1-ol	29	27	-2	-14
9	*n*-eicosane	36	42	6	2
9	1-octadecanol	35	34	-1	-12
9	*n*-docosane	34	35	1	-8
9	(3*R*,6*E*)-nerolidol	19	30	11	12
9	neocembrene	22	54	32	54
9	*δ*-cadinene	19	15	-4	-18
9	dodec-3-yn-1-ol	35	31	-4	-18
9	geranylgeraniol	20	44	24	38
10	hexane	17	22	5	
10	neocembrene	20	39	19	28
10	geranylgeraniol	17	41	24	38
11	hexane	6	11	5	
11	neocembrene	19	46	27	44
11	geranylgeraniol	24	34	10	10
12	hexane	28	26	-2	
12	neocembrene	31	56	25	54
13	hexane	41	37	-4	
13	neocembrene	17	38	21	50
13	geranylgeraniol	8	28	20	48
13	(3*Z*,6*Z*)-dodecadien-1-ol	15	13	-2	4
13	(3*Z*)-dodecen-1-ol	18	20	2	12
13	(3*Z*,6*Z*,8*E*)-dodecatrien-1-ol	12	13	1	10
13	*n*-eicosane	15	18	3	14
13	1-octadecanol	7	11	4	16
13	*n*-docosane	7	11	4	16
13	(3*R*,6*E*)-nerolidol	27	19	-8	-8
13	*δ*-cadinene	27	23	-4	0
13	dodec-3-yn-1-ol	18	30	12	32
14	hexane	25	21	-4	
14	neocembrene	18	68	50	108
14	geranylgeraniol	15	22	7	22
14	(3*Z*,6*Z*)-dodecadien-1-ol	28	15	-13	-18
14	(3*Z*)-dodecen-1-ol	32	26	-6	-4
14	(3*Z*,6*Z*,8*E*)-dodecatrien-1-ol	20	24	4	16
14	*n*-eicosane	21	17	-4	0
14	1-octadecanol	30	23	-7	-6
14	*n*-docosane	27	24	-3	2
14	(3*R*,6*E*)-nerolidol	7	9	2	12
14	*δ*-cadinene	13	11	-2	4
14	dodec-3-yn-1-ol	8	8	0	8
15	hexane	9	8	-1	
15	(3*Z*,6*Z*)-dodecadien-1-ol	24	21	-3	-4
15	(3*Z*)-dodecen-1-ol	24	29	5	12
15	(3*Z*,6*Z*,8*E*)-dodecatrien-1-ol	13	14	1	4
15	*n*-eicosane	8	19	11	24
15	1-octadecanol	23	19	-4	-6
15	*n*-docosane	30	26	-4	-6
15	(3*R*,6*E*)-nerolidol	9	16	7	16
15	neocembrene	12	40	28	58
15	*δ*-cadinene	9	9	0	2
15	dodec-3-yn-1-ol	16	8	-8	-14
15	geranylgeraniol	10	24	14	30
16	hexane	13	7	-6	
16	neocembrene	18	38	20	52
16	geranylgeraniol	9	26	17	46
16	(3*Z*,6*Z*)-dodecadien-1-ol	15	12	-3	6
16	(3*Z*)-dodecen-1-ol	12	25	13	38
16	(3*Z*,6*Z*,8*E*)-dodecatrien-1-ol	11	13	2	16
16	*n*-eicosane	15	18	3	18
16	1-octadecanol	7	13	6	24
16	*n*-docosane	9	10	1	14
16	(3*R*,6*E*)-nerolidol	7	13	6	24
16	*δ*-cadinene	12	13	1	14
16	dodec-3-yn-1-ol	8	18	10	32
17	hexane	16	14	-2	
17	neocembrene	7	32	25	54
17	geranylgeraniol	8	14	6	16
17	(3*Z*,6*Z*)-dodecadien-1-ol	10	7	-3	-2
17	(3*Z*)-dodecen-1-ol	18	8	-10	-16
17	(3*Z*,6*Z*,8*E*)-dodecatrien-1-ol	17	9	-8	-12
17	*n*-eicosane	7	8	1	6
17	1-octadecanol	17	9	-8	-12
17	*n*-docosane	14	10	-4	-4
17	(3*R*,6*E*)-nerolidol	8	8	0	4
17	*δ*-cadinene	9	14	5	14
17	dodec-3-yn-1-ol	9	10	1	6

Table S11. SSR dose response data for neocembrene and *P. simplex* neocembrene sensillum. Related to Fig. 5.

		Δ Spikes/s										
	replicate	1	2	3	4	5	6	7	8	9	10	11
Dose	0.01 ng	62	44		18		14	8	30	10	4	18
	0.1 ng	76	24	20	64	90	22	42	36	12	10	42
	1 ng	90	46	54	86	106	14	30	38	20	12	36
	10 ng	84	44	50	88	120	22	14		16	28	46
	100 ng	104	54	34	112	124	36	8		36	38	40

Table S12. Nucleotide and protein sequences of PsimOR14. Related to Fig. 6.

PsimOR14

ATGATTCGATCAAAGAGAAAGGAGAGCCAAGCAAACGAAACAAAACACACATTAACAAGTGAAGAGCAACCTTCTGATTG
TGACGTGAAGATCATGACACTCAGTATTATGCTGAATGCGGCTGGCCTCCTACCTCCAGCCAAATCGTCATCATTGATCA
GACTGGCCTACAAAGTATTTGTAGTATTTATTCACATACTTTTCGTCTTAACGCTGATAGGACAGATAATGGCAGTAGTG
GTTTACTGGGGAGACATTCCTCTAATTGCAACCACAATAAGCTTGATGACTAGTCTGATTGGATCGATGAGTTCATCCAT
AAATTTTCTTCTAAACAGAAAGAAGTACATGCGTCTTGCGGACACGTTGAAAACAGAATTTGTTGCCAAATTGAAATCAA
AATATATCAAAATTATTTTAAATGCTGAACGTCAGGTTGTATTCTGTGGGATACTCGTATGTATTGTAGCTGTATGTATT
GGATTTATTTGGATAGTCGTGCCATTTTTAAGTACCAACACCCCATTTGACTTTGCAAATGAAAAAAGTGTCAAAGAAGG
AAGCCGCATGGAGGAATTAATTCTTGTGATGTGGCTCCCTTCTAAATTTGAACAGTCCCCTCAATTTGAAATAATAGTTT
TTTTACAAATCTTTGTCGTAACGTTTGCATTAGCAATGATCTATTCAGTTGATATGATGTTACTATCTCTGATGAGCCAC
GCTGCTGCACAGTTCAGGGTTTTGAATGCCATGCTGAATGACATGCACGAAAATGTTCGTGAAGACGAGATTCACAGAAC
AAGAAACATGGCTTCATTGGTCACTGGCACTGACATCTCGTACATGGAGTTCTCTTCTACCAATTCTTGGAATGGAAACA
CAGAGCATTCTGGAAGCGCTGGTGTTGAGTTGGACAGCCTAAAAAATGAAGACTGTGAAGAAGATCCTGTCCGACAGTAC
CTCGTTGAGTGCATTAGATATCACCAGGCTGTAATTGAGTTTGTTGACCAACTGAACGAGGTGTTCGGCGCAGTGAGCTT
CGTGAAGATGCTTGACTGGCCTTTTGCGATTTGTATGACAGGATTTCAGTTGACACAGACTGTAGAGAGCCAGGAGGATT
TACTTAAATTCATCTCCCTGTTTGCTGGGGTTGTATATCTAATAATCTCTTACATTTGGTTCGGACAGCAAGTAATTGAC
GAGAGCGAGGAAGTAGCAACAGCGTTGTACAGCACTGACTGGTACAACCAGGCACCAGGGTTCAAACGTCTGCTGCCTGT
AGCCATCATGCGGGCTTCGAATTCTGTCAAAGTTAAAGCTGGGGTGTTCTTTGACATGTCTTGCGTCACGTTAGCTTCGA
TTATGAATGCATCTTACACGTATTTTATGATGCTAATTCATCTACACGACTCCTAA

PsimOR14

MIRSKRKESQANETKHTLTSEEQPSDCDVKIMTLSIMLNAAGLLPPAKSSSLIRLAYKVFVVFIHILFVLTLIGQIMAVV
VYWGDIPLIATTISLMTSLIGSMSSSINFLLNRKKYMRLADTLKTEFVAKLKSKYIKIILNAERQVVFCGILVCIVAVCI
GFIWIVVPFLSTNTPFDFANEKSVKEGSRMEELILVMWLPSKFEQSPQFEIIVFLQIFVVTFALAMIYSVDMMLLSLMSH
AAAQFRVLNAMLNDMHENVREDEIHRTRNMASLVTGTDISYMEFSSTNSWNGNTEHSGSAGVELDSLKNEDCEEDPVRQY
LVECIRYHQAVIEFVDQLNEVFGAVSFVKMLDWPFAICMTGFQLTQTVESQEDLLKFISLFAGVVYLIISYIWFGQQVID
ESEEVATALYSTDWYNQAPGFKRLLPVAIMRASNSVKVKAGVFFDMSCVTLASIMNASYTYFMMLIHLHDSX

Table S13. MM/PBSA calculated interaction energies of ligands with PsimOR14 decomposed into per-residue contributions.

Interaction energy (kcal/mol)	neocembrene	geranylgeraniol	(+)-limonene
	mean ± SD		
Cys154	-0.90 ± 0.58	-0.71 ± 0.35	-0.17 ± 0.27
Ala157	-0.68 ± 0.46	-1.02 ± 0.38	-0.45 ± 0.38
Val158	-1.16 ± 0.77	-1.72 ± 0.56	-0.23 ± 0.44
Gly161	×	-0.82 ± 0.38	×
Phe162	×	-1.08 ± 0.67	×
Ile165	×	-0.66 ± 0.49	×
Ile217	×	-1.03 ± 0.47	×
Val220	×	-0.72 ± 0.31	×
Thr221	-1.00 ± 0.53	-1.19 ± 0.47	-0.17 ± 0.35
Leu224	-1.09 ± 0.58	-1.41 ± 0.39	-0.78 ± 0.46
Ala225	-0.93 ± 0.6	-0.97 ± 0.45	-0.17 ± 0.29
Tyr228	-1.10 ± 0.72	-1.06 ± 0.49	-0.47 ± 0.4

Table S14. Differential expression of *P. simplex* ORs (DESeq2 and edge R analyses), based on heads (including antennae) of workers and soldiers (three replicates). Related to Fig. 7.

OR	DESeq2			edgeR	
	log_2 fold change (worker vs soldier)	lfcSE	p-value	log_2 fold change (worker vs soldier)	p-value
PsimOR1	-0.5905	0.3426	0.0848	-0.6679	0.0186
PsimOR10	-0.4006	0.9211	0.6636	-0.4375	0.5905
PsimOR11	0.3565	0.5005	0.4763	0.262	0.5589
PsimOR12	-0.2703	1.2658	0.8309	-0.4127	0.8431
PsimOR13	0.1677	0.6478	0.7957	0.0539	1
PsimOR14	-1.8565	0.8841	0.0357	-1.8989	0.0036
PsimOR15	-0.578	0.8735	0.5082	-0.6829	0.4084
PsimOR16	-0.4973	1.1753	0.6722	-0.5878	0.613
PsimOR17	-0.7328	3.7695	0.8459	-0.5892	1
PsimOR18	1.2163	1.6983	0.4739	1.0486	0.5486
PsimOR19	0.6517	1.0553	0.5369	0.5408	0.5589
PsimOR2	1.2943	0.7769	0.0957	1.1238	0.1342
PsimOR20	-2.9803	0.7045	0	-3.0603	0
PsimOR22	0.5913	1.1359	0.6027	0.5019	0.7071
PsimOR23	-0.0816	1.3315	0.9511	-0.1249	1
PsimOR24	-1.3934	0.8105	0.0856	-1.4649	0.025
PsimOR25	0.9132	1.4392	0.5257	0.6897	0.6457
PsimOR26	-0.879	0.1926	0	-0.9787	0
PsimOR27	0.2988	1.1656	0.7977	0.2	1
PsimOR28	0.3981	1.1226	0.7229	0.3443	0.722
PsimOR29	-0.4531	1.3799	0.7426	-0.45	0.6812
PsimOR3	-0.037	1.156	0.9744	-0.1663	0.8475
PsimOR30	0.7053	1.184	0.5514	0.5977	0.6758
PsimOR31	0.1924	0.5699	0.7357	0.0691	0.9348
PsimOR32	-0.2186	1.4043	0.8763	-0.288	1
PsimOR34	-0.4167	0.4244	0.3261	-0.5383	0.1738
PsimOR35	-1.0587	2.6395	0.6883	-0.8036	0.5553
PsimOR36	-0.3664	0.9102	0.6873	-0.5093	0.5249
PsimOR37	0.3495	1.2265	0.7756	0.2614	0.8477
PsimOR39	-0.0669	0.6154	0.9135	-0.1886	0.7502
PsimOR4	0.0586	0.7043	0.9336	-0.0669	1
PsimOR40	-0.5383	0.34	0.1134	-0.6076	0.0395
PsimOR41	-0.3886	0.2793	0.164	-0.5129	0.0916
PsimOR42	NA	NA	NA	0	1
PsimOR43	-0.5866	1.4600	0.6878	-0.5596	0.7796
PsimOR44	0.1981	1.6775	0.906	0.128	1
PsimOR45	-1.5455	1.331	0.2456	-1.4406	0.1817
PsimOR46	-3.0579	1.863	0.1007	-2.9	0.0445
PsimOR47	2.375	1.7303	0.1699	2.2464	0.1134
PsimOR48	0.0016	1.2033	0.9989	-0.0757	1
PsimOR49	-1.0692	1.6425	0.5151	-0.9962	0.3814
PsimOR5	0.4942	0.6163	0.4227	0.4152	0.4609
PsimOR50	0.229	4.0805	0.9553	1.6045	1
PsimOR6	-0.0086	0.5823	0.9882	-0.0515	1
PsimOR7	0.161	0.4781	0.7363	0.1071	0.8517
PsimOR8	0.4963	0.6856	0.4692	0.3467	0.6466
PsimOR9	2.0761	0.9969	0.0373	1.8932	0.0303

Table S15. Differential sensitivity of *P. simplex* workers and soldiers to neocembrene inferred from EAG responses to the dose of 10 ng. Related to Fig. 7.

EAG response normalized to air stimulation		$\log_2$ value	
worker	soldier	worker	soldier
199.52	92.67	7.64	6.53
322.81	116.73	8.33	6.87
132.44	136.93	7.05	7.10
142.77	78.81	7.16	6.30
124.07	120.01	6.96	6.91
135.73	120.49	7.08	6.91
192.41	136.59	7.59	7.09
146.41	116.43	7.19	6.86
122.17	176.51	6.93	7.46
201.83	122.48	7.66	6.94
123.71	110.96	6.95	6.79
142.15	139.64	7.15	7.13
115.99	138.32	6.86	7.11
164.7	132.45	7.36	7.05
167.08	152.31	7.38	7.25

Table S16. List of primers.

Primer Name	Sequence (5' to 3' direction)	Use
PsimOR14_F	ATGATTCGATCAAAGAGAAAGG	Cloning
PsimOR14_R	TTAGGAGTCGTGTAGATGAAT	Cloning
PsimO31_F	ATGGAATACATAAAAAATGAAACATATTCTCA	Cloning
PsimO31_R	TCAACCTACGACATGTGAGTTATT	Cloning
PsimOR9_F	ATGGACAGCCTTTACGACCAATCTT	Cloning
PsimOR9_R	TCATTCAGTGACTGAGGGATCCTT	Cloning
PsimO30_F	ATGGAGCACAGGAAATACAAAGTGACAA	Cloning
PsimO30_R	TTACGTTCCCTGATTTGTGTCGGTAT	Cloning
PsimOrco_F	ATGTACAAGTTCAGGTTACACG	cDNA check
PsimOrco_R	CTAGTTGAGCTGTACCAACAC	cDNA check
GW1	GTTGCAACAAATTGATGAGCAATGC	Sanger Sequencing & Colony PCR
GW2	GTTGCAACAAATTGATGAGCAATTA	Sanger Sequencing & Colony PCR
UAS1	TAGCGAGCGCCGGAGTATAAATAG	Sanger Sequencing
UAS2	ACTGATTTCGACGGTTACCC	Sanger Sequencing
DmOr22a_F	TCTCCAGCATCGCCGAGTGT	Single-Wing PCR
DmOr22a_R	CGGCAGAGGTCCAGTCCGAT	Single-Wing PCR
PsimOR14_SW_F	GAGAGCCAAGCAAACGAAAC	Single-Wing PCR
PsimOR14_SW_R	TTTAGAAGGGAGCCACATCAC	Single-Wing PCR
PsimO31_SW_F	GCTGGGTTAATCCCGATCAT	Single-Wing PCR
PsimO31_SW_R	GCATGGCACCAAATAGTTCTTC	Single-Wing PCR
PsimOR9_SW_F	TGGGCGAAACTGAGGATATG	Single-Wing PCR
PsimOR9_SW_R	CGAGCCGACATAGAAGAAGAG	Single-Wing PCR
PsimO30_SW_F	TGCCATCACCAGCAGATAAA	Single-Wing PCR
PsimO30_SW_R	CACCGACTGACTCAGCATATT	Single-Wing PCR

Table S17. Characteristics and origin of *D. melanogaster* lines used.

Fly line	Source
w^{1118}	Biology Centre CAS Czech Republic
w-; Bl/Cyo; TM2/TM6B	MPI-Jena, Germany
w; $Or22ab^{GAL4}$	Benton Lab, Switzerland
w-; +/+; UAS-OR(w+)/UAS-OR(w+)	BestGene Inc, USA

Table S18. Origin of chemicals.

Panel	Compound	Provider	Purity
1	*n*-eicosane	Merck	99%
1	*n*-docosane	Merck	99%
1	1-octadecanol	Merck	99%
1	(3*Z*)-dodecen-1-ol	IOCB	in house synthesis, see supplementary methods, GC purity 95%
1	(3*Z*,6*Z*)-dodecadien-1-ol	IOCB	in house synthesis, see supplementary methods, GC purity 94%
1	(3*Z*,6*Z*,8*E*)-dodecatrien-1-ol	IOCB	in house synthesis, see supplementary methods, GC purity 96%
1	dodec-3-yn-1-ol	IOCB	in house synthesis, see supplementary methods,GC purity 93%
1	*δ*-cadinene	Chemenu	95%
1	(3*R*,6*E*)-nerolidol	IOCB	in house synthesis (Havlíčková et al. 2019), 96%
1	neocembrene	IOCB	purified from natural resource (Sillam-Dussès et al., 2005), GC purity 96%
1	geranylgeraniol	Merck	98%
2	myrcene	Sigma Aldrich	≥90%
2	eucalyptol	Sigma Aldrich	99%
2	(+)-3-carene	Sigma Aldrich	90%
2	(+)-limonene	Thermo-Fisher	97%
2	(+)-α-pinene	Sigma Aldrich	98%
2	p-cymene	Sigma Aldrich	99%
2	γ-terpinene	Sigma Aldrich	97%
2	(-)-β-caryophyllene	Sigma Aldrich	98%
2	(+)-longifolene	Phyto Lab	≥90%
2	terpinolene	Sigma Aldrich	≥85%
2	toluene	VWR Chemicals	99%
2	(2*E*)-hexenal	Thermo-Fisher	98%
2	sabinene	Chemenu	≥95%
2	pentyl acetate	Sigma Aldrich	≥99%
2	ethyl acetate	VWR Chemicals	99%
2	γ-nonalactone	Sigma Aldrich	98%
2	heptanal	Thermo-Fisher	98%
2	isoamyl propionate	Sigma Aldrich	≥98%
2	ethanol	VWR Chemicals	≥99%
2	(2*E*)-hexen-1-ol	Sigma Aldrich	96%
3	*β*-bisabolene	Thermo-Fisher	96%
3	(*E*)-myrcenol	FytoFarm	95%
3	(-)-trans-pinocarveol	Sigma Aldrich	≥96%
3	isoamyl acetate	Sigma Aldrich	≥99%
3	2-phenylethyl acetate	J&K Scientific Ltd.	≥98%
3	α-camphorene	Synergy Ltd	≥90%
3	(*E*)-β-ocimene	TRC Canada	98%
3	nonan-1-ol	Thermo-Fisher	95%
3	octan-1-ol	Honey well	99%
3	benzyl alcohol	Thermo-Fisher	99%
3	p-cresol	Sigma Aldrich	≥99%
3	cryptone	Chemenu	≥95%
3	(+)-cis-carveol	BOC Sciences	95%
3	methyl jasmonate	Sigma Aldrich	≥98%
3	eucarvone	MuseChem	≥95%
3	ethyl (2*E*,4*Z*)-decadienoate	Sigma Aldrich	95%
4	(-)-verbenone	Merck	94%
4	acetophenone	Sigma Aldrich	99%
4	2-phenylethanol	Acros organics	99%
4	(±)-myrtenol	Sigma Aldrich	95%
4	geranyl acetone	Sigma Aldrich	≥97%
4	oct-1-en-3-ol	Thermo-Fisher	98%
4	4-vinylanisole	Sigma Aldrich	97%
4	4-ethylguaiacol	Sigma Aldrich	≥98%
4	hexan-1-ol	Sigma Aldrich	99%
4	oct-1-en-3-ol	Sigma Aldrich	≥97%
4	styrene	Thermo-Fisher	99%
4	2,3-dihydrobenzofuran	Thermo-Fisher	99%
4	2-methylbutan-1-ol	J&K Scientific Ltd.	98%
4	2-methylbutyl acetate	Sigma Aldrich	99%
4	4-methylanisole	Sigma Aldrich	97%
4	linalool	Thermo-Fisher	97%
4	methyleugenol	Sigma Aldrich	98%
4	(±)-camphor	Sigma Aldrich	≥95%
4	benzaldehyde	Sigma Aldrich	≥99%
4	isoamyl alcohol	VWR Life Science	≥98%

SUPPLEMENTARY METHODS

Organic synthesis

Unless noted otherwise, all reactions were carried out under argon in oven-dried glassware. Solvents were distilled from drying agents as indicated and transferred under nitrogen: THF (Na/benzophenone), toluene (Na/benzophenone). All starting materials were used as purchased (Sigma Aldrich, Combi-Blocks), unless otherwise indicated. Chromatography was performed using Fluka silica gel 60 (0.040 - 0.063 mm). For TLC analysis, F254 – coated aluminum sheets were used. The spots were detected both in UV and by the solution of $Ce(SO_4)_2 \cdot 4H_2O$ (1%) and $H_3P(Mo_3O_{10})_4$ (2%) in 10% sulfuric acid. ^1H- and ^{13}C NMR spectra were recorded at 400 MHz and 100 MHz, respectively, with a Bruker 400 MHz instrument at 25 °C (the solvents are indicated in parentheses). Chemical shifts are reported in ppm relative to TMS. The residual solvent signals in the ^1H and ^{13}C NMR spectra were used as an internal reference ($CDCl_3$: δ = 7.26 for ^1H and δ = 77.23 for ^{13}C). The compounds were analyzed using the gas chromatograph TRACE 1310 (ThermoFisher Scientific, Waltham, MA, USA), equipped with a nonpolar Zebron ZB-5MS column (30 m × 0.25 mm × 0.25 µm film; Phenomenex, Torrance, CA, USA) connected to a ThermoFisher Scientific ISQ LT mass-selective detector (70eV ionization voltage, source temperature 200 °C, transferline heated to 260 °C). The column temperature was held at 50 °C for 1 min, gradually increased to 320 °C at 8 °C/min and then held at 320 °C for 20 min. Helium was used as carrier gas at a flow 1.2 mL/min. Split/splitless port was heated to 200 °C, and samples were injected in splitless mode with a purge time of 1 min.

Scheme 1.

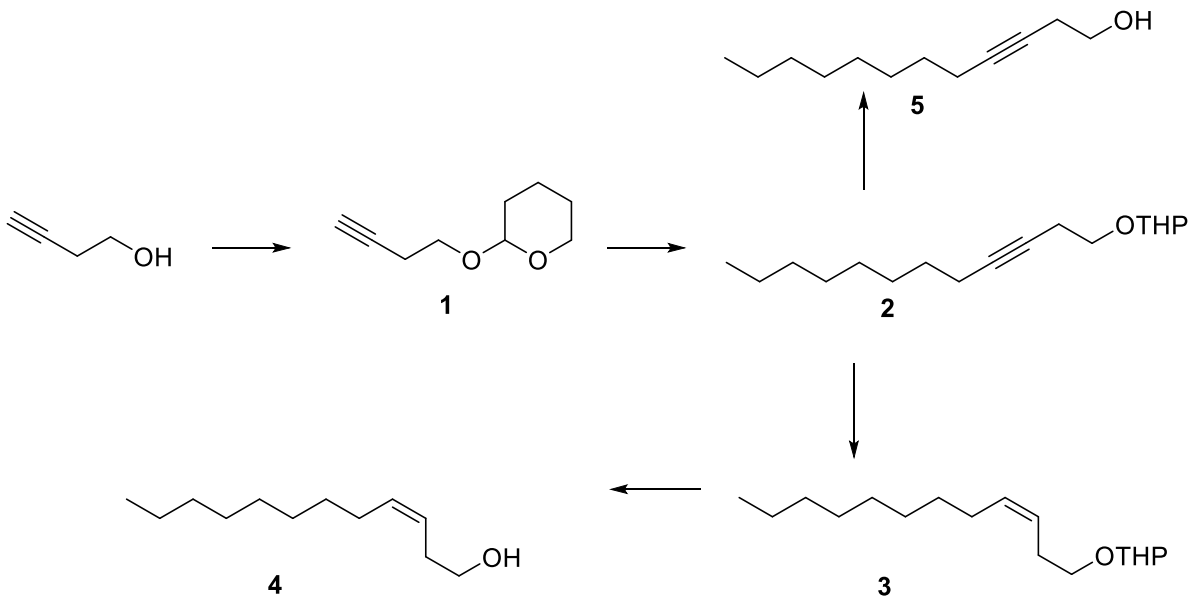

2-(But-3-yn-1-yloxy)tetra-2H-hydropyran (Allegretti & Ferreira, 2011) (1)

To a solution of 3-butyn-1-ol (3.0 g; 42.79 mmol) in DCM (100 mL) at 0 °C was added 3,4-dihydro-2*H*-pyran (3.78 g; 44.93 mmol) followed by addition of *p*-toluenesulfonic acid monohydrate (0.080 g; 0.427 mmol). After stirring at 0 °C for 5 min, the reaction was warmed to room temperature and stirred for 90 min. The reaction was quenched with saturated solution of $NaHCO_3$ (20 mL), and the layers were separated. The aqueous layer was extracted with DCM (50 mL), and the combined organic layers were dried over $MgSO_4$ and concentrated in vacuo. The residue was purified by a column chromatography (silica gel; cyclohexane/EtOAc 4:1) to give **4** as colorless oil (0.53 g, 64%). ^{1}H NMR (401 MHz, $CDCl_3$) δ 4.67 (dd, *J* = 4.2, 2.9 Hz, 1H), 3.97 – 3.81 (m, 2H), 3.65 – 3.49 (m, 2H), 2.52 (td, *J* = 7.0, 2.7 Hz, 2H), 2.00 (t, *J* = 2.7 Hz, 1H), 1.93 – 1.78 (m, 1H), 1.78 – 1.69 (m, 1H), 1.69 – 1.46 (m, 4H). EI-MS (70 eV): *m/z* (%): 153 (1.4), 125 (2), 99 (9), 85 (100), 79 (9), 67 (21), 53 (33), 41 (22).

2-(Dodec-3-yn-1-yloxy)tetrahydro-2*H*-pyran (2)

To a solution of acetylene **1** (1.0 g; 6.48 mmol) in THF (10 mL) at -40 °C under argon atmosphere was added *n*-BuLi (2.6 mL, 2.5 M in hexanes, 6.5 mmol), followed with addition of HMPA (1 mL) and the resulting solution was stirred for 40 min at -40 °C. Then a solution of octyl bromide (1.25 g; 6.48 mmol) in THF (2.00 mL) was added rapidly. The resulting mixture was stirred at -40 °C for 60 min, and then warmed to room temperature and stirred for 2 h. The reaction mixture was quenched by addition of water (10 mL) and was diluted with EtOAc (20 mL). The layers were separated, and the aqueous layer was extracted with EtOAc. The combined organic layers were washed with water and brine and concentrated under reduced pressure. The residue was purified by a column chromatography (silica gel; cyclohexane/EtOAc 9:1) to give **2** as colorless oil (1.12 g, 86%). ^{1}H NMR (401 MHz, $CDCl_3$) δ 4.67 (dd, *J* = 4.2, 2.9 Hz, 1H), 3.91 (ddd, *J* = 11.2, 8.1, 3.3 Hz, 1H), 3.82 (dt, *J* = 9.7, 7.2 Hz, 1H), 3.61 – 3.47 (m, 2H), 2.48 (tt, *J* = 7.2, 2.4 Hz, 2H), 2.16 (tt, *J* = 7.1, 2.4 Hz, 2H), 1.94 – 1.79 (m, 1H), 1.74 (tdd, *J* = 9.2, 3.9, 2.9 Hz, 1H), 1.67 – 1.43 (m, 6H), 1.43 – 1.24 (m, 10H), 0.95 – 0.86 (m, 3H). ^{13}C NMR (101 MHz, $CDCl_3$) δ 98.7, 81.4, 66.3, 62.2, 31.9, 30.6, 29.2, 29.2, 29.0, 28.9, 25.5, 20.3, 19.4, 18.8, 14.1. EI-MS (70 eV): *m/z* (%): 265 (0.002), 211 (0.4), 195 (0.7), 153 (2), 115 (4), 101 (7), 85 (100), 81 (8), 67 (17), 55 (13), 41 (12).

2-[((*Z*)-Dodec-3-enyl)oxy)]-tetrahydro-2*H*-pyran (3)

To a solution of borane-dimethylsulfide complex (0.44 g; 5.78 mmol) in THF (10 mL) at -10 °C under argon atmosphere cyclohexane (0.95 g; 11.57 mmol) was added. After the addition was complete, the mixture was slowly warmed to room temperature over 3 hr, yielding a white slurry. The mixture was cooled to -20 °C and a solution of substrate 2 (0.77 g; 2.89 mmol) in THF (3 mL) was added dropwise. The reaction mixture was slowly warmed to 0 °C over 3 hr, and stirred at 0 °C for a further 3 hr. Then acetic acid (1.40 g; 23.1 mmol) was then added dropwise, and the reaction mixture was stirred overnight. The reaction mixture was cooled to 0 °C, and a solution of NaOH (1.9 g) in water (8 mL) was added over 10 min, followed by dropwise addition of hydrogen peroxide (0.7 mL, 30% solution in water). The stirred mixture was warmed to room temperature and poured in into water. Crude product extracted with cyclohexane and then concentrated under reduced pressure. The residue was purified by column chromatography (silica gel; cyclohexane/EtOAc 9:1) to provide **3** as colorless oil (0.71 g, 91%). ^{1}H NMR (401 MHz, $CDCl_3$) δ 5.56 – 5.28 (m, 2H), 4.63 (dd, *J* = 4.4, 2.7

Hz, 1H), 3.97 – 3.85 (m, 1H), 3.75 (dt, *J* = 9.5, 7.2 Hz, 1H), 3.61 – 3.48 (m, 1H), 3.48 – 3.36 (m, 1H), 2.46 – 2.32 (m, 2H), 2.06 (td, *J* = 7.1, 1.3 Hz, 2H), 1.86 (ddt, *J* = 10.7, 7.8, 5.3 Hz, 1H), 1.80 – 1.70 (m, 1H), 1.69 – 1.50 (m, 4H), 1.38 – 1.28 (m, 10H), 0.94 – 0.87 (m, 3H). ^{13}C NMR (101 MHz, $CDCl_3$) δ 132.1, 125.4, 98.8, 67.1, 62.3, 31.9, 30.7, 29.7, 29.5, 29.4, 29.2, 28.90, 27.4, 22.7, 19.6, 14.1. EI-MS (70 eV): *m/z* (%): 268 (0.1), 166 (3), 115 (2), 101 (15), 85 (100), 67 (13), 55 (11), 41 (8).

(*Z*)-Dodec-3-en-1-ol (4)

A mixture of *Z*-alkene **3** (0.71 g; 2.64 mmol), and *p*-toluenesulfonic acid monohydrate (0.025 g; 0.13 mmol) in methanol (2 mL) was stirred at room temperature for 3 hr. Then the reaction mixture was poured into an ice-cold solution of sodium bicarbonate and was extracted with diethyl ether (2×10 mL). The combined organic layers were washed with brine (5 mL), dried over $MgSO_4$ and evaporated. The residue was purified by column chromatography (silica gel; cyclohexane/EtOAc 9:1) to provide **4** as colorless oil (0.43 g, 87%). ^{1}H NMR (401 MHz, $CDCl_3$) δ 5.66 – 5.48 (m, 1H), 5.46 – 5.31 (m, 1H), 3.67 (t, *J* = 6.5 Hz, 2H), 2.40 – 2.32 (m, 2H), 2.13 – 1.98 (m, 2H), 1.43 – 1.21 (m, 12H), 0.97 – 0.86 (m, 3H). ^{13}C NMR (101 MHz, $CDCl_3$) δ 133.6, 124.9, 62.4, 31.9, 30.8, 29.7, 29.5, 29.3, 29.3, 27.4, 22.7, 14.1. EI-MS (70 eV): *m/z* (%): 184 (0.1), 166 (5), 138 (6), 124 (8), 110 (18), 96 (39), 81 (79), 68 (100).

Dodec-3-yn-1-ol (5)

A mixture of THP-protected alkyne **2** (0.30 g; 1.12 mmol), and *p*-toluenesulfonic acid monohydrate (0.04 g; 0.022 mmol) in methanol (5 mL) was stirred at room temperature for 3 hr. Then the reaction mixture was poured into an ice-cold solution of sodium bicarbonate and was extracted with diethyl ether (2×10 mL). The combined organic layers were washed with brine (5 mL), dried over $MgSO_4$ and evaporated. The residue was purified by column chromatography (silica gel; cyclohexane/EtOAc 4:1) to provide **5** as colorless oil (0.20 g, 98%). ^{1}H NMR (401 MHz, $CDCl_3$) δ 3.70 (t, *J* = 6.2 Hz, 2H), 2.46 (tt, *J* = 6.2, 2.4 Hz, 2H), 2.18 (tt, *J* = 7.2, 2.4 Hz, 2H), 1.57 – 1.46 (m, 2H), 1.39 – 1.22 (m, 8H), 0.94 – 0.86 (m, 3H). ^{13}C NMR (101 MHz, $CDCl_3$) δ 82.9, 76.2, 61.4, 31.8, 29.2, 29.1, 29.0, 28.9, 23.2, 22.7, 18.8, 14.1.

Scheme 2.

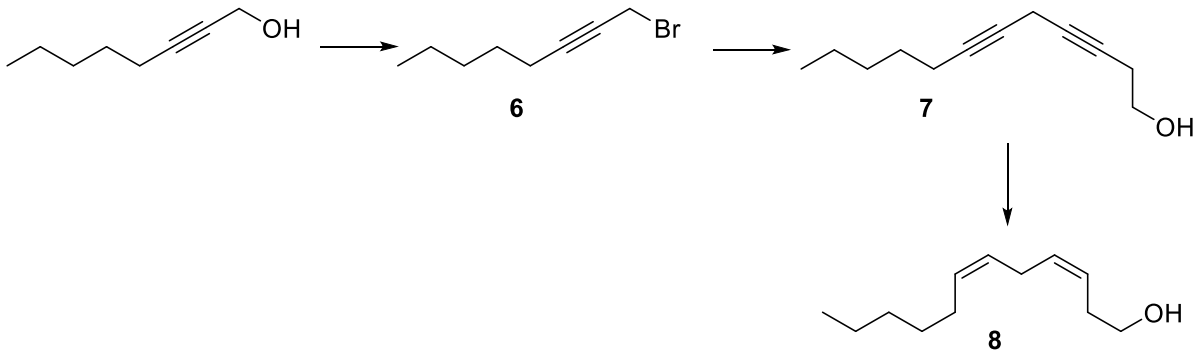

1-Bromooct-2-yne (6)

A mixture of 2-octynol (2.0 g; 15.87 mmol), triphenylphosphine (4.57 g; 17.46 mmol), and tetrabromomethane (6.30 g; 19.04 mmol) in DCM (40 mL) was stirred at 0 °C for 2 hr and then it was diluted with cyclohexane and filtered. The filtrate was evaporated, and a column chromatography (silica gel; eluent cyclohexane) of the residue afforded 3.70 g (90%) of bromide **5** as a pale oil. ^{1}H NMR (401 MHz, $CDCl_3$) δ 3.95 (t, *J* = 2.4 Hz, 2H), 2.25 (ddt, *J* = 7.2, 4.7, 2.4 Hz, 2H), 1.59 – 1.46 (m, 2H), 1.44 – 1.27 (m, 4H), 0.96 – 0.88 (m, 3H). ^{1}H NMR data match published spectrum (Sigurjónsson & Haraldsson, 2024).

Dodeca-3,6-diyn-1-ol (Liu et al. 2018) (7)

To a stirred solution of but-3-yn-1-ol (0.90 g; 12.76 mmol) in anhydrous DMF (30 mL) under an argon atmosphere at room temperature was added cesium carbonate (3.45 g; 10.63 mmol), sodium iodide (1.60 g; 10.63 mmol) and copper(I) iodide (2.02 g; 10.63 mmol). The reaction mixture was stirred for 30 min. Then a solution of 1-bromooct-2-yne (2.0 g; 10.63 mmol) in anhydrous DMF (10 mL) was added dropwise and stirring was continued for another 2 hr. The reaction mixture was quenched by addition of saturated aqueous NH_4Cl and extracted with Et_2O. The combined organic layers ware washed with water, brine, and concentrated under reduced pressure. The residue was purified by a column chromatography (silica gel; cyclohexane/EtOAc 4:1) to provide diynol **7** as colorless oil (0.90 g, 45%). ^{1}H NMR (401 MHz, $CDCl_3$) δ 3.73 (t, *J* = 6.2 Hz, 2H), 3.16 (t, *J* = 2.4 Hz, 2H), 2.47 (tt, *J* = 6.2, 2.4 Hz, 2H), 2.17 (tt, *J* = 7.2, 2.4 Hz, 2H), 1.56 – 1.46 (m, 2H), 1.43 – 1.22 (m, 4H), 0.98 – 0.85 (m, 3H). EI-MS (70 eV): *m/z* (%): 178 (0.2), 163 (0.7), 149 (2), 135 (4), 121 (14), 117 (20), 105 (37), 91 (100), 79 (41).

(3*Z*,6*Z*)-Dodeca-3,6-dien-1-ol (Liu et al. 2018) (8)

To a stirred suspension of $Ni(OAc)_2{\cdot}H_2O$ (0.81 g; 3.25 mmol) in EtOH (10 mL) under an argon atmosphere at room temperature was added $NaBH_4$ (0.12 g; 3.25 mmol). Then the flask was filled with hydrogen and balloon with hydrogen gas was attached to the reaction flask for the rest of the experiment. Ethylenediamine (0.78 g; 13.02 mmol) was added to the reaction mixture after 30 min and then the reaction mixture was stirred for another 30 min. Then a solution of diynol **7** (0.58 g; 3.25 mmol) in EtOH (2 mL) was added and the mixture was stirred for another 2 hr. The reaction mixture was diluted with water and EtOAc (5+5 mL) and the P-2 catalyst was filtered through a pad of Celite. The filtrate was concentrated under reduced pressure and partitioned between water and Et_2O. The organic layer was separated, the aqueous phase was extracted with Et_2O, and the combined organic layers were washed with brine and concentrated under reduced pressure. The residue was purified by a column chromatography (silica gel; cyclohexane/EtOAc 4:1) to provide dienol **8** as colorless oil (0.29 g, 49%). ^{1}H NMR (401 MHz, $CDCl_3$) δ 5.65 – 5.48 (m, 1H), 5.47 – 5.27 (m, 2H), 3.68 (t, *J* = 6.5 Hz, 2H), 2.89 – 2.75 (m, 2H), 2.44 – 2.32 (m, 2H), 2.13 – 1.99 (m, 2H), 1.47 – 1.22 (m, 6H), 0.98 – 0.86 (m, 3H). ^{13}C NMR (101 MHz, $CDCl_3$) δ 131.6, 130.7, 127.4, 125.3, 62.3, 31.5, 30.8, 29.3, 27.3, 26.9, 25.8, 22.6, 14.1. EI-MS (70 eV): *m/z* (%): 182 (2), 164 (5), 138 (5), 135 (8), 121 (16), 107 (19), 93 (48), 79 (100), 67 (66).

Scheme 3.

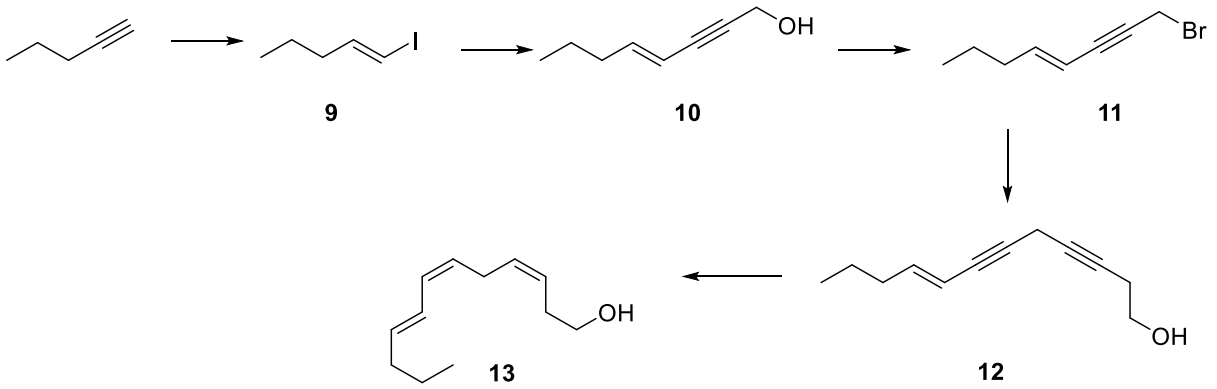

(*E*)-1-iodopent-1-ene (Saran et al., 2018) (9)

Diisobutylaluminum hydride in hexanes (1 M, 50 mL, 50 mmol) was added dropwise to a solution of pent-1-yne (3.7 g; 54 mmol) in hexanes cooled to -40 °C. The resulting mixture was stirred for 30 min, then slowly warmed to room temp over 3 hr, and was allowed to stir overnight. The mixture was warmed to ~50 °C for 4 hr, then cooled to -40 °C, and a solution of iodine (12.7 g; 50 mmol) in THF (20 mL) was added dropwise over 30 min. The resulting dark brown suspension was allowed to warm to room temperature with stirring overnight. The solution was cooled in an ice bath, and slowly quenched with dropwise addition of ice-cold diluted sulfuric acid (5 mL of 96% acid in 60 mL of water) with vigorous stirring. After stirring for 30 min, the layers were separated, and the organic layer was washed with dilute $NaHSO_3$ solution and brine and dried over $MgSO_4$. The resulting solution was filtered through a short pad of silica gel, rinsing with pentane. Obtained solution was concentrated by rotary evaporation without heating (rotavap was set to 100 Torr pressure). This procedure gave 12.24 g of crude alkenyl iodide **9** that was used in the next step. EI-MS (70 eV): *m/z* (%): 155 (4), 141 (3), 127 (5), 73 (69), 55 (100).

(*E*)-Oct-4-ene-2-yn-1-ol (Saran et al., 2018) (10)

To a mixture of bis(triphenylphosphine)palladium(II) dichloride (1.45 g; 2.0 mmol), copper(I) iodide (0.72 g; 3.8 mmol), and pyrrolidine (50 mL) under argon atmosphere the crude (*E*)-1-iodopent-1-ene (12.2 g) was added dropwise, followed by dropwise addition of propargyl alcohol (4.92 g; 87.8 mmol). The mixture was immersed into water bath until the exothermic reaction ended. After cooling the mixture to room temperature, the mixture was stirred for 3 hr. Then the reaction mixture was poured into an ice-cold mixture of saturated aqueous NH_4Cl and 2 M HCl (150+150 mL) and extracted several times with diethyl ether. The combined organic layers were washed with aqueous solution of citric acid (10% solution), water, brine, concentrated under reduced pressure. The residue was purified by a column chromatography (silica gel; eluent DCM) to provide alcohol **10** as colorless oil (2.22 g). ^{1}H NMR (401 MHz, $CDCl_3$) δ 6.19 (dt, *J* = 15.9, 7.1 Hz, 1H), 5.57 – 5.47 (m, 1H), 4.48 – 4.36 (m, 2H), 2.11 (qd, *J* = 7.2, 1.6 Hz, 2H), 1.71 – 1.51 (m, 1H), 1.45 (q, *J* = 7.4 Hz, 2H), 0.93 (t, *J* = 7.4 Hz, 3H). EI-MS (70 eV): *m/z* (%): 124 (74), 109 (14), 95 (44), 81 (100), 67 (49), 53 (33).

(*E*)-1-Bromooct-4-ene-2-yne (11)

To a stirred solution of alcohol **10** (2.22 g; 17.9 mmol) and triphenylphosphine (5.16 g; 19.7 mmol) in dry DCM (30 mL) under an argon atmosphere at 0 ºC was added solution of tetrabromomethane (7.12 g; 21.5 mmol) in dry DCM (10 mL). The reaction mixture was stirred at 0 ºC for 10 min and then an ice bath was removed, and the reaction mixture was allowed to stir for 3 hr. The reaction mixture was concentrated to half the volume and cyclohexane (30 mL) was added. The mixture was stirred for 30 min. Then the mixture was filtered through a pad of Celite, and the solvent was evaporated. A column chromatography (silica gel, eluent cyclohexane) of the residue gave 3.00 g (90%) of bromide **11** as colorless oil. ^{1}H NMR (401 MHz, $CDCl_3$) δ 6.22 (dt, *J* = 15.9, 7.1 Hz, 1H), 5.58 – 5.47 (m, 1H), 4.08 (d, *J* = 2.3 Hz, 2H), 2.12 (qd, *J* = 7.2, 1.6 Hz, 2H), 1.51 – 1.37 (m, 4H), 0.93 (t, *J* = 7.4 Hz, 3H). ^{13}C NMR (101 MHz, $CDCl_3$) δ 146.7, 108.8, 85.8, 82.5, 35.2, 26.9, 21.8, 15.8, 13.6. EI-MS (70 eV): *m/z* (%): 188 (21), 186 (23), 107 (100), 91 (55), 79 (49), 65 (66).

(*E*)-Dodeca-8-en-3,6-diyn-1-ol (12)

To a stirred solution of but-3-yn-1-ol (1.58 g; 22.58 mmol) in anhydrous DMF (30 mL) under an argon atmosphere at room temperature was added cesium carbonate (6.11 g; 18.81 mmol), sodium iodide (2.82 g; 18.81 mmol) and copper(I) iodide (3.57 g; 18.81 mmol). The reaction mixture was stirred for 30 min. Then a solution of bromide **11** (3.50 g; 18.81 mmol) in anhydrous DMF (10 mL) was added dropwise and stirring was continued for another 2 hr. The reaction mixture was quenched by addition of saturated aqueous NH_4Cl and extracted with Et_2O. The combined organic layers ware washed with water, brine, and concentrated under reduced pressure. The residue was purified by a column chromatography (silica gel; cyclohexane/EtOAc 3:1) to provide alcohol **12** as colorless oil (2.0 g, 60%). ^{1}H NMR (401 MHz, $CDCl_3$) δ 6.14 (dt, *J* = 15.9, 7.1 Hz, 1H), 5.52 – 5.42 (m, 1H), 3.73 (t, *J* = 6.2 Hz, 2H), 3.33 – 3.26 (m, 2H), 2.52 – 2.42 (m, 2H), 2.14 – 2.03 (m, 2H), 1.51 – 1.36 (m, 2H), 0.92 (t, *J* = 7.4 Hz, 3H). ^{13}C NMR (101 MHz, $CDCl_3$) δ 144.7, 109.3, 81.9, 79.4, 77.2, 76.3, 61.1, 35.1, 23.2, 21.9, 13.6, 10.4. HRMS (ESI): *m/z* calcd for $C_{12}H_{16}ONa^+$: 199.1093 $[M+Na]^+$; found: 199.1094. EI-MS (70 eV): *m/z* (%): 176 (4), 161 (3), 147 (14), 128 (36), 115 (67), 103 (45), 91 (100), 77 (62).

(3*Z*,6*Z*,8*E*)-Dodeca-3,6,8-trien-1-ol (13)

To a stirred suspension of $Ni(OAc)_2{\cdot}H_2O$ (1.41 g; 5.68 mmol) in EtOH (8 mL) under an argon atmosphere at room temperature was added a suspension of $NaBH_4$ (0.21 g; 5.68 mmol) in EtOH (5 mL). Then the flask was filled with hydrogen and balloon with hydrogen gas was attached to the reaction flask for the rest of the experiment. Ethylenediamine (1.36 g; 22.7 mmol) was added to the reaction mixture after 30 min and then the reaction mixture was stirred for another 30 min. Then a solution of diynol **12** (1.0 g; 5.68 mmol) in EtOH (2 mL) was added and the mixture was stirred for another 2 hr. The reaction mixture was diluted with water and EtOAc (5+5 mL) and the P-2 catalyst was filtered through a pad of Celite. The filtrate was concentrated under reduced pressure and partitioned between water and Et_2O. The organic layer was separated, the aqueous phase was extracted with Et_2O, and the combined organic layers were washed with brine and concentrated under reduced pressure. The residue was purified by a column chromatography (silica gel; cyclohexane/EtOAc 4:1) to provide trienol **13** as colorless oil (0.40 g, 40%). ^{1}H NMR (401 MHz,

$CDCl_3$) δ 6.42 – 6.25 (m, 1H), 6.12 – 5.93 (m, 1H), 5.72 (dt, *J* = 14.6, 7.0 Hz, 1H), 5.65 – 5.53 (m, 1H), 5.50 – 5.38 (m, 1H), 5.28 (dt, *J* = 10.6, 7.5 Hz, 1H), 3.69 (t, *J* = 6.5 Hz, 2H), 2.45 – 2.35 (m, 2H), 2.12 (qd, *J* = 7.5, 1.4 Hz, 2H), 1.51 – 1.44 (m, 2H), 0.94 (t, *J* = 7.3 Hz, 3H). ^{13}C NMR (101 MHz, $CDCl_3$) δ 135.5, 131.1, 129.1, 127.1, 125.7, 125.4, 62.3, 35.0, 30.9, 26.2, 22.5, 13.8. EI-MS (70 eV): *m/z* (%): 180 (13), 137 (8), 119 (20), 105 (41), 91 (100), 79 (75), 67 (42).

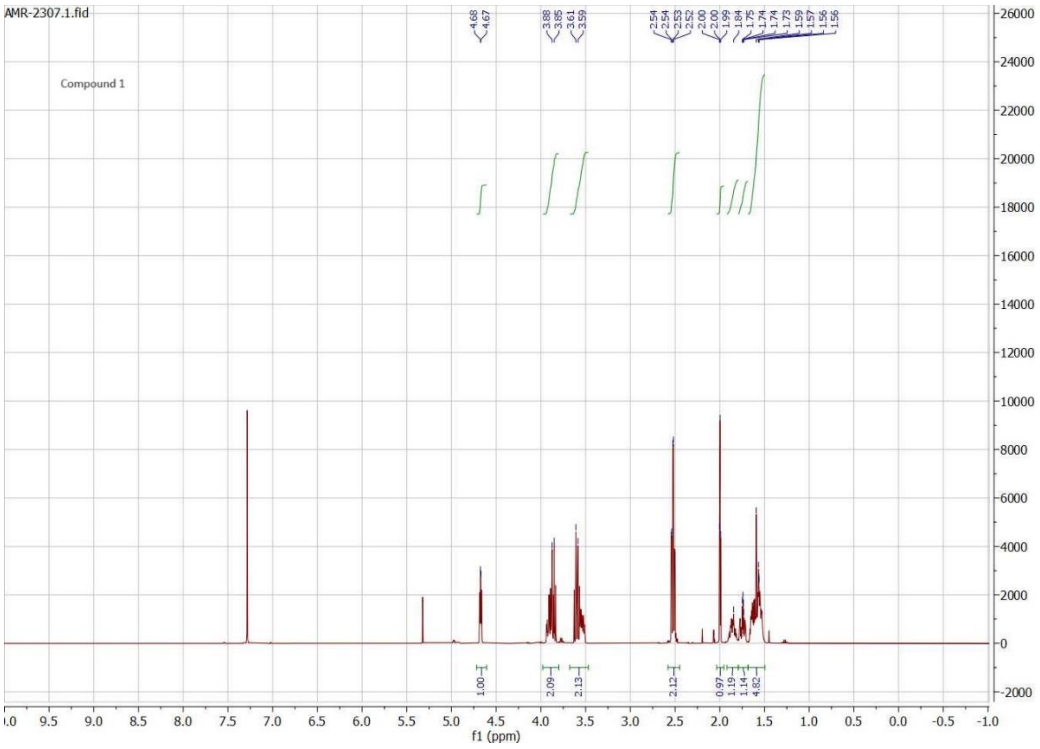

^{1}H NMR spectrum of the compound 1.

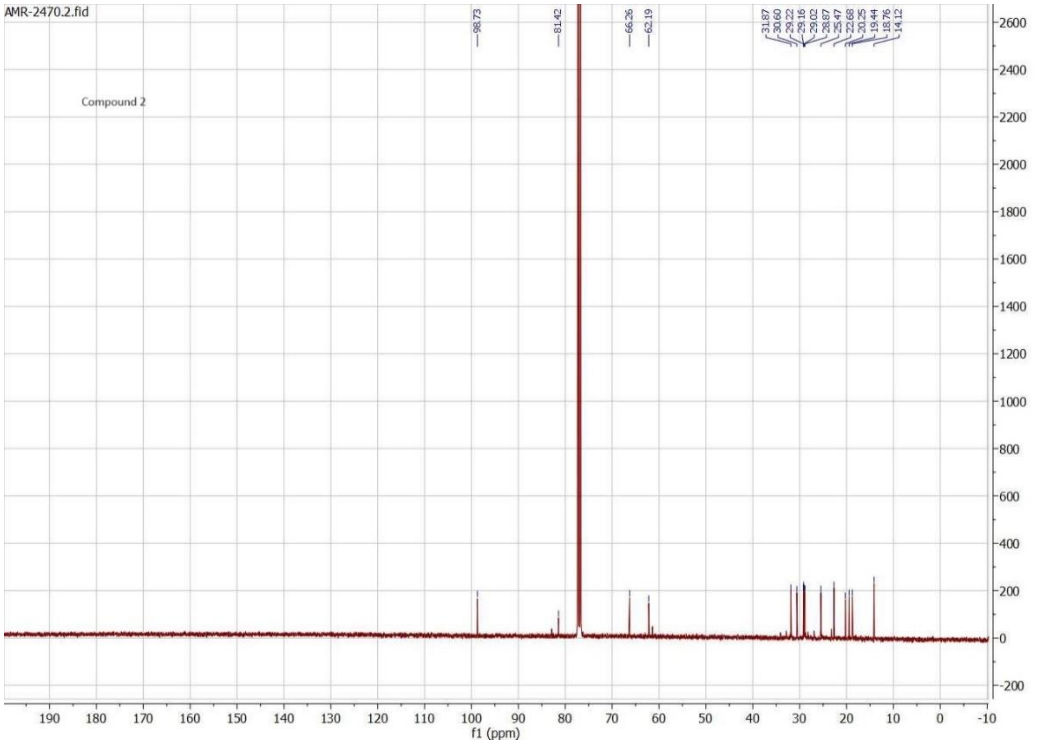

^{13}C NMR spectrum of the compound 2.

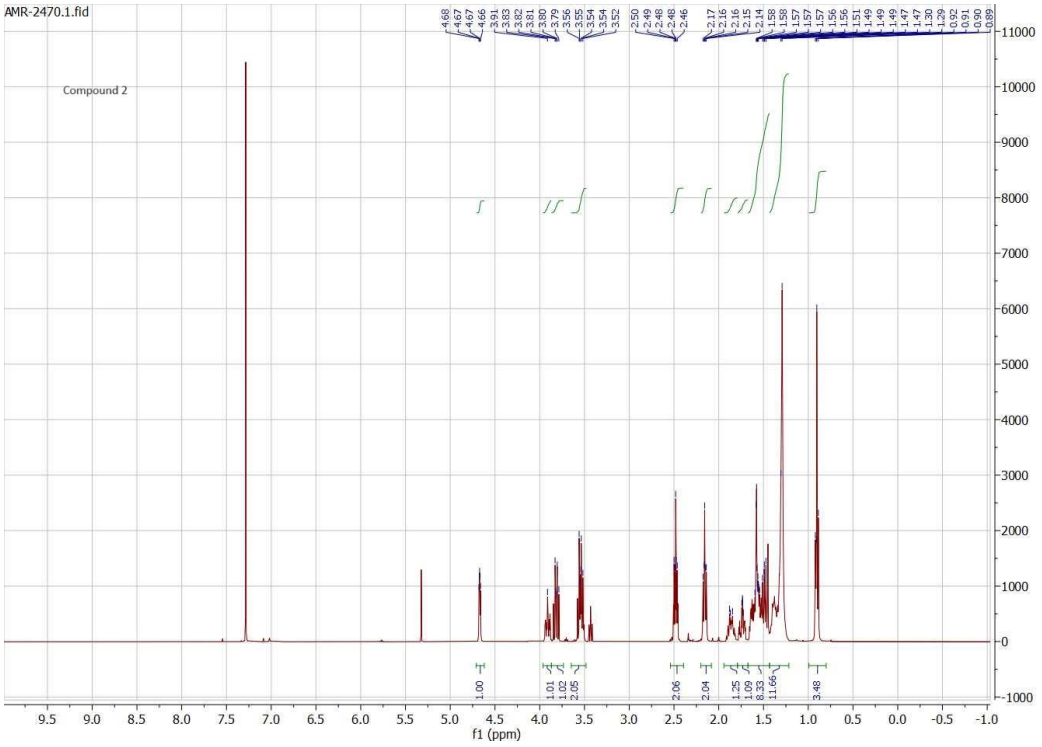

^{1}H NMR spectrum of the compound 2.

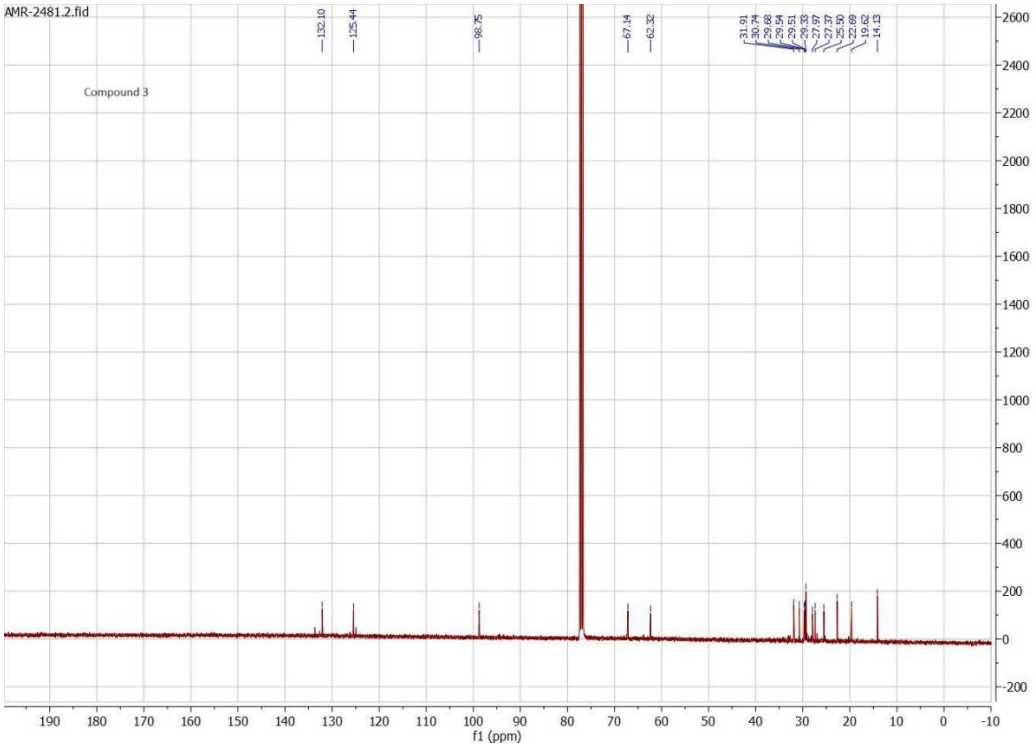

^{13}C NMR spectrum of the compound 3.

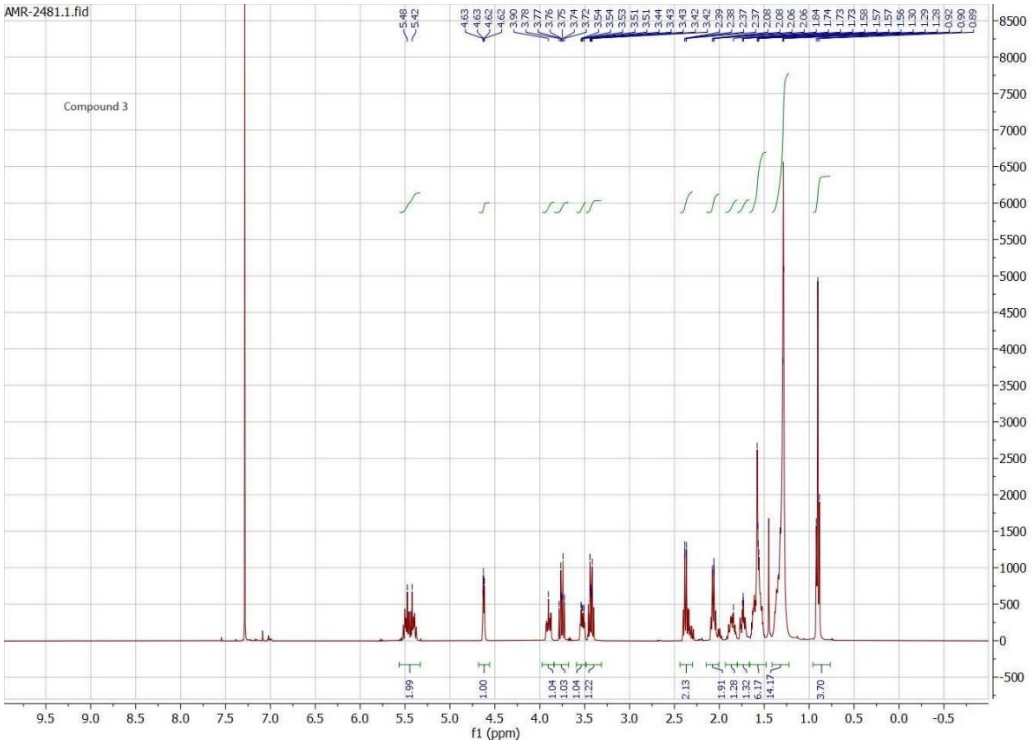

^{1}H NMR spectrum of the compound 3.

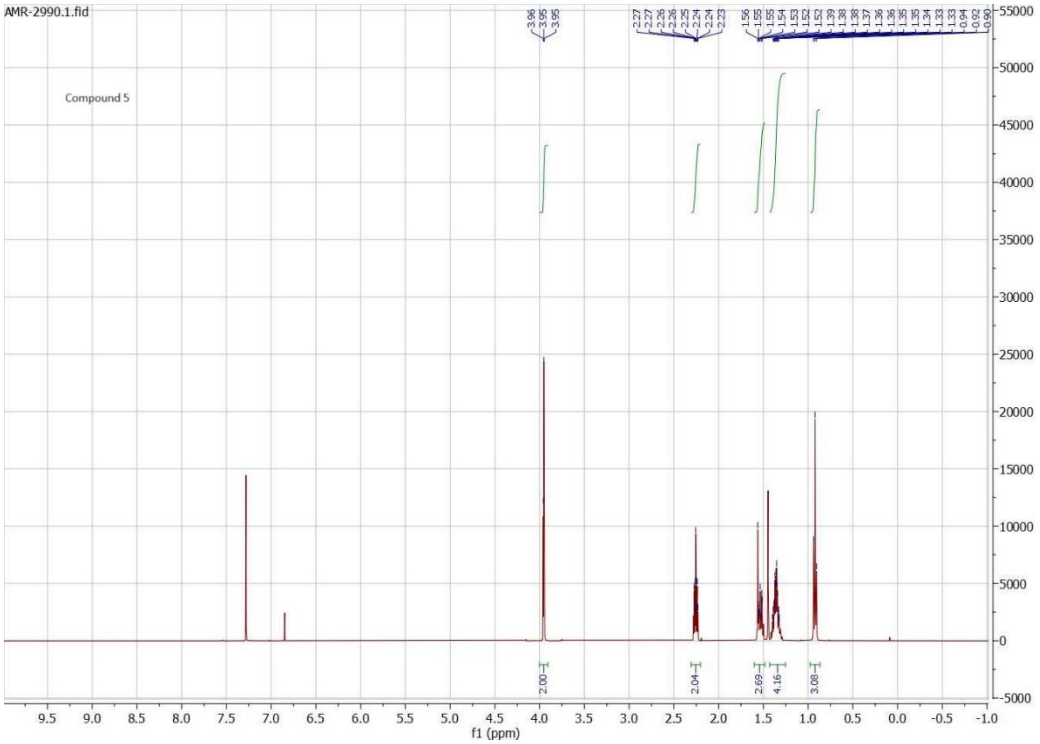

^{1}H NMR spectrum of the compound 5.

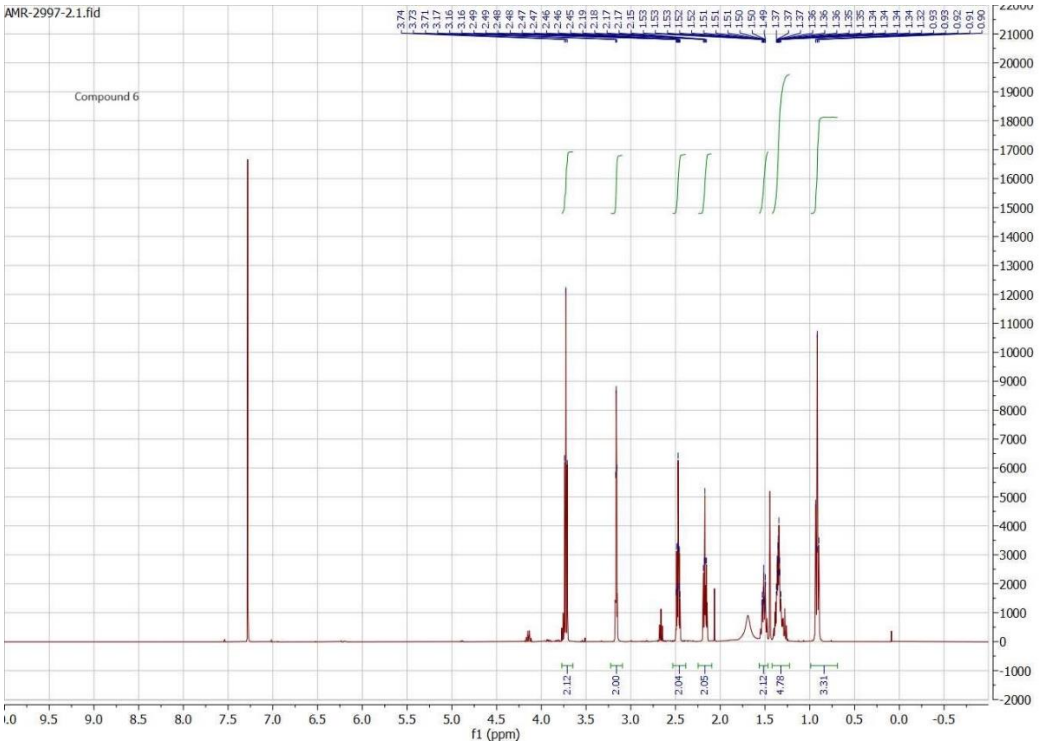

^{1}H NMR spectrum of the compound 6.

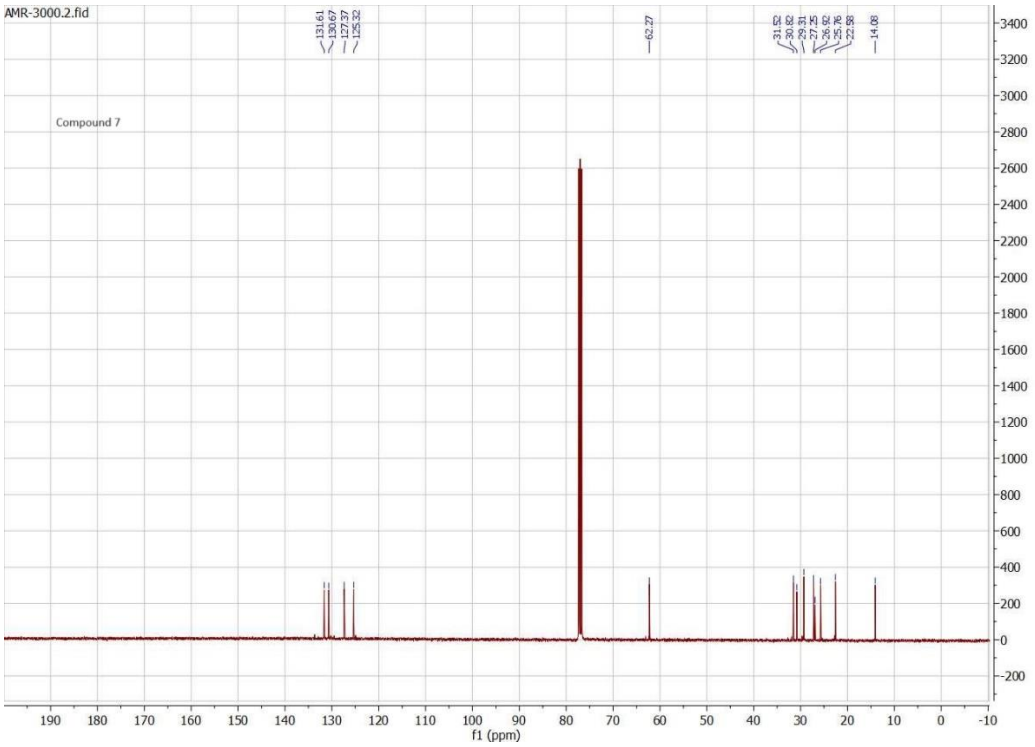

^{13}C NMR spectrum of the compound 7.

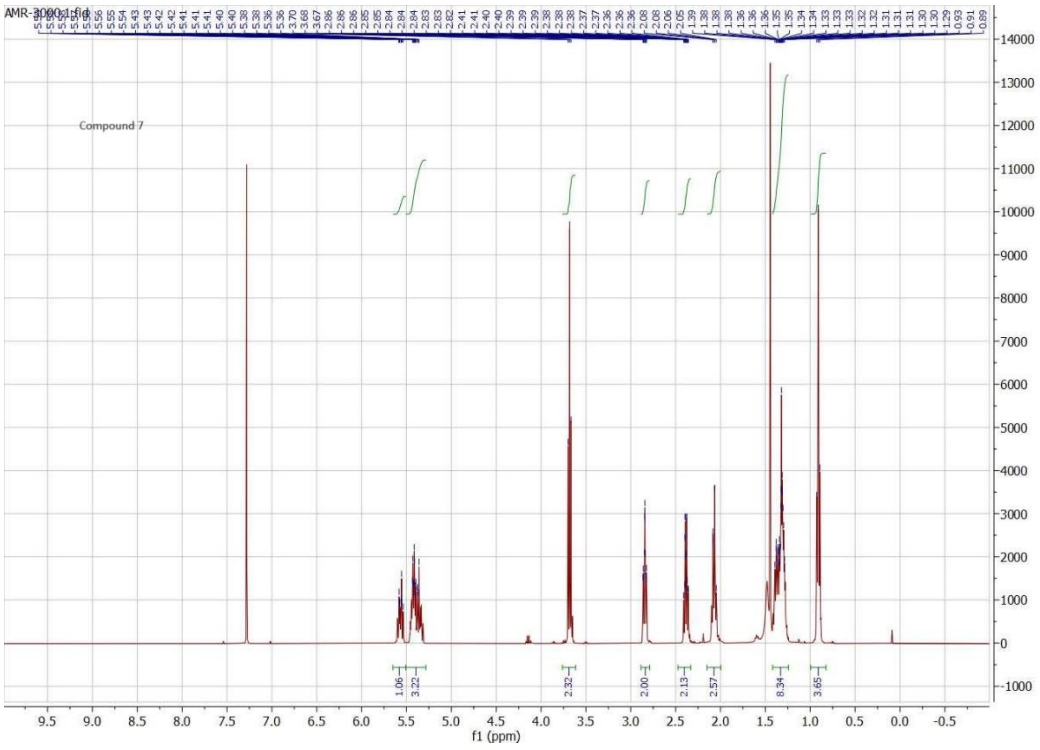

^{1}H NMR spectrum of the compound 7.

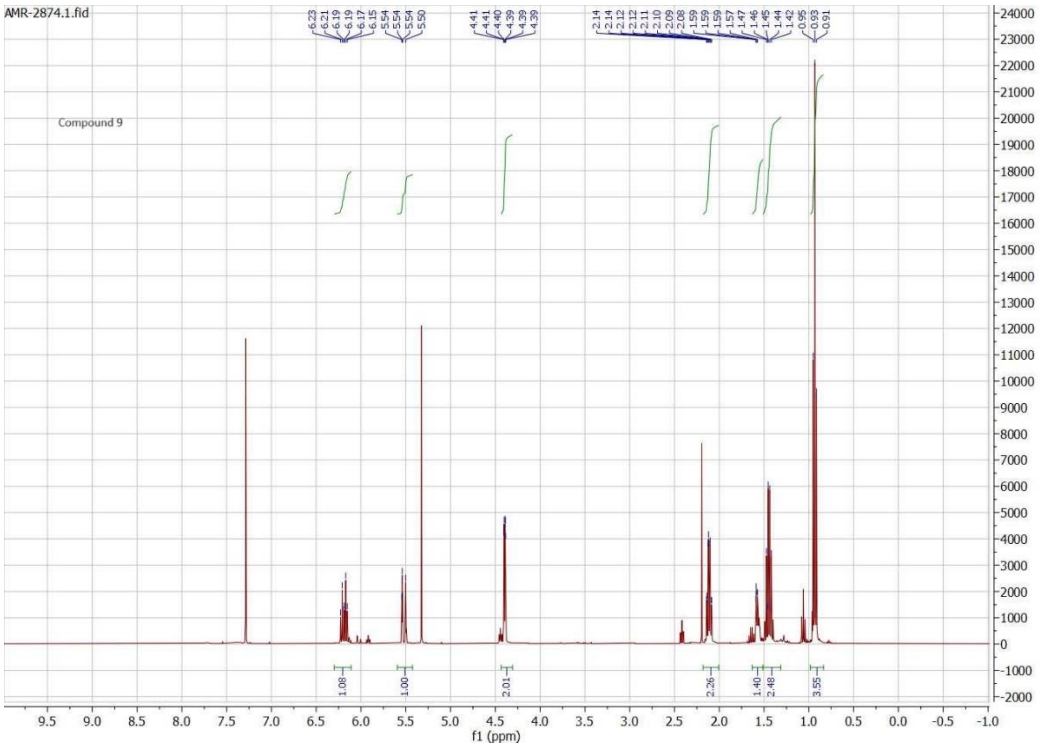

^{1}H NMR spectrum of the compound 9.

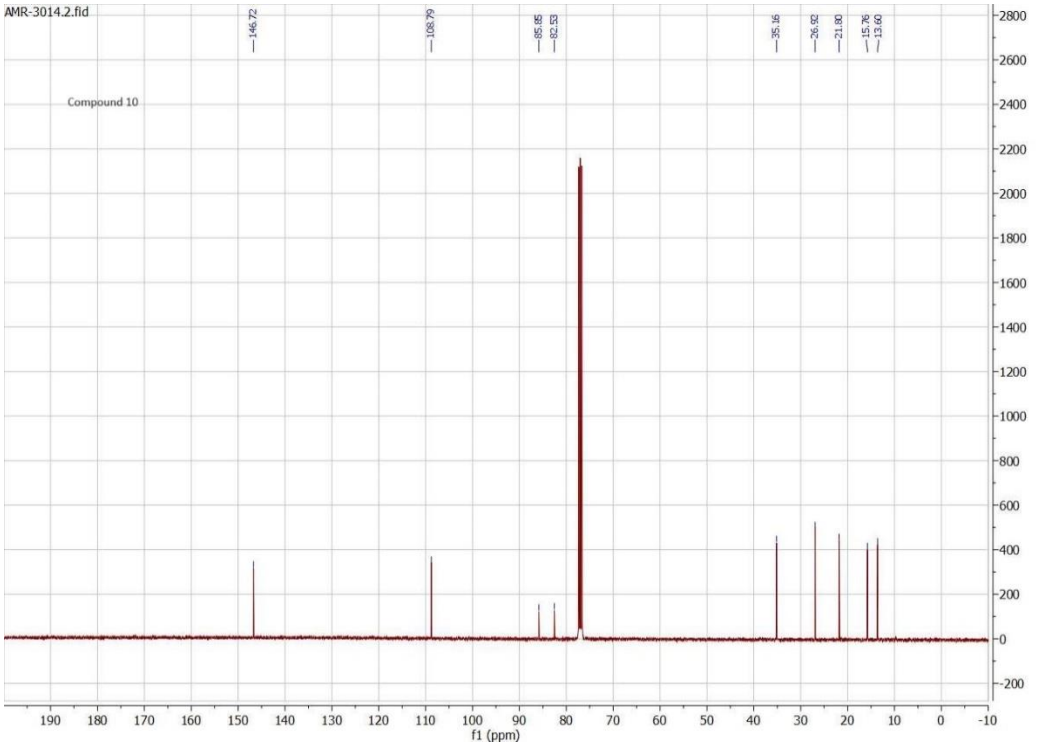

^{13}C NMR spectrum of the compound 10.

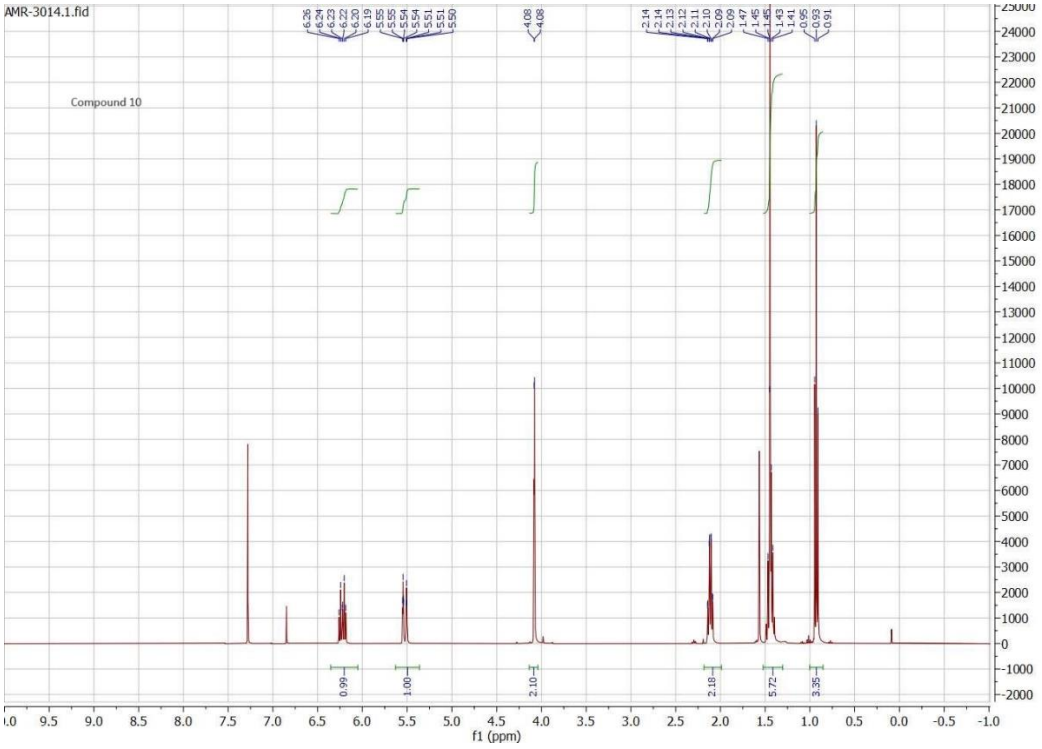

^{1}H NMR spectrum of the compound 10.

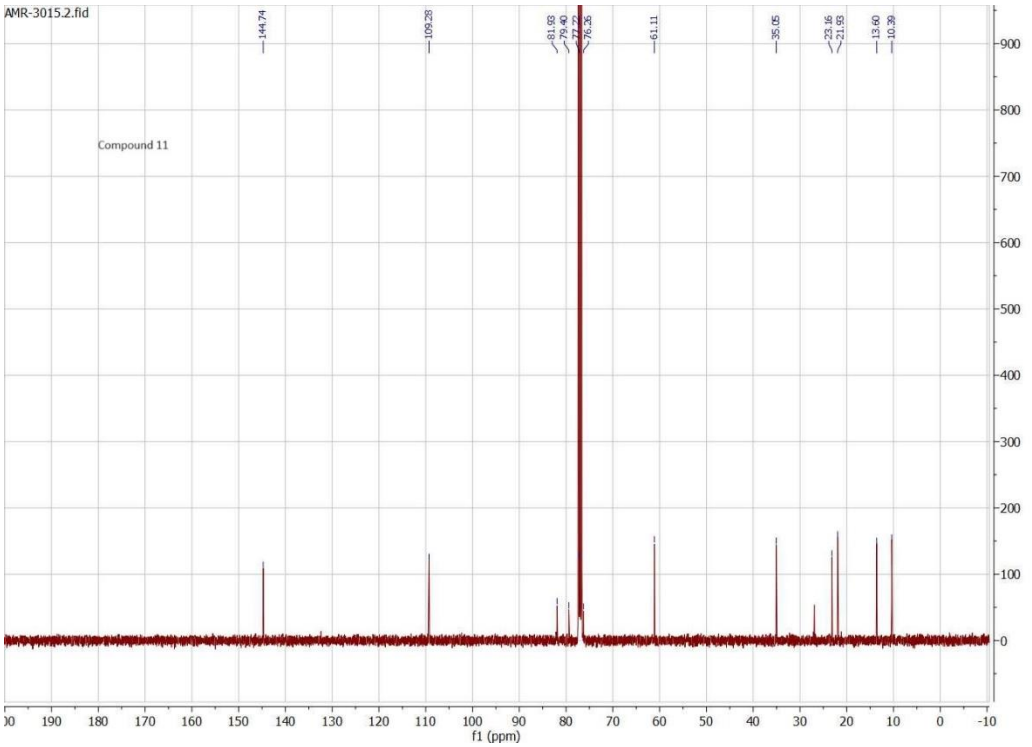

^{13}C NMR spectrum of the compound 11.

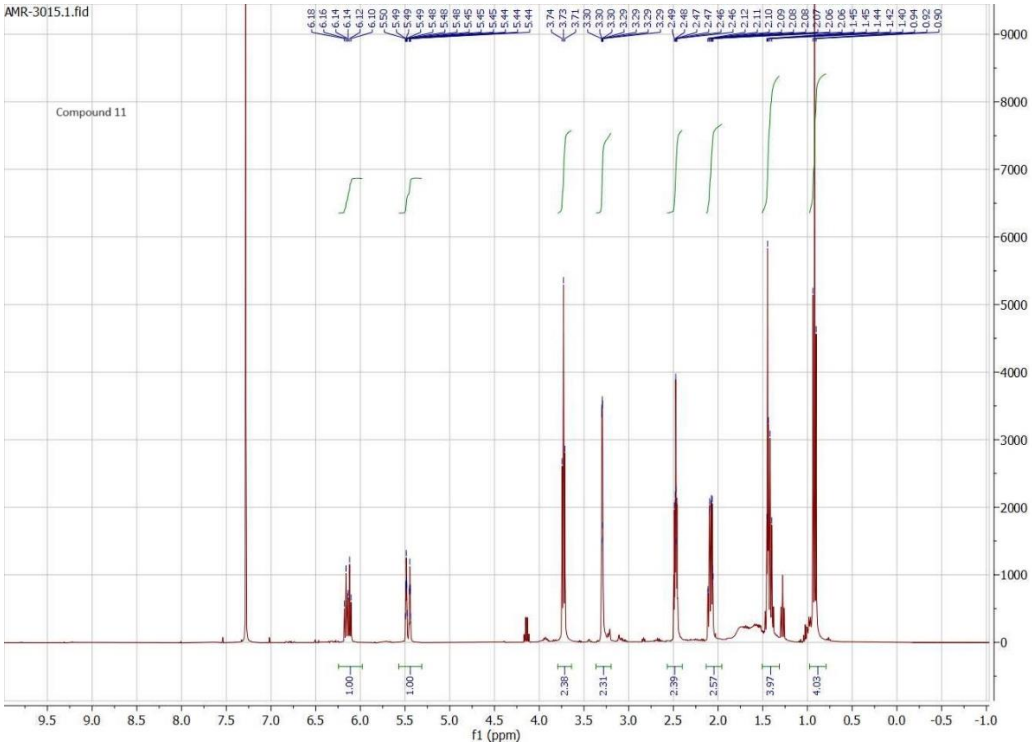

^{1}H NMR spectrum of the compound 11.

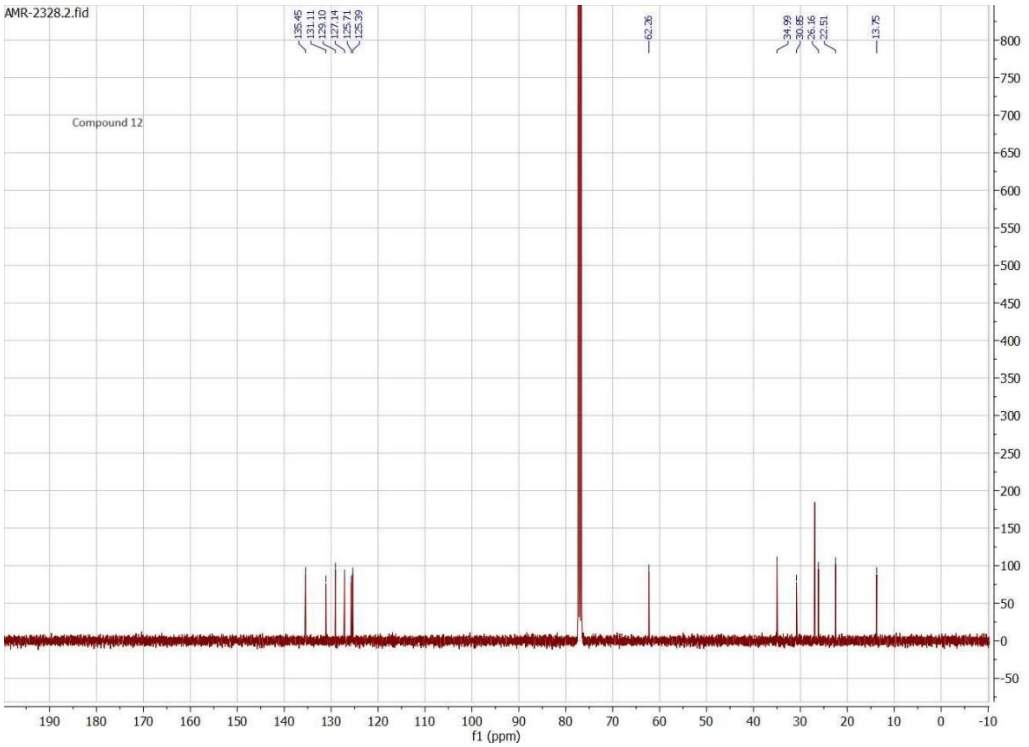

^{13}C NMR spectrum of the compound 12.

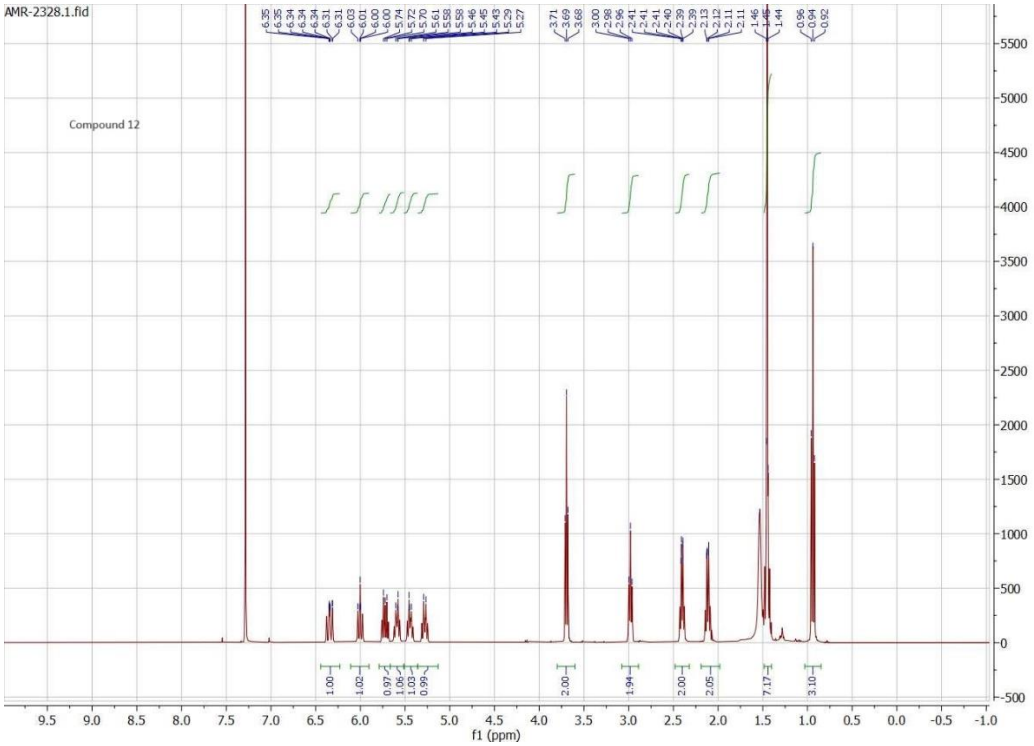

^{1}H NMR spectrum of the compound 12.

Supplementary references:

Allegretti, P. A. & Ferreira, E. M. (2011) Generation of α,β-unsaturated platinum carbenes from homopropargylic alcohols: Rearrangements to polysubstituted furans. *Org Lett* **13**, 5924-5927.

Liu, Y. P., Ji, L. P., Eno, M., Kudalkar, S., Li, A. L., Schimpgen, M. et al. (2018) (*R*)-*N*-(1-Methyl-2-hydroxyethyl)-13-(*S*)-methyl-arachidonamide (AMG315): A novel chiral potent endocannabinoid ligand with stability to metabolizing enzymes. *J Med Chem* **61**, 8639-8657.

Saran, R. K., Millar, J. G. & Rust, M. K. Role of (3,6,8)-dodecatrien-1-ol in trail following, feeding, and mating behavior of *Reticulitermes hesperus*. *J Chem Ecol* **33**, 369-389.

Sigurjónsson, S. & Haraldsson, G. G. (2024) Asymmetric synthesis of methoxylated ether lipids: Total synthesis of polyunsaturated C18:3 omega-3 and omega-6 MEL triene derivatives. *Molecules* **29**, 223.